Interactions of inhaled nanoparticles with the alveolar-capillary barrier of the human respiratory tract

Dissertation
zur Erlangung des Grades
„Doktor der Naturwissenschaften“

am Fachbereich Biologie
der Johannes Gutenberg-Universität in Mainz

Jennifer Yvonne Kasper

Geb. in Saarbrücken

Mainz, der 22.08.2011

Dekan:
Tag der mündlichen Prüfung: 13. 12. 2011

Partial results of this thesis have been published in the following publications

Kasper J, Hermanns MI, Bantz C, Maskos M, Stauber R, Pohl C, Unger RE, Kirkpatrick CJ: **Inflammatory and cytotoxic responses of an alveolar-capillary coculture model to silica nanoparticles: Comparison with conventional monocultures**. *Part Fibre Toxicol* 2011, **8**(1):6.

Hermanns MI, Kasper J, Dubruel P, Pohl C, Uboldi C, Vermeersch V, Fuchs S, Unger RE, Kirkpatrick CJ: **An impaired alveolar-capillary barrier in vitro: effect of proinflammatory cytokines and consequences on nanocarrier interaction**. *J RSocInterface*, 2010, **7 Suppl 1**:S41-S54.

Contents

List of Abbreviations

AJ	adherens junctions
AJC	apical junctional complex
ALI	acute lung injury
AM	alveolar macrophage
AmorSil	amorphous Organosiloxane particles
ANOVA	analysis of variance
ARDS	acute respiratory distress syndrome
aSNP	amorphous silica nanoparticles
ATI	alveolar type I cell
ATII	alveolar type II cell
BB	biological barriers
Bcl-2	B-cell lymphoma 2
BFGF	basic fibroblast growth factor
CatD	cathepsin-D
Cav	caveolin-1
CCP	clathrin-coated pits
CCV	clathrin-coated vesicles
CHC	clathrin heavy chain
COPD	chronic obstructive pulmonary disease
DNA	desoxyribonucleic acid
DIC	differential interference contrast
DLS	dynamic light scattering
dNTP	desoxyribonukleosidtriphosphate
DPPC	dipalmytoylphosphatidyl-cholin
ECBM	endothelial cell basal medium
EEA1	early endosome antigen 1
ELISA	enzyme-linked immunosorbent assay
ER	endoplasmatic reticulum
F12	siRNA for flotillin-1 and -2 in combination
FCS	fetal calf serum
Flot1	flotillin-1
Flot2	flotillin-2
G-CSF	granulocyte-colony stimulating factor
HIF-1a	hypoxia-inducible factor alpha
HPMEC	primary human pulmonary microcascular endothelial cells
ICAM-1	intercellular adhesion molecule-1
IF	immunofluorescence
IL-1	interleukin-1
IL-1ß	interleukin-1 beta
IL-6	interleukin-6
IL-8	interleukin-8
Lamp-1	lysosomal-associated membrane protein 1

LDH	lactate dehydrogenase
LPS	lipopolysaccharide
M6PR	mannose-6-phosphate receptor
MCP-1	monocyte chemoattractant protein-1
MTS	3-(4,5-dimethylthiazol-2-yl)-5-(3-carboxymethoxyphenyl)-2-(4-sulfophenyl)-2H-tetrazolium, inner salt
Neg	non-trageted siRNA
NP	nanoparticle
OG	oregon green
PCR	polymerase chain reaction
PECAM-1	platelet endothelial cell adhesion molecule
PEI	polyethyleneimine
Pen/Strep	penicillin/streptomycin
PFA	paraformaldehyde
PLGA	DL-lactide/glycolide copolymers
PM_{10}	particulate material with a diameter <10 µm
$PM_{2.5}$	particulate material with a diameter <2.5 µm
PMA	phorbol 12-myristate 13-acetate
PMEC	pulmonary microvascular endothelial cells
RANTES	regulated upon activation, normal T-cell expressed, and secreted
RFU	relative fluorescent unit
RNA	ribonucleic acid
ROS	*produce reactive oxygen species*
sICAM-1	soluble intercellular adhesion molecule-1
siRNA	small interferring
SNPs	silica nanoparticles
SP-(A, B, C, D)	surfactant protein-(A, B, C, D)
TEM	transmission electron microscopy
TER	trans-bilayer electrical resistance
TGF-β	transforming growth factor-β
TGN	*trans*-Golgi network
TJ	tight junctions
TNF-a	tumor necrosis factor alpha
VCAM-1	vascular cell adhesion molecule 1
VEGF	vascular endothelial growth factor
WHO	world health organisation
XIAP	X-linked inhibitor of apoptosis protein

List of Figures

1 Introduction

1.1 The alveolar-capillary barrier

The lung is the respiratory organ of vertebrates and is composed of two different sections: 1. the conducting zone, which contains the bronchi, the bronchioles as well as the terminal bronchioles 2. the respiratory zone, which contains the respiratory bronchioles, the alveolar ducts and finally the alveoli (see Figure 1). The conducting zone comprises the pulmonary airway. Its function is it to enable the airflow via inhalation from the external environment, beginning at the nose and mouth and terminating in the alveoli, which are situated at the distal end of the bronchioles. The alveoli are sacs which are arranged in clusters and constitute the alveolar-capillary barrier, the terminal respiratory unit [1]. The function of the alveoli is in the first place to mediate gas exchange with the blood to maintain the respiratory metabolism of the organism. The barrier is permeable for gases such as oxygen and carbon dioxide as well as many other gases. The lung contains approximately 300 million alveoli, which makes a surface area of around 140 m^2 which would cover an entire tennis court. To permit sufficient gas diffusion the barrier is extremely thin, and in some areas it is merely 500 nm [2]. However, this also makes the alveolar-capillary barrier a target site for harmful substances from the external environment encountering the organism via the inhalation route. Nevertheless, it maintains a tight barrier which protects the body from external hazards.

1.1.1 The alveolar capillary barrier in detail

The balance of supporting sufficient gas diffusion and simultaneously providing a protective barrier is due to the finely tuned interplay of cell types of which the alveolar-capillary barrier is composed. The main cell types are the alveolar epithelial cells, which face the alveolar lumen and cover the entire alveolar surface, and the microvascular endothelial cells, which are polarized to the capillary lumen. Between both cell types, which separate the alveolar lumen

from the capillary lumen, there is a continuous, thin, collagen-containing basement membrane.

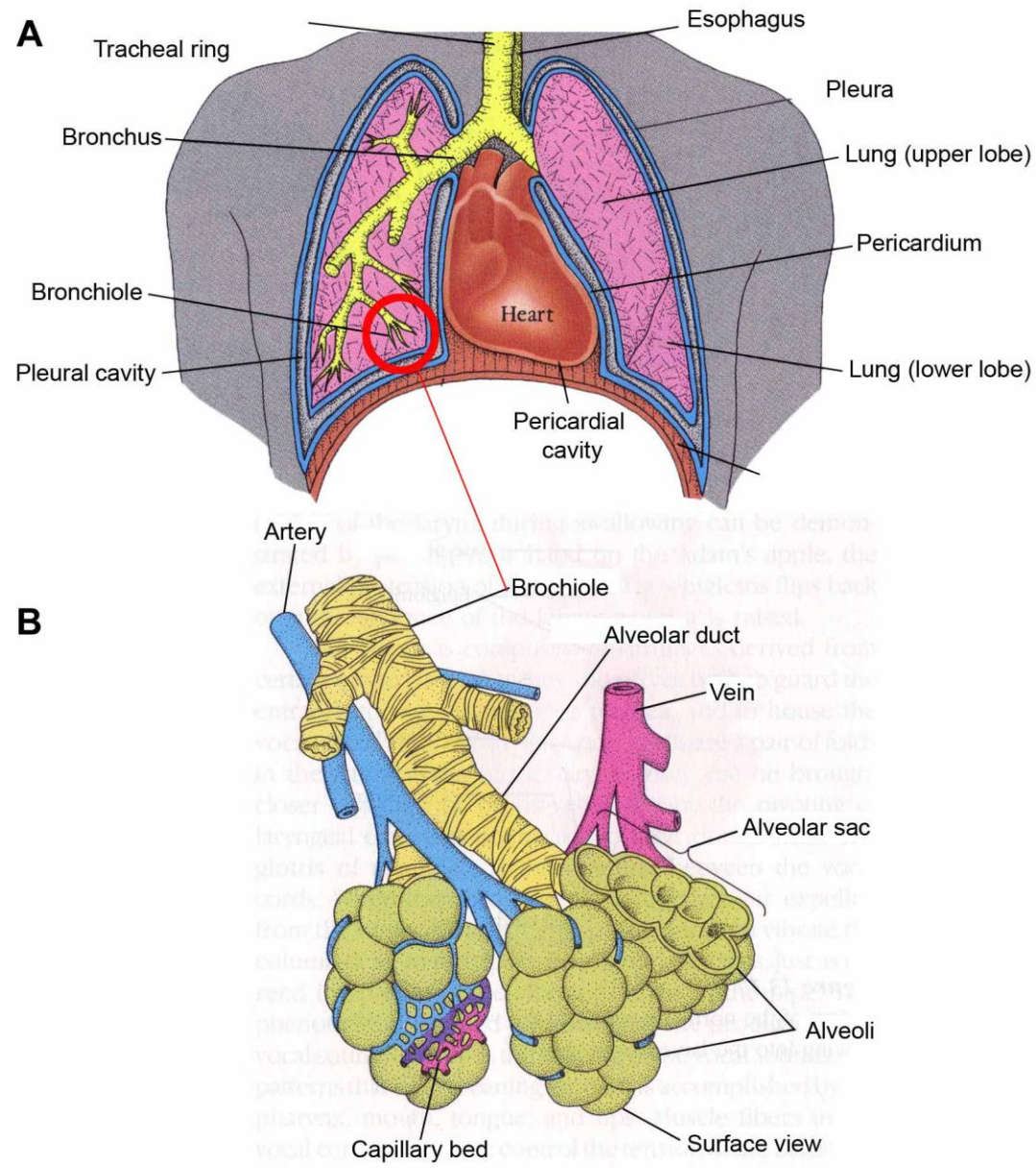

Figure 1: A: The human respiratory system. B: Termination of the respiratory passages (Alveoli), modified from Dorit/Walker/Barnes (Zoology) [1].

Alveolar epithelial cells can be distinguished as alveolar type I (ATI) and alveolar type II (ATII) cells. ATI cells cover approximately 95% of the alveolar surface and are mainly responsible for the tight epithelial barrier formation. Their morphology is perfectly adapted to permit efficient gas exchange between

the alveolus and the blood. The ATII cover the remaining 5% of the alveolus [3]. In addition to their crucial role in fluid balance and ion transport across the alveolar epithelium, they are mainly responsible for surfactant synthesis, secretion and recycling [4]. The alveolar surfactant is indispensable for the regulation of the surface tension in the alveolus. Alveolar surfactant is composed of ca. 90 % lipids [5]. The lipid compound consists predominantly of dipalmytoylphosphatidyl-choline (DPPC), which plays a crucial role in reducing the surface tension in the alveolar space. The other 10 % of the alveolar surfactant is made up by specific surfactant proteins. Surfactant protein SP-B and SP-C lower and modulate the alveolar surface tension [6]. Surfactant protein SP-A and SP-D belong to the collectins and play a crucial role in the innate immune system concerning recognition, binding and clearing of invading viral, fungal and bacterial pathogens from the alveolar space. SP-A and SP-D either directly kill pathogens or enhance their phagocytosis by macrophages [7, 8].

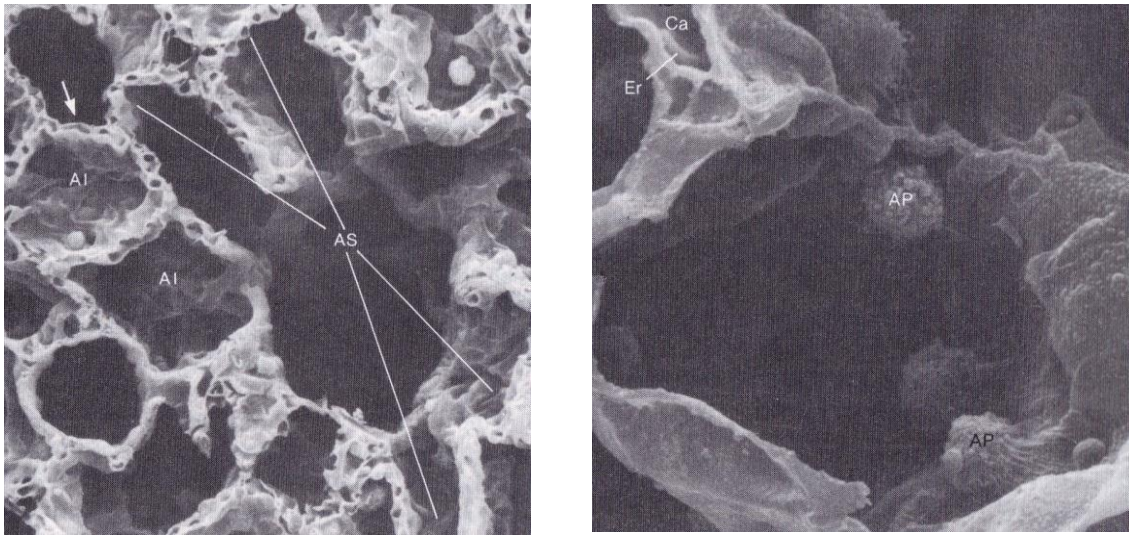

Figure 2: Scanning electron micrograph of a group of alveoli (Al) branching from an alveolar sac (AS). Several capillaries (arrows) situated between alveoli (from Dorit/Walker/Barnes (Zoology) [1]).

The synthesis of surfactant material (lipids, SP-Band -C) encompasses the endoplasmic reticulum, the Golgi complex, multivesicular bodies and composite bodies. Subsequently, the surfactant material is stored in specific storage

organelles, the so called lamellar bodies, prior to secretion onto the alveolar epithelial surface. Surfactant is also recycled via the lamellar bodies [9].

Another crucial cell type in the alveoli is the **alveolar macrophage (AM)**. As the first line of defence in the deep lung against particles such as dust or microorganisms, the so called “dust” cell eliminates dust or infectious material through phagocytosis and intracellular degradation and responds with the release of several inflammatory mediators such as IL-1, IL-6, TNF-α or IL-8. AMs are known to play a central role in controlling lung immunity. Under homeostatic conditions the AM closely adheres to the alveolar epithelium. Upon recognition of infectious material the AM detaches from the epithelium and executes its innate immune functions such as phagocytosis and secretion of proinflammatory cytokines [10].

Pulmonary microvascular endothelial cells (PMEC) constitute a surface area of approximately 130 m^2. For many years the pulmonary vascular endothelium was considered to be merely a monolayer, with semipermeable barrier properties, which separates the blood lumen from the alveolar space. However, the vascular endothelium has a high metabolic activity and comprises a variety of physiological, immunological and synthetic functions [11]. PMECs contribute to a crucial extent to the maintainance of fluid homeostasis. It expresses i.e. the ACE-complex (angiotensin converting enzyme) on the surface, which is responsible for the conversion of angiotensin-I to angiotensin-II. Thus, the pulmonary vascular endothelium has a regulating function on blood pressure [12]. Furthermore, its immunological functions involve the expression of adhesion molecules, such as ICAM-1 or E-selectin [13, 14] and the release of cytokines, such as MCP-1, IL-6, IL-8 or RANTES [13, 15-17].

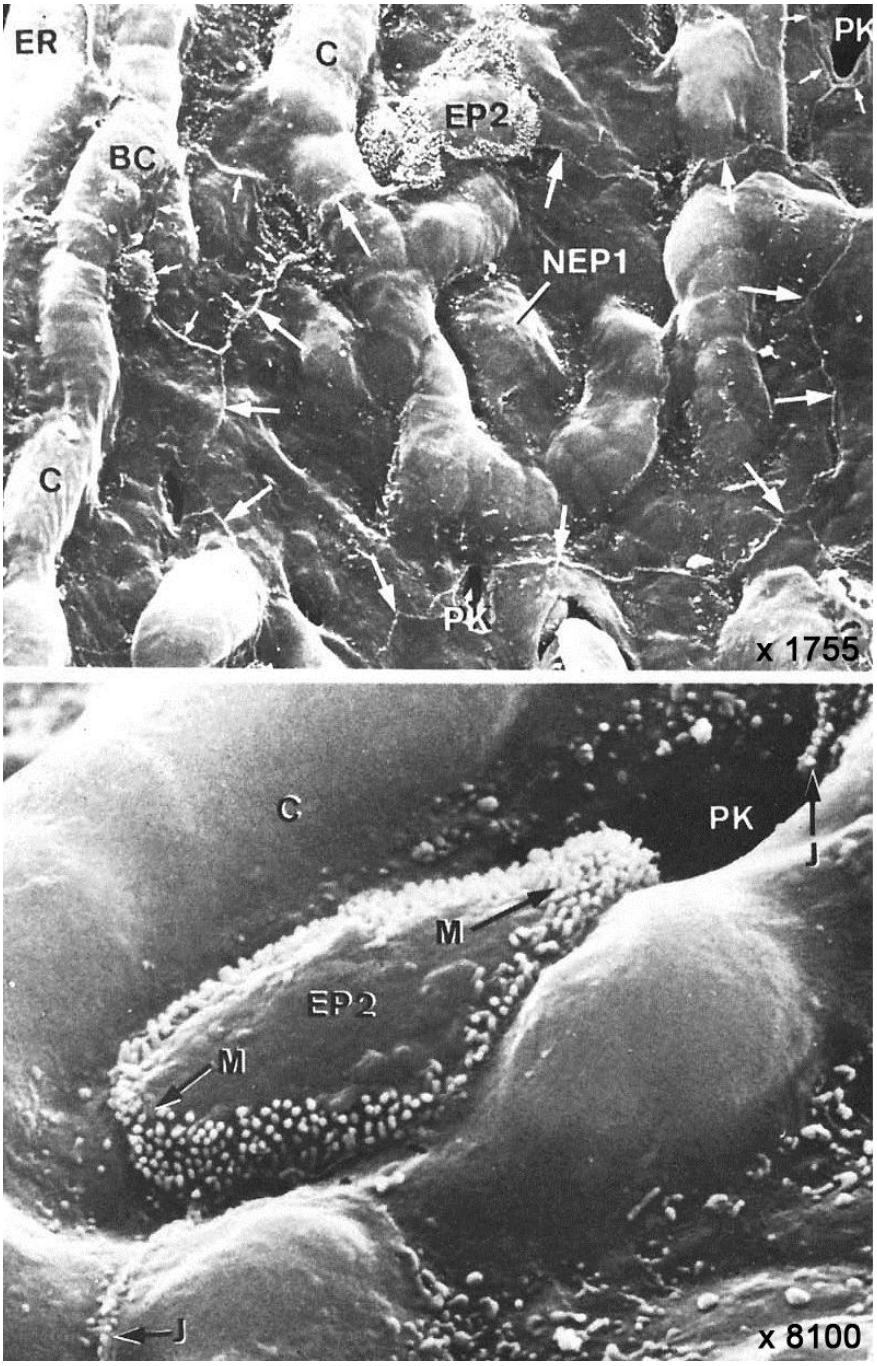

*Figure 3: Scanning electron micrograph of an alveolar epithelium. White arrows mark cell-borders of a single **EP1**: alveolar type I cell (ATI), **NEP1**: nucleus of the ATI, **BC, C**: bulging capillaries, **EP2**: alveolar typ II cell (ATII), **M**: microvilli, **PK**: interalveolar pore. This Figure is modified from Gehr et. al., The Normal Human Lung: **Ultrastructure and Morphometric Estimation of Diffusion Capacity**, Respiration Physiology (1978) [18].*

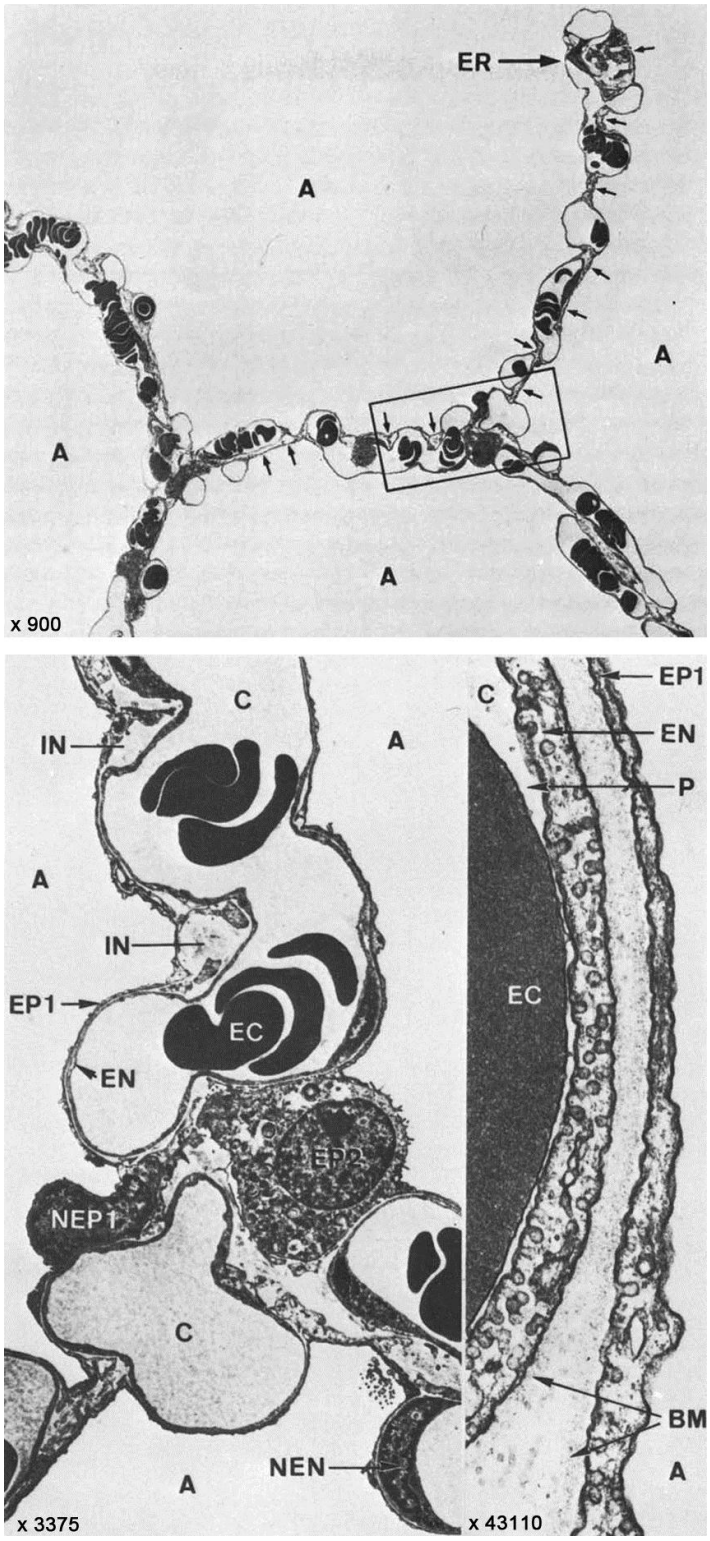

Figure 4: Electron micrograph of the alveolar capillary barrier A: alveolar space, ER: entrance ring, reinforced border of a septum, EP1, EP2: alveorar type I/II cells (ATI/II), NEP1: nucleus of a ATI, EN: endothelium, C: capillaries, EC: erythrocyte, IN: interstitial space, BM basalmembrane, P: bood plasma. This Figure is modified from Gehr et. al., The Normal Human Lung: ***Ultrastructure and Morphometric Estimation of Diffusion Capacity****, Respiration Physiology (1978) [18]*

1.2 Barrier integrity: Cell-cell contacts

ATI and ATII cells are arranged as a monolayer and form a tight epithelial barrier towards the environmental site. To do so, they develop tight cell-cell contacts, the so-called tight junctions (TJ) and adherens junctions (AJ).

Tight junctions are arranged at the most apical region of the lateral membrane of epithelial cells. They form a circumferential belt around the cell and engage a tight contact to adjacent cells. On the one hand they have a fence function which maintains the apical/basolateral polarity of the cell by preventing the diffusion of apical membrane components towards basolateral and vice versa. On the other hand they execute a gate function which regulates the paracellular transport of water, ions or molecules as well as immune cells across the epithelial barrier. Paracellular transport of solutes through TJ is passive; it is driven by diffusion or electro-chemical gradients generated by active transcellular (vesicle-mediated) transport mechanisms.

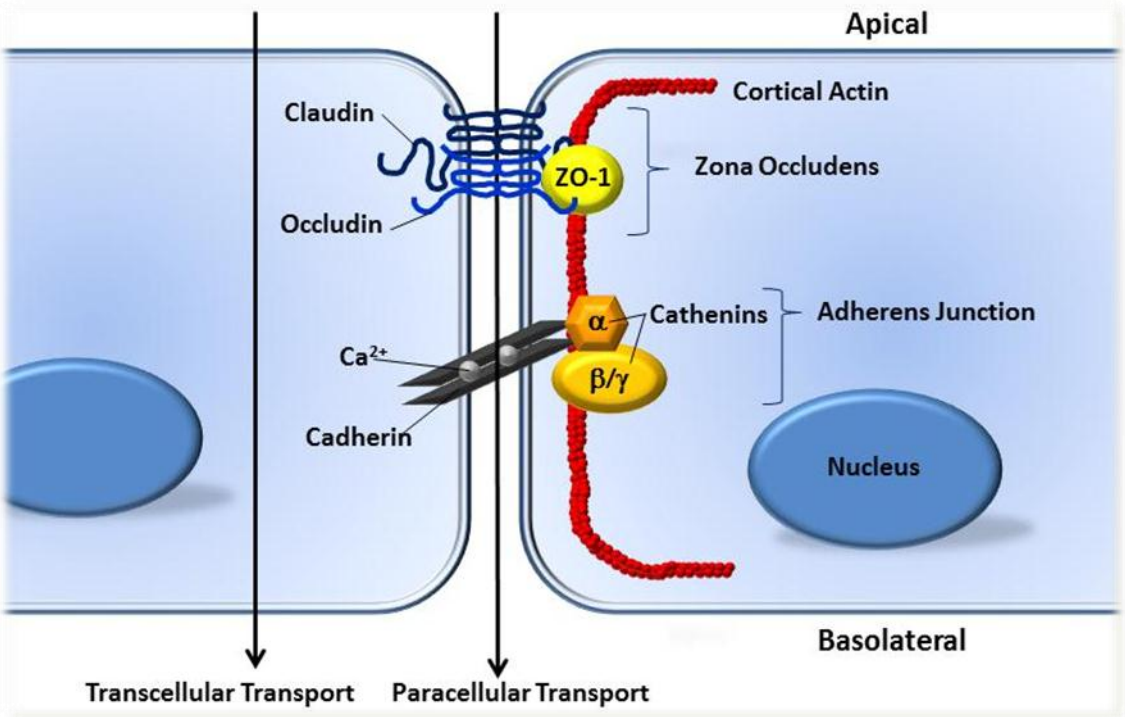

Figure 5: Cell-cell contacts in general: Tight junctions (TJ) are composed of claudins, occludins and ZO-1, forming the zona occludens. Adherens junctions (AJ) are i.a. composed of cadherins and catenins. This figure is based on Dudek and Garcia (2001) [19].

TJs are composed of several proteins which assemble the paracellular seal. Pivotal TJ-proteins are ZO-1 (zona occludens protein-1) and occludin. Occludin is an integral plasma-membrane protein which contributes to the paracellular seal by exposing loops to the paracellular space which form the tight contact to adjacent cells. Occludin is linked to ZO-1 which is located at the cytosolic side and anchored to the cortical actin cytoskeleton [20, 21]. Other fundamental TJ-proteins are the claudins. Claudins as well as occludin form charge and size selective pores between two cells with a size of about 8-9 A° (ca. 0.8 - 0.9 nm) [22, 23]. A recent study has shown, that claudin-3, claudin-4 and claudin-5 are expressed in ATII, whereas especially claudin-5 is expressed throughout the alveolus [24].

Adherens junctions are another type of intercellular junctions and are arranged basolaterally to TJs. They function in a calcium-dependent manner and are composed of transmembrane-proteins such as cadherins, which are linked to catenins (α, β or γ), which are in turn anchored to the actin cytoskeleton [25]. AJ and TJs compose, concomitant with desmosomes, the apical junctional complex (AJC).

As lining cells, pulmonary microvascular endothelial cells (PEC) also possess a cortical actin-ring associated with TJs, AJ and PECAM-1 related contacts, which are located basally to AJs [19]. In contrast to alveolar epithelial cells, they develop less tight cell-cell-contacts, which is accompanied by a higher water permeability through the paracellular space.

1.3 Nano-sized material

Humans are in contact with nano-sized material throughout their entire evolutionary lifespan. Naturally occurring sources of nanomaterial origin are, for example, volcanic eruptions, forest fires, physical and chemical weathering of rocks or desert sand. Nanoparticles (NPs) are defined as having, at least in one structural dimension, at most 100 nm in size [26]. Recently, other definitions for nanoparticles have been suggested. Since the size, which is regarded as the pivotal characteristic factor of a nanoparticle closely correlates with its surface area, it has been proposed that the definition of a nanoparticle should refer to a

specific NP-surface area of about 60 m^2/cm^3. The surface-parameter is regarded as a prevailing factor with respect to the reactivity and toxicity of nanomaterials [27].

Over the past 10 years nanoparticulate material has gained tremendously in importance for industrial applications. But also the antique Greeks and Romans used nanotechnology. They used a nano-paste composed of lead oxide and calcium hydroxide to stain grey hair.

Nano-sized material has been demonstrated to exhibit different features than the same material in bulk form [28]. Nearly any material can be used to synthesise engineered nanoparticles. Carbon-based NPs are used for example in lubricants, coatings, catalysts and electro-optical devices. Titaniumdioxide NPs are applied in toothpaste, white paints and also sunscreens or in the textile industry as coating with self-cleaning effects. Nano-silver is also used as a textile-coating with antimicrobial properties [29, 30]. Silica-based (SiO2) NPs (SNPs) are of particular interest for contemporary nanotechnology. Silica appears in two different forms: 1. The crystalline form which is arranged in tetrahedral SiO_4 units (such as α-quartz, α-tridymite etc.), 2. the amorphous form which does not have such a long-range order of the positions of the atoms. Fumed SNPs are i.e. used to optimise adhesives and sealants. It is also applied in catalyst carriers, paints and coatings. Synthetic amorphous silica NPs (aSNPs) are processed in e.g. photovoltaic, tyre compounds or electrical and thermal insulation material [31]. They are also a component of products which are directly exposed to humans, e.g. cosmetics or toothpaste. SNPs are even added to powdered food ingredients to avoid caking [32, 33].

1.4 Nanoparticles encounter the human lung

Nanoparticles are able to enter the body by passing through biological diffusion barriers such as the skin (epidermis), the gastrointestinal tract (gastrodermis) or the lung (respiratory epithelium) i.e. the alveolar-capillary barrier. Physiologically, biological barriers are designed to handle the interplay of two different aspects. On the one hand they allow the passage of external substances that are essential for the organism (e.g. gas exchange at the

alveolar-capillary barrier), while on the other hand biological barriers protect the body from hazardous exterior substances. Nevertheless, inhaled NPs embody a health-risk in the form of environmental and occupational lung diseases. Hence, research addressing the toxicity of industrially fabricated NPs or the suitability of particles specially synthesized for drug and gene delivery should focus on the interaction of these NPs with biological barriers as putative entrance routes.

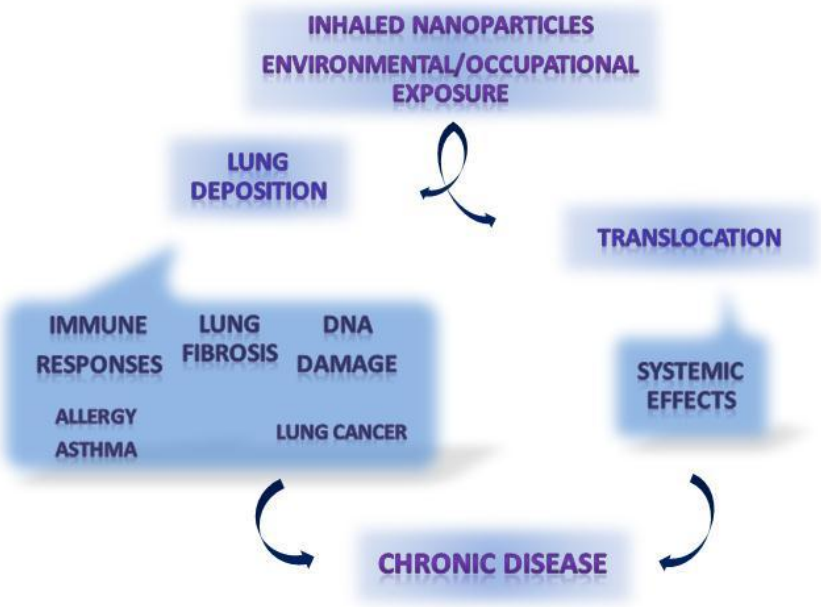

Figure 6: Biological endpoints that should be examined to enlighten the potential health risks of inhalated nanoparticles [34]

1.4.1 Pulmonary diseases caused by nanoparticles

The term pneumoconiosis is used when inhaled particles cause occupational lung diseases. Different types of particles cause different responses in the lung. Depending on the particle or dust type there are different terms for the caused lung disease:

Coal workers' pneumoconiosis (black lung) is caused by carbon particles.

A milder form (anthracosis) occurs to at least some extent in all city residents or tobacco smokers and proceeds normally asymptomatically. The more complicated form occurs in all mine and coal workers and leads to so-called industrial bronchitis. Industrial (chronic) bronchitis is characterised by cough and sputum for at least three months a year. [35].

Asbestosis is caused by asbestos fibres (naturally occurring silicate minerals) and manifests itself as interstitial fibrosis in the lower zones of the lungs due to accumulation of asbestos bodies. The latency period from the first exposure to the first symptoms may vary from 15 to 20 years. Shortness of breath, dry cough, and decreased diffusion capacity with time are the most common symptoms and signs of asbestosis [36].

Silicosis is caused by inhalation of high doses of crystalline silica during sandblasting, silica flour milling, stonecutting or ceramic manufacture which leads generally to a progressive fibrotic lung, pulmonary edema and inflammation.The silicotic lung is typified by silica-nodules composed of SNPs enclosed in collagen fibres arranged in concentric layers and enriched with macrophages, lymphocytes and fibroblasts in the periphery [26] attended by an accumulation of surfactant-rich fluid within the alveoli [37]. Epidemiologic studies indicate that the silicotic disease pattern progresses further even after the silica exposure has ended [38, 39]. Silica exposure does not only progress to silicosis, it also exerts influence in increasing other diseases, such as tuberculosis, rheumatoid arthritis or COPD (chronic obstructive pulmonary disease) [40].

Furthermore, silica and especially asbestos are reported to possess cancerogenic features [41-43]. Cancer affecting the lung and bronchus is, compared to other cancer forms, the most common and deadliest of cancers globally [44]. Therefore, it is of special interest to minimize exposure to silica and asbestos at occupational sites. Especially occupational asbestos exposure leads to severe lung cancer forms including bronchial carcinoma, or even mesothelioma (affecting the cavity lining of the lung, heart, or abdomen). Even workers who come in contact with low-doses of asbestos, such as construction workers, car mechanics, and plumbers, should be counselled on exposure risks [45].

1.4.2 Deposition, translocation of NPs and systemic effects

According to Borm and coworkers [46] five `Ds` have to be taken into account in order to determine and interpret properly the potential toxicity of inhaled nanomaterial: (1) **Dose**, (2) **Deposition**, (3) **Dimension**, (4) **Durability**, and (5) **Defense**. Primarily, the deposited dose depends on the mass concentration and the dimensions (size and porosity) of the particulate matter. With regard to the respiratory tract, the deposition probability of NPs increases as particle size decreases. From this, it follows that the major fraction of nano-sized material deposits on the alveolar epithelium, where the gas exchange takes place. Another deciding factor is the durability. The poorer the solubility and degradation of the deposited material, the higher the accumulation at the deposition site over time and the more toxicity it can display [46]. The lung is equipped with several defence mechanisms to handle such foreign material. The first line of defence is located in the upper airways and is called mucocilliary clearance (MCC), which is a self-clearing mechanism of the bronchi. In the deep lung alveolar macrophages (AM) take over this task by phagocytosis of deposited nanomaterial. Nonetheless, the transport of phagocytosed NPs by AMs towards the larynx to link up with the MCC is very slow and may remove just about a third of the entire deposited material [47].

Direct effects: Instantaneous effects upon NP exposure to the alveolar surface are not yet completely understood. In a sub-toxic dose range, which is NP-dependent, alveolar macrophages and alveolar epithelial cells may be damaged or triggered to implement inflammatory responses [46]. In the first place, NP-exposed alveolar epithelial cells are known to produce *reactive oxygen species* (ROS), such as $OH^{\cdot}$, NO, hydrogen peroxide or superoxide, which act as a general defence mechanism to eliminate invading pathogens. Under optimal conditions these radicals are generated at low frequency since they tend to react with proteins, lipids and DNA, which causes cellular damage [48]. Cristalline silica, to give one example, is known to initiate ROS production when inhaled in the deep lung [49]. Either the SNP-surface can trigger ROS production by interacting with extracellular matrix components or the failure of the clearing-process by macrophages can initiate ROS generation directly by

macrophages. As a result NP-induced increased ROS levels inter alia prompt inflammatory processes in the lung [50]. Inflammatory cytokines are crucial mediators in inflammatory lung diseases. In this scenario the alveolar macrophages function as an essential initiator by releasing so-called early-response cytokines such as IL-1ß and TNF-α, which in turn activate other AMs, epithelial cells as well as endothelial cells to produce further cytokines. Interleukin-8 (IL-8) is besides other cytokines such as IL-6, MCP-1 and RANTES, the most important cytokine regarding the recruitment of further immune cells, originating from the blood, into the alveolus [51-55]. Furthermore, adhesion molecules, such as ICAM-1 and VCAM-1, which are also expressed by alveolar epithelial and pulmonary microvascular endothelial cells upon stimulation, also play a pivotal role in the attraction of further immune cells [56, 57]. The recruitment of leukocytes to the alveolar compartment by moving across the alveolar-capillary barrier is an indispensable defence mechanism in inflammatory processes and occurs generally in acute and chronic inflammatory lung injury [58, 59].

Systemic effects: Epidemiological studies have revealed that particulate air pollution (PM_{10}) increases the frequency of cardiac diseases [60, 61]. PM_{10} (particulate material with a diameter less than 10 µm) is identified by the WHO (World Health Organisation) as the most hazardous component of air pollution. Furthermore, only $PM_{2.5}$ (diameter <2.5 µm) is able to penetrate the bronchioles and alveoles to a marked extent [62]. Recently conclusions have been drawn that elevated concentrations of PM in the air may increase the risk of myocardial infarction within 2 to 24 hours after exposure [63]. However, plausible explanations from the biological perspective are still lacking. Nevertheless, it is currently discussed that the pulmonary release of cytokines and mediators into the circulation that is triggered by inhaled NPs causes extrapulmonary effects [64]. It is also suggested that these systemic effects are a result of inhaled PM_{10} accessing the systemic circulation and the following translocation to various organs [62, 65].

1.4.3 Intracellular trafficking of nanomaterial in lung cells and its application to nanomedicine

Going into more detail of biological barriers (BB), the plasma membrane of cells takes on special significance. The smallest unit of a biological barrier is the plasma membrane of the cell, which is the basic functional unit of live. In the case of alveolar epithelial cells the plasma membrane separates the interior of the cell from the alveolar lumen, which has access to external environment. The plasma membrane consists of a phospholipid bilayer containing *inter alia* several proteins and is semipermeable for ions and some organic molecules, to name two important interaction partners. Thus, the plasma membrane regulates the influx and efflux of the cellular unit. Consequently, nanoparticulate matter has in the first instance to overcome this basic unit of biological barriers to enter cells and finally the organism.

1.4.3.1 Putative entry-routes for NPs: Endocytosis pathways

A variety of external substances which are essential for cellular metabolism are either too large or on account of their polarity cannot pass through the hydrophobic, cellular plasma membrane. Therefore, the cell incorporates such substances and molecules via endocytosis. Endocytosis is a process in which the cell engulfs external material such as fluid or macromolecules by budding off vesicles originating from the plasma membrane. The vesicles transport their cargo along actin filaments or microtubules with involvement of molecules such as myosin, kinesin and dynein. A variety of endocytosis pathways can be distinguished, depending on the cargo or transport- ype: **Pinocytosis** forms include macropinocytosis, clathrin-mediated endocytosis and caveolin-mediated endocytosis. All three pathways transport their load to the early sorting station (early endosomes). From there, the cargo is taken via carrier vesicles (multivesicular bodies) to late endosomes. Cargo which is designated for degradation is sent to lysosomes, whereas reclaimable cargo is transferred to the *trans*-Golgi network (TGN) for further processing. Vesicles undergo a recycling process and return to the plasma membrane via so-called recycling vesicles [66].

Clathrin-mediated endocytosis involves clathrin-coated pits (CCP), in which clathrin is arranged in a polygonal lattice on the inner surface of the plasma membrane. Those CCPs bud and pinch off the membrane in a dynamin-depenent manner and form clathrin-coated vesicles (CCV). Several hundreds to thousands of CCV can form in a period of a few minutes. Once budded from the plasma membrane the CCV have a lifetime of a few seconds. After shedding the clathrin-coat, the remaining vesicles fuse with other vesicles and proceed through the endocytosis pathway, whereas the shed coats constitute the cytosolic reservoir of clathrin that is recycled to the plasma membrane to form new CCPs. The clathrin–dependent pathway is receptor-mediated and its ligands are, for example, low density lipoprotein, transferrin or growth factors [67-69].

Caveolae comprise one type of clathrin-independent endocytotic pathway. They are a special type of lipid rafts and form invaginations of the plasma membrane with a size of about 50-100 nm. Caveolae are primarily composed of an intergral membrane protein named caveolin-1 which is essential for the formation and stability of the caveolae. Caveolae can bud off the membrane and fuse either with so-called caveosomes or early endosomes. Caveolae are involved in endocytosis (fusing with early endosomes directed to late endosomes and lysosomes) as well as transcytosis by fusing with the TGN (trans-Golgi-networt) or ER (endoplasmatic reticulum). Transcytosis is a transport of macromolecules across cells to a target site and occurs in all epithelial cells and particularly in vascular endothelial cells. Caveolae have been suggested to be involved in transcytosis iof albumin [70], iron-transferrin [71], insulin [72] or even chemokines like MCP-1 (monocyte chemoattractant protein-1) [73].

Phagocytosis is the pathway which is responsible for the uptake of solid particles. Similar to the pinocytotic pathway, internalized materials are transported to stations similar to the pinocytosis pathway. Thus, phagosomes are similar to early endosomes and lysophagosomes are similar to late endosomes and lysosomes [66]. Figure 7 summarises the principal endocytosis pathways. It should also be stressed that different cell types are specialized for

specific uptake mechanisms. Thus, phagocytosis occurs primarily in phagocytes (i.e. alveolar macrophages), whereas the pinocytosis machinery is prevalent in several cell types (i.e. alveolar epithelial cells and microvascular endothelial cells).

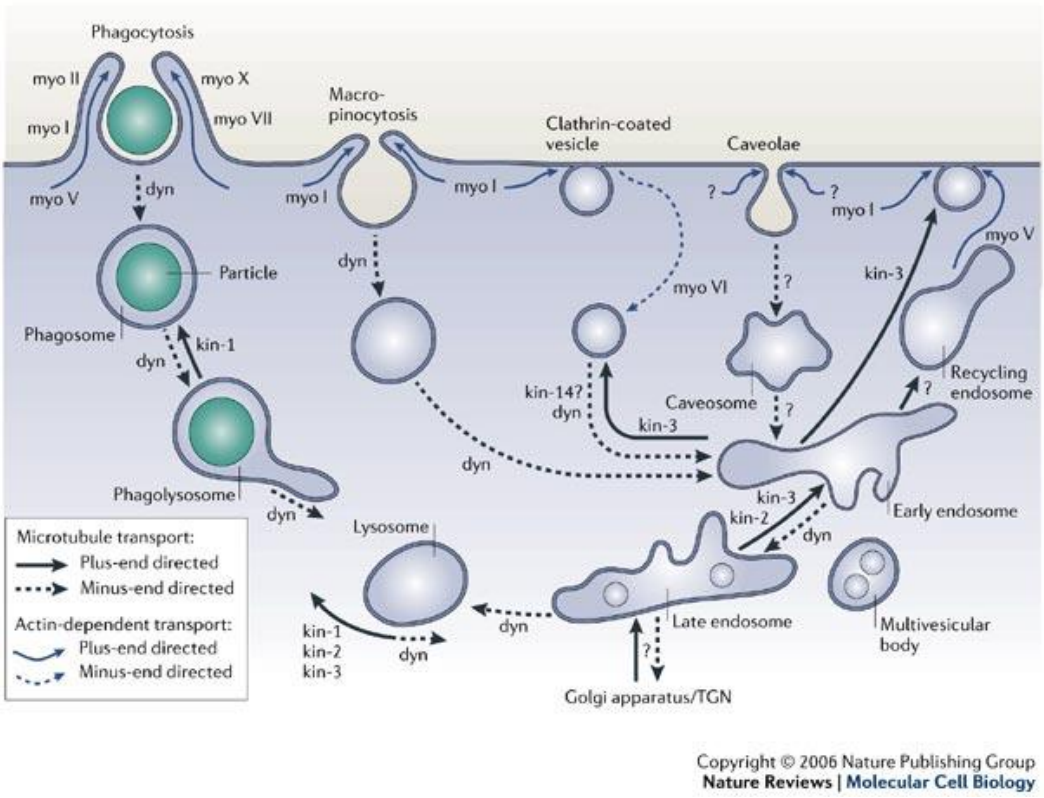

Copyright © 2006 Nature Publishing Group
Nature Reviews | Molecular Cell Biology

Figure 7: Overview of the prevalent endocytosis mechanisms: Phagocytosis and pinocytosis (macropinocytosis, clathrin-mediated endocytosis, caveolin-mediated (clathrin-independent) endocytosis). Microtubule transport: myosin (myo), kinesin (kin) or dynein (dyn). The figure is a resume based on Soldati and Schliwa et. al. 2006 [66].

Nanoparticles can enter cells by either direct penetration of the phospholipid bilayer of the plasma membrane or via the above mentioned endocytosis mechanisms. Great effort has already been invested by several research facilities to reveal the uptake behaviour of NPs in cells. The main interest has been placed on internalisation of surface-modified nanomaterial functioning as nanocarriers for drug and gene delivery, which are intended to target distinct endocytosis pathways, such as clathrin- or caveolae-mediated uptake. Examples are drug-loaded PLGA (DL-lactide/glycolide copolymers) or polybutylcyanoacrylate nanospheres [74-76]. Recent research activity involves

the development of nanovehicles loaded with for example anti-asthmatic drugs [77].

The lung is an ideal target organ for drug and gene delivery via nanoparticles for both systemic and local applications (asthma, COPD, cystic fibrosis). This is due to the large alveolar surface area, which offers better drug absorption, the relatively thin epithelial barrier, which has to be overcome, the extensive vascularisation of the organ and, in particular, the exclusion of first-pass metabolism, by which the concentration of an applied drug is drastically reduced before reaching the systemic circulation, not to mention the targeted organ [78].

1.5 *In vitro* cell culture models of the alveolar-capillary barrier

Simulating the *in vivo* situation using *in vitro* coculture models: The lung is composed of many different cell types which act in concert. Thus, complex coculture systems which are assembled with more than one cell-type are of great importance in elucidating cytotoxicity and induced cellular communication by diverse substances.

To form an alveolar-capillary barrier, an *in vitro* coculture system has been developed using the two principal cell types – alveolar epithelial and alveolar capillary endothelial cells. For the lower respiratory tract epithelium, the epithelial cell line, NCI H441 (with characteristics of type II pneumocytes and Clara cells) [79], and for the capillary endothelial cells of the lung, the human microvascular endothelial cell (MEC) line, ISO-HAS-1 [80, 81] are used. Both cells are seeded on opposite sides of a transwell filter membrane. After 10 days of cultivation epithelial and endothelial cells differentiate into polarized, barrier-forming cells, which develop circumferential cell-cell contacts expressing the tight junctional (TJ) protein, ZO-1, and the adherens junction (AJ) proteins, E-Cadherin, $\alpha-$ and β-Catenin. In addition, the barrier develops trans-bilayer electrical resistance (TER) values that average $560 \pm 6\ \Omega * cm^2$.

Figure 8: Cross section of a coculture with H441 seeded on top and ISO-HAS-1 seeded on the lower surface of a transwell filter membrane

Simulating more closely the *in vivo* situation by adding the alveolar macrophage: For the alveolar-capillary barrier there are non-specific mechanisms (coughing, sneezing, as well as the mucocillary escalator clearance mechanism), that prevent environmental, pathogenic or toxic material from passing through the thin cellular barrier from the airspace to the capillary blood. Should a material evade these clearing mechanisms, then the specific defence mechanisms of the respiratory system (the innate immune system) come into force. The first line of defence in the deep lung against particles such as dust or microorganisms is the alveolar macrophage (AM), the so called “dust” cell. As the alveolar macrophage plays a central defence role against invading pathogens or dust material, its addition to the well-established coculture model of the alveolar-capillary barrier [82] would be a major step forward in simulating more closely the *in vivo* situation. To represent the alveolar macrophage in our coculture model composed of H441 and ISO-HAS-1, the human acute monocytic leukemia cell line, THP-1, was chosen. Upon stimulation with PMA (phorbol 12-myristate 13-acetate) the THP-1 cells differentiate to cells with alveolar macrophage features and are can be applied to the epithelial monolayer.

1.6 Inflammatory and cytotoxic responses of an alveolar-capillary coculture model to aSNPs

Comparison with conventional monocultures: Since the health hazards of the crystalline form of silica nanoparticles, which among other things causes silicosis, have been well documented for the micrometer scale [83], the amorphous form has been considered as having low toxicity. Therefore, amorphous silica nanoparticles are used as an FDA-approved food additive [84]. Furthermore, aSNPs are used as a low toxic reference material in cytotoxicity experiments [85].

However, several cytotoxicity studies on nanoscaled amorphous silica NPs (aSNPs) indicate a possible serious hazard for human health. Napierska et al. [86] and Lison et al. [87] demonstrated via MTT and LDH assays a concentration-dependent cytotoxicity of aSNP on an endothelial cell line EA.hy926, the epithelial cell line, A549, and on monocyte-macrophages J774. Additionally, Waters et al. [32] employed a macrophage cell model to demonstrate that non-opsonised aSNPs stimulate inflammatory protein secretion such as RANTES, TNF-α, VEGF and G-CSF. In this latter study NP interaction with cells in coculture was compared to interaction with the conventional monoculture, in which the cells are seeded on tissue culture plastic 24h prior to the experiment. This study demonstrates that not only the polarized nature of cells in coculture but also the close proximity of epithelial and endothelial cells play an important role in the effects caused by aSNP exposure.

1.7 Aim of the study

The aim of this study is it to demonstrate the relevance of multicellular *in vitro* coculture systems for investigations of nanoparticle interactions with biological interfaces such as the lower respiratory tract, the so called alveolar-capillary barrier. Three different types of NPs have been chosen for this study: amorphous silica (aSNP), organosiloxane (AmorSil) and polyethyleneimine (PEI). All three NPs find increasing application in biomedical as well as industrial applications, although they may also represent serious health risks. The experimental design focussed on

- **cytotoxicity and inflammatory** responses of the alveolar-capillary unit following nanoparticle (NP) exposure. Comparison of different culture systems: sophisticated coculture *versus* conventional monoculture
- **Nanoparticle uptake:** Comparison of epithelial cells (H441) under conventional monoculture and coculture conditions
- possible **cellular uptake mechanisms** for nanoparticles, including cathrin- or caveolae-mediated as well as cathrin- or caveolae-independent endocytosis pathways
- **involvement of flotillins in cellular uptake** of nanoparticles and their **contribution to the viability** of NP-treated cells

Two principal hypotheses were tested within the scope of this thesis:

- Cells in multicellular coculture display more closely the polarized phenotype of the alveolar epithelium and endothelium, and additionally, the close proximity of these two barrier-forming cells permits cellular cross-talk as it may occur *in vivo* following nanoparticle exposure.
- Flotillins (flotillin-1 and -2) play an important role in regard to cellular uptake mechanisms, intracellular trafficking or storage of internalized nanoparticles and hence may influence the viability of NP-exposed cells

2 Material and Methods

2.1 Chemicals, Material and Devices

2.1.1 List of Chemicals

Table 1: list of chemicals

Albumin, bovine 35 % dilution, sterile	Sigma, Taufkirchen A 7409
Albumin, bovine fraction V	Sigma, Taufkirchen, 1000595748
AmorSil20	Physical Chemistry, Universitiy of Mainz (Maskos)
Aqua Braun	Braun ad iniectabilia, Braun Melsungen AG
beta-Mercaptoethanol	Sigma-Aldrich, M7522
Blockingreagence	Roche, Mannheim 1112589
Dexamethasone	Sigma, D1756
Di-Sodiumhydrogenphosphate-Dihydrate	Merck, Darmstadt 6580
DNAse	Qiagen, 79254
Dulbecco´s Phosphate buffered saline	GIBCO, 01852
ECL (Western Lightning™-ECL)	PerkinElmer, Rodgau, NEL100001EA
EGTA (Ethylenglycol-bis(ß-aminoethyl)-N,N,N`,N`-	Sigma, Taufkirchen E 4378
Essigsäure 99-100%	Baker, Griesheim 6152
Ethanol	Riedel de Haen, Seelze, 34923
Fluoromount-G™	Southern Biotech, Birmingham, 0100-01
Formaldehyde 37%	Merck, Darmstadt 40031000
Glucose	Merck, Darmstadt 4074
Glutaraldehyde	Serva, Heidelberg ,23114
Glycerine	Sigma, Taufkirchen G 7757
Hepes (N-[2-Hydroxyethyl]piperazin-N`-[2-ethansulfonsäure])	Sigma, Taufkirchen H 9136
Hoechst 33342	Sigma, Taufkirchen B-2261
hydrogen peroxide 30 %	Merck, Darmstadt 108597
Ibidi Mounting Medium (IMM)	ibidi, Martinsried, 50001
Lipopolysaccharid (LPS) von E.coli	Sigma, Taufkirchen L 2630
Ludox TM-40	Sigma, Taufkirchen, 420786
Methanol p.A.	Baker, Griesheim 8045
Natriumacetate	Merck, Darmstadt 6268
Natriumbicarbonat	Sigma, Taufkirchen 54019
Natriumchlorid	Merck, Darmstadt 6528
NexSil™ Aqueous Colloidal Silica	NYACOL®, Nano Technologies, Inc.
o-Phenylene-diamine-dihydrochloride [OPD]-tablets	Sigma, P 7288
Paraformaldehyde (PFA)	Merck, Darmstadt 4005
Percoll™PLUS	GE Healthcare, München, 17-5445-01

Phorbol 12-myristate 13-acetate (PMA)	Sigma, 79346
Polyetheleneimine	Polymer Chemistry & Biomaterials Research Group, Ghent University (Peter Dubruel)
Polyethyleneglykol	Sigma, Taufkirchen E 4378
Sicastar Red, 30 nm	Micromod, 40-00-301
Sucrose	Serva, Heidelberg 35579
TRIS	Roth, Karlsruhe 48552
Triton X-100	Sigma, Taufkirchen T 6878
Tween 20	Sigma, Taufkirchen P 1379

2.1.2 Devices

Table 2: devices

cell counter	CASY® Cell Counter and Analysis System
Centrifuges	Biofuge stratos, Heraeus Instruments
	Megafuge 1.0R, Heraeus Instruments
	MICRO 120, Hettich Zentrifugation
Chemiluminescence system	Chemi-Smart 5100 (peqlab, Erlangen)
clean bench	antair BSK, Heraeus
clean water system	ELGA, Elgastat Maxima.VF
ELISA-Reader	TECAN GENios Plus
Fluorescencemikroskope	Leica DMIL
	Leica DMI 6000B
	DetlaVision, AB, Applied Precision
Incubators	HERA cell 150
	UNIMAX1010, Heidolph
Intelli-Mixer	NeoLab
light microscope	Leica DMIL
Magnet	MPC-1, DYNAL
microplate washer	TECAN hydroFLEX
NanoDrop®	Thermo Scientific
pH-meter	inolab WTW series pH 730
Real-Time PCR machine	7300 Real Time PCR System, AB
special accuracy weighing machine	Sartorius Analytic
steam steriliser	H+P Labortechnik, Varioklav Typ 500
Steriliser	WTC Binder, TYP 18115300002020
TER measurment instrument	WPI, EVOM
Thermoblock	TECHNE DRI-Block® DB 2D
VORTEX GENIE2™	Scientific Industries Si
Waterbath	Julabo, SW-20C
	Julabo 5 VC

2.1.3 Material

Tabelle 1: Material list

15 ml Tubes	BD Falcon™, REF352096
50 ml Tubes, CELLSTAR®	greiner bio-one, 227261
24 well plates	TPP #92024
6 well plates	TPP #92406
96 well plates	TPP #92696
Cell culture flask 25 cm^2	TPP #90025
Cell culture flask 75 cm^2	TPP #90076
Eppendorf Safe-Lock Tubes (1.5/2ml)	Eppendorf AG, 0030 123.328/120.094
HTS-Transwell® 24 well plates	Costar®, Corning, NY14831
Ibidi µ-Slides 8 well (ibiTreat, tissue culture treated)	Ibidi #80826
Lab-Tek™ chamberslides	Nalge Nunc, 154534
MicroAmp™ Optical 96-well reaction plate	AB, Applied Biosystems, #N801-0560
Nalgene Syringe Filter, 0,2 µm	Nalgene®, Thermo Scientific, 1909920
Nylon filter, Cell Strainer (40/100 µm)	BD Falcon™, REF352346/352360
single-use syringe	Braun Melsungen AG, REF460602
Thermanox™ Coverslip	Nunc #174969

2.1.4 Cell culture

Table 3: cell lines

Cell lines	Type	Medium	company
NCI H441	epithelial	RPMI1640, 1 % P/S, 10% FCS	ATCC, HTB-174
ISO-HAS-1	endothelial	RPMI1640, 1 % P/S, 10% FCS	[80, 81]
THP-1	monocyte	RPMI1640, 1 % P/S, 10% FCS	ATCC, TIB-202

Table 4: primary cells

Primary cells	notation	Medium	source
ATII	Alveolar type II cells	SAGM, 1% P/S, 1%FCS, Supplements	Human lung tissue
HPMEC	Human pulmonary microvascular endothelial cells	ECBM, 1%P/S,15 % FCS	

Primary human cells were used in accordance with the rules of the responsible ethical commission.

Table 5: surface coatings for cell culture

Fibronectin	Sigma, Taufkirchen, F3648
Gelatine	2%Typ B bovine skin Sigma, Taufkirchen G1393
Collagen Type I, rat tail	BD, Biosciences, 354236

Table 6: culture media

ECGM-MV [PC-Medium]	PromoCell, Heidelberg C-90320
Medium 199 [M199], Hepes Mod.	Sigma, Taufkirchen M 7528
RPMI 1640	Gibco, Karlsruhe 61870-010
SAGM	CellSystems, St. Katharinen CC-4124

Table 7: medium supplements and growth factors

Antibiotics and fungicides	
Penicillin/Streptomycin (P/S)	Gibco, Karlsruhe 15140-114
Fungizone	Gibco, Karlsruhe #15290-026
Ciprobay 200	Bayer, Leverkusen 82420402 PZN-7802062
Supplements and growthfactors	
L-Alanyl-L-Glutamin [Glutamax I]	Gibco, Karlsruhe 35050-038
Fetal calf serum [FCS]	Gibco, Karlsruhe 10270-106
Heparin	Sigma, Taufkirchen H-3149
BFGF	Sigma, Taufkirchen, F0291
SAGM™SingleQuots®	Clonetics®, MD USA, CC-4124
Supplement-Mix for ECBM medium	Promocell, C-39255

Table 8: Enzymes for cell dissociation

Trypsin/EDTA	Gibco, Karlsruhe, 25200-056
Dispase [EC 3.4.21.4]	Sigma, Taufkirchen, P3417
Elastase [EC 3.4.21.36]	Calbiochem,Darmstadt, 324682

2.1.5 Kits and assays

2.1.5.1 Cytotoxicity

Table 9: Kits for cytotoxicity studies

MTS (CellTiter 96® AQueous One Solution Cell Proliferation Assay	Mitochondrial activity	Promega, G3582
LDH CytoTox 96® Non-Radioactive Cytotoxicity Assay	Membrane integrity	Promega, G1780.
Crystal violet	Cell number measurement	Merck, Darmstadt 1407

2.1.5.2 Apoptosis

Table 10: Apoptosis Kits

notation	endpoint	company
Casp-Glo assay	Caspase 3/7 activity	Promega,
BCA-Kit	Protein assay	Pierce , 23225
Proteome Profiler™ Array Human Apoptosis Array Kit	Several apoptosis markers	R&D,ARY009

2.1.6 Antibodies

Table 11: Endosomal markers for Immunofluorescence, Methanol/Ethanol fixation, 15 min, RT

Antibody	Dilution	Company	animal
EEA1	1:250	BD, 610456	mouse
Lamp1	1:100	BD, 611042	mouse
D-Catepsin	1:100	BD, 610800	mouse
Clathrin HC	1:100	BD, 610499	mouse
Caveolin-1	1:300	SantaCruz,sc-894	rabbit
Mannose-6-P-R.	1:100	Abcam	mouse
Flotillin-1	1:100	BD, 610821	mouse
Flotillin-2	1:100	BD, 610383	mouse

Table 12: Cell-cell contact markers for Immunofluorescence, PFA-Fixation

Antibody	Permeabilisation	Dilution	Company	animal
ß-Catenin	0.5% TritonX100, 20`RT	1:400	BD, 610154	mouse
E-Cadherin	0.5% TritonX100, 20`RT	1:40	Monosan, 7024	mouse
VE-Cadherin	0.5% TritonX100, 20`RT	1:100	BD, C 26120	mouse
ZO-1	2% TritonX100, 20`RT	1:200	Zymed 61-7300	rabbit
Occludin	0.5% TritonX100, 20`RT	1:200		mouse
PECAM	0.5% TritonX100, 20`RT	1:50	Dako, M 0823	mouse

Table 13: macrophages markers for immunofluorescence

Antibody	Permeabilisation	Dilution	Company	animal
CD 14	0.5% TritonX100, 20`RT	1:100	SantaCruz,sc19588	mouse
CD 11a	0.5% TritonX100, 20`RT	1:200	BD, 610826	mouse

Table 14: antibodies for immunomagnetic cell separation

Antibody		Company
Dynabeads®CD31	Endothelial Cell	Dynal Biotech, 111.28

Table 15: secondary antibodies for immunofluorescence

Antibody		Dilution	Company	animal
Alexa 488	anti-mouse		Invitrogen, A11029	goat
Alexa 546	anti-mouse	1:1000	Invitrogen, A11030	goat
Alexa 488	anti-rabbit		Invitrogen, A21206	donkey
Alexa 546	anti-rabbit		Invitrogen, A11010	goat

2.1.7 Molecular biology

Table 16: siRNAs

Target	Product line	Locus ID	siRNA ID	company
Flotillin-1	*Silencer®Select siRNA*	10211	s19914	
Flotillin-2	*Silencer®Select siRNA*	2319	s5286	Applied Biosystems
Non targeted	Silencer® Negative Control #1 siRNA		AM4611	

Table 17: transfection reagences

GenCarrier™ 1		Epoch Biolabs, 31-00110
Organelle Lights		Molecular Probes
	Endosomes-GFP	O10104
	Lysosomes-RFP	O10100
	PM-GFP	O36214
	PM-RFP	O36214

Table 18: RNA-Isolation and Reverse Transcription

RNAlater™	Ambion, 7021
RNeasy Mini Kit	Qiagen, 74104
Qiashredder columns	Qiagen,79654
Omniscript Reverse Transcriptase-System	Qiagen, 205113
oligo-dT primer	Qiagen,SP230
RNase inhibitor	Promega,N 2111
Taq DNA polymerase-Kit	Qiagen,201203

Table 19: Primers for Real-time PCR

GenBank accession	**Sequence 5´-3´**	**Strand**	**Tm [°C]**	**Company**
Flotillin 1				
AF089750.2	GCCTGAATGATCCTCCTGTT	forward	59	Microsynth
	CCTTCAAGACAAGGCACAAA	reverse	58.9	
Flotillin 2				
NM_004475.2	CCTTATCTCGAAGGGACCAG	forward	58.7	Microsynth
	GGAGAGGAAGAGGAGGAGGT	reverse	58.8	
RPL13 large ribosomal protein (house keeping)				
NM_000977	CCTGGAGGAGAAGAGGAAAGAGA	foreward	59.5	Microsynth
	TCCGTAGCCTCATGAGCTGTT	reverse	57.4	

Table 20: Real.time PCR Master Mix

Power SYBR® Green PCR Master Mix	Applied Biosystems, 4367659

2.2 Methods

2.2.1 Cell culture and cell isolation

2.2.1.1 Cell culture

The human microvascular endothelial cell line, ISO-HAS-1 [80, 81], the human lung adenocarcinoma cell line, NCI H441 (purchased from ATCC, ATCC-HTB-174, Promochem, Wesel, Germany), as well as the human acute monocytic leukemia cell line, THP-1 [88], were kept in RPMI 1640 supplemented with 10% FCS (fetal calf serum), 1 % P/S (penicillin/streptomycin). ISO-HAS-1 and H441 were passaged every third day in a dilution of 1:3 until passage 50 and 35 respectively. The THP-1 cell line was kept in a dilution of 7.5 x 10^4 cells/ml to 1.2 x 10^6 cell/ml in the presence of 0.1 nM ß-mercaptoethanol.

2.2.1.2 Monocultures of ISO-HAS-1 and H441

Prior to seeding of cells, the 96-well plates (TPP, Switzerland) or 8-well µ-slides were coated with 50/300 µl fibronectin for 1h at 37°C (5µg/ml, Roche Diagnostics, Mannheim). The cells were seeded (ISO-HAS-1: 1.6 x 10^4 cells/well, H441: 3.2 x 10^4 cells/well) from a confluent culture flask on 96-well plates in RPMI 1640 medium (Gibco) with L-glutamine supplemented with 10% FCS and Pen/Strep (100 U/100 µg/ml) and cultivated at 37°C, 5% CO_2 for 24h to a confluent cell-layer prior to NP exposure.

2.2.1.3 The coculture model of the alveolar capillary barrier

The procedure of coculture was performed as described in [89] with some alterations. Briefly, HTS 24-Transwell® filters (polycarbonate, 0.4 µm pore size; Costar, Wiesbaden, Germany) were coated with rat tail collagen type-I (12.12 µg/cm^2, BD Biosciences, Heidelberg, Germany). ISO-HAS-1 cells (1.6 x 10^4/well ≙ 5 x 10^4/cm^2) were seeded on the lower surface of the inverted filter membrane. After 2h of adhesion at 37°C and 5% CO2, H441 (8.4 x 10^3/well ≙ 2 x 10^4/cm^2) were placed on the upper side of the membrane. The cells were cultured for about 10 days in RPMI 1640 medium with L-glutamine supplemented with 5% FCS, Pen/Strep (100 U/100 µg/ml). From day 4 of

cultivation the H441 were treated with dexamethasone (1µM). As a control, monocultures of H441 or ISO-HAS-1 were seeded on transwells and kept under the same culture conditions as described for the cocultures. From day 10 on, they show trans-bilayer electrical resistance (TER) values that average 560 ± 6 $\Omega * cm^2$.

Primary cocultures were prepared as described previously by Hermanns et al. [90]. Primary human pulmonary microvascular endothelial cells (HPMEC) from native human lung tissue (1.6 x 10^4/well ≙ 5 x 10^4/cm^2) were seeded on the lower surface of the inverted filter membrane. They were maintained in ECBM supplemented with 15% FCS, 1% P/S, 0.2% BFGF and 0.02% sodium-heparin. After 4h of adhesion at 37°C and 5% CO_2, primary human alveolar epithelial cells (AT II): (8 x 10^4/well ≙2.4 x 10^5/cm^2) were placed on the upper surface of the membrane. They were cultured in SAGM (small airway epithelialcell growth medium supplemented with 1% P/S, 1% FCS and SAGM™SingleQuots®). After a cultivation period of 10 days the coculture shows trans-bilayer electrical resistance (TER) values that average 800±209Ω * cm^2.

2.2.1.4 Isolation of primary human pulmonal microvascular endothelial cells (HPMEC) from native human lung tissue:

Lung tissue was obtained from the St. Hildegardis Hospital (KKM, Katholisches Klinikum, Mainz). At first peripheral lung tissue was removed from the subpleural lung parenchyma. After removal and before further preparation the tissue was kept in special tissue buffer (M-199 Medium, 15% FCS, 1.2% Fungizone, 1.2% P/S, 1.2% Ciprobay 200, 0.4%). The pleura visceralis was thoroughly removed to avoid contamination with mesothelial cells. The residual parenchyma was cut into small pieces with scissors and checked for vasculature which was separated from the tissue pieces and discarded to avoid contamination with macrovascular endothelial cells. Subsequently the pieces were further thoroughly cut into small pieces, washed with cold Hepes-BSA 0.2% and put through a 40 µm nylon filter to remove debris and erythrocytes. The tissue was treated with Dispase (10 ml Dispase (2.36 U/ml) per 2 g tissue diluted with 10 ml tissue buffer) for at least 18 h on a rollmixer at 4°C. After the 18h enzymatic treatment the tissue was rinsed with 10 ml Hepes-BSA through a

100 µm nylon filter.The filtrate containing alveolar macrophages was discarded. Afterwards the tissue was treated with elastase (1 ml elastase (30U/ml), 0.9 ml trypsin/EDTA, 1.1 ml Hepes-BSA 0.2% per gram lung tissue) in a water-bath for 30 minutes at 37°C. The enzymatic digestion was then stopped by adding the tissue suspension to 5 ml FCS through a 100 µm nylon filter and the tissue was resuspended with a 10 ml pipette. Before centrifugation for 10 min at 1000 rpm the suspension was put again through a 40 µm nylon filter. After centrifugation, the supernatant was discarded and the cell pellets were resuspended in 5 ml PC complete (ECBM with 5% supplement-mix, 1% P/S) and placed on a gelatin (coating: 2 ml 0.2% gelatin in PBS, 30 minutes at 37°C) -coated T25 flask. After culturing for 4h at 37°C and 5% CO_2, the microvascular endothelial cells (HPMEC) attached to the surface of the flask. The supernatant, still containing the alveolar epithelial cells, is removed for further processing as described in 2.2.1.5 and the HPMEC remain in the flask with 5 ml complete PC.

Purification of freshly isolated HPMEC: PECAM-separation

After approx. one week of proliferation, cells underwent a PECAM-separation using Dynabeads®CD31 as described as follows:

- Wash 1.5 – 3 µl T25 in 10 ml PBSA 0.1% in a 15 ml tube
    - Put the tube to the magnet (MPC-1, DYNAL)
    - Wait 1 minute until beads attract to the magnet and withdraw the solution carefully
    - Reconstitute the beads with 5 ml PC complete
- Wash HPMEC with 5 ml PBS
- Apply the beads to the T25 on the cells
    - Incubate ca. 5 min until antibodies are bound to the cells (visual control)
- Wash with 5 ml PBS
- Add 1 ml Trypsin/EDTA and detach the cells (visual control)
- Stop enzymatic reaction with 5 ml cold PBS/5% FCS
- Apply detached cells in a 15 ml tube at the magnet and wait 1 minute
- Withdraw the solution and resuspend cells with 10 ml PBSA 0.1%

- Incubate on a roll mixer for 10 minutes at 4°C
    - Repeat washing step twice
- Resuspend cells in 5 ml warm PC complete and put the cells on a Gelatine (0.2 %) coated T25

After reaching confluence (approx. one week) repeat PECAM-separation with 10-15 µl Dynabeads.

2.2.1.5 Isolation of human alveolar epithelial cells (AT II):

Subsequently, the supernatant was centrifuged for 10 minutes at 300*g*. In the meantime the percoll-gradient was prepared as follows:

- Pipett Percoll-High and Percol-Low as decribed inTable 21:
  mix thoroughly, avoid bubbles, pipette FCS at the end

Table 21: Percoll-gradient

Percoll-High (10 ml)	**Percoll-Low (10 ml)**
1ml 10x PBS	1ml 10x PBS
6.49 ml Percoll	2.72 ml Percoll
2.5 ml Aqua ad injectable	6.28 ml Aqua ad injectable
50 µl FCS	50 µl FCS

- Take Percoll-High and overlay carefully with 10 ml Percoll-Low
- After centrifugation, withdraw the medium to a rest of 5 ml and resuspend the pellet thoroughly
- Add the resuspension carefully on top of the gradient and centrifuge for 20 min at 250*g* and 10°C (switch off deceleration)
- After centrifugation, withdraw the interphase which contains 80-90% pure AT II and add it to 35 ml cold Hepes-BSA 0.2% and centrifuge again for 10 min at 300*g.*
- Reconstitute the AT II in SAGM (small airway epithelial cell growth medium supplemented with 1% P/S, 1% FCS and SAGM™SingleQuots®) and count cells in a Neubauer counting chamber.

2.2.2 Nanoparticle characterization

NexSil20 and Ludox TM-40 are commercial available colloidal amorphous silica nanoparticles in aquous dispersion with a diameter of about 30 nm (NexSil20: NYACOL®, Nano Technologies, Inc., Ludox TM-40: Sigma, Taufkirchen, 420786).

AmorSil: AmorSil nanoparticles were synthezised and delivered by Stefanie Utech (Department of Physical Chemistry of the Johannes Gutenberg Universitiy of Mainz,). It is a core-shell nanoparticle with a magnetic ironoxide core that averages 3.2 nm in radius wich is incorporated into a polyorganosiloxane network composed of trimethoxymethylsilane, diethoxydimethylsilane and the functional monomer (chloromethylphenyl)-trimethoxysilane. The magnetic nanocapsules have a particle radius below 60nm. Detailed information on synthesis and characterisation of AmorSil can be found in Utech et. al. [91, 92].

Sicastar Red: Sicastar Red is an amorphous silica nanoparticle (30, 70 and 300 nm in size) in aquous dispersion which contains rhodamin B covalently incorporated in the entire SiO_2-matrix. The manufacturing technique is decribed by micromod Partikeltechnologie GmbH [93].

Poly(ethyleneimine)-nanoparticles (PEI): Polyethyleneimine-nanoparticles were delivered by Peter Dubruel (Polymer Chemistry & Biomaterials Research Group, Ghent University). Branched PEI (polyetheleneimine, MW: 25 000 g/mol) was purchased from Aldrich (Bornem, Belgium) and OG488-X succinimidyl ester (OG) was obtained from Molecular Probes (Leiden, The Netherlands) and was used as received from Peter Dubruel. Characterisation of PEI-OG is described previously by Peter Dubruel [94].

The characterization of nanoparticles was conducted by the providers of the nanomaterial: Silica-based nanoparticles (NexSil20 and AmorSil) were obtained from the department of Physical Chemistry of the Johannes Gutenberg Universitiy of Mainz (Michael Maskos, Christoph Bantz).

Christoph Bantz carried out the experiments concerning characterization of nanoparticle solutions and the following interpretations and draftings as already described in Kasper et. al. [95]: The nanoparticles were characterised with

respect to shape, size and size distribution in the dry state, as well as in solution. Transmission Electron Microscopy (TEM) imaging was performed using a Philips EM420, operating at 120 kV, on carbon coated copper grids. The apparent hydrodynamic diameter $\langle D_h \rangle_z$ was determined by dynamic light scattering (DLS), both in a ready-to-use instrument (Malvern Zetasizer Nano ZS, single angle measurements at 173°, He-Ne-Laser with λ = 633 nm) and a fully equipped setup with a Coherent Verdi V2 diode-pumped solid-state laser (λ = 532 nm), an ALV-SP125 goniometer with single photon detector SO-SIPD and an ALV-5000 Multiple-Tau digital correlator. Angle-dependent measurements were carried out between 30° and 150° and the data were evaluated by exponential fitting and q = 0 extrapolation; μ2 values as an estimate for the polydispersity of the sample were determined at 90° (assuming a Gaussian distribution, a μ2 value of <0,04 approximately corresponds to a standard deviation of <28%). In addition to the DLS measurements, the zeta potential of the particles was measured with the Zetasizer (measuring angle for the zeta potential: 17°) to study the aggregation behaviour of the nanoparticle dispersions.

2.2.3 Nanoparticle effects on cells

2.2.3.1 Exposure to nanoparticles

To avoid nanoparticle aggregation predilutions of the NP dispersions were made in pure water (Braun ad injectabilia, Braun Melsungen AG, Melsungen) or serum-free Medium (PEI). Due to nanoparticle aggregation in serum-containing medium, serum-free medium was used for cell exposure. All dilutions were applied 1:10 in serum-free medium to the cells (10µl NP dispersion + 90 µl serum-free medium). Since both culture systems used (mono- and coculture) have the same culture area/well, the volume of the applied NP dispersion was adjusted to 100 µl in both systems. After an exposure time of 4h the cells were either evaluated or washed twice with serum-free medium and cultured for a further 20h period under normal culture conditions (medium with respective supplements). After 4h and 20h recovery the effect on cell viability was studied by various assays. For the coculture, NPs were exclusively applied to the apical

side of the H441 layer on top of the 24 well transwells. In the case of aSNPs, a concentration of 6000 µg/ml might not mimic realistic inhalative exposure conditions as they might occur, for example, in the case of a ceramic worker. Nevertheless, this high concentration of aSNPs was included as a positive control with a significant cytotoxic effect observed in our mono- and cocultures.

2.2.3.2 Endotoxin contamination of nanoparticle dispersions

Prior to all experiments the particles were checked for endotoxin contamination by E-selectin induction on endothelial cells via ELISA (Duoset ELISA Kit (R&D Systems®, Wiesbaden, Germany) and immunofluorescence. For the ELISA-assay cells were seeded on 96-well plates and exposed to aSNPs as described above. From the supernatant, that was taken after 24h soluble E-selectin was measured. As positive control cells were incubated with TNF-α (300 U/ml $\cong$ 0.732 g/ml) or lipopolysaccharide from E.coli (LPS, 1µg/ml, Sigma). For the immunocytochemical E-selectin staining cells were seeded (ISO-HAS-1: 8 x 10^4 cells/well) on Lab-Tek™ chamberslides (Nunc, Wiesbaden, Germany) and exposed to aSNPs for 4h as described above. Subsequently, they were fixed with paraformaldehyde (3.7%) in CS buffer (PIPES 0.1M, EGTA 1mM, 4% polyethylene glycol 800, NaOH 0.1M) for 20 min at room temperature, and washed three times. Cell membranes were then permeabilized with 0.2% Triton X-100 in PBS for 10 minutes. After washing three times in PBS cells were stained with primary antibodies (in PBS + 1% BSA for 1h at room temperature) obtained from Monosan (CellSystems, St. Katharinen, Germany). The secondary antibody (Alexa fluor 488-conjugated, anti-mouse) was added for 1h after washing three times in PBS. Terminal cells were counterstained with Hoechst 33342 (Sigma) and mounted with Fluoromount-G™ (SouthernBiotech). Visual examination was conducted by means of a fluorescent microscope (personalDV, Applied Precision, Issaquah, USA).

2.2.3.3 Viability after NP exposure on conventional monocultures (MTS)

On the cell layer CellTiter 96® AQueous One Solution Cell Proliferation Assay (MTS) was used to study cytotoxicity of NPs. This assay is a colorimetric method which determines the number of viable cells. It contains a novel tetrazolium compound [3-(4,5-dimethylthiazol-2-yl)-5-(3-carboxymethoxy-phenyl)-2-(4-sulfophenyl)-2H-tetrazolium, inner salt; MTS] and an electron coupling reagent (phenazine ethosulfate; PES). The cells reduce the tetrazolium compound (Owen's reagent) to a colored formazan product that is soluble in tissue culture medium. Dehydrogenase enzymes in metabolically active cells produce NADPH or NADH which is responsible for the conversion [96].

The MTS-assay was conducted as follows:

- Remove supernatant after incubation of NPs and wash twice
- Add the MTS-reagent to the cells in a ratio of 1:10 with medium with supplements as described for standard culture conditions and incubate 45-60 minutes at 37°C and 5% CO_2.
- After incubation pipette the substrate-solution into a new 96-well plate and measure adsorption at 492 nm

At aSNP concentrations of 600µg/ml or higher, interference with the MTS reagent occurred. To avoid false positive results due to particle-dye interactions supernatant (in total 100µl) was removed after aSNP exposure. Thereafter, the cells were washed with PBS and incubated with fresh medium containing MTS reagent (dilution 1:10) for 1h before absorbance measurements at 492 nm.

2.2.3.4 Membrane integrity measured by lactate-dehydrogenase (LDH) release upon NP treatment

50µl of the collected supernatant was used in the LDH CytoTox 96® Non-Radioactive Cytotoxicity Assay (Promega, Mannheim, Germany) to determine lactate dehydrogenase (LDH) release following membrane disruption. This enzyme is present in the cytosol and catalyses the lactate-to-pyruvate reaction. Disruption of plasma membrane integrity leads to a release of LDH into the supernatant, resulting in the conversion of the tetrazolium salt into a red formazan product (absorbance at 490 nm).The experimental procedure is described as follows:

- Dilute the substrate with 12 ml assay-buffer as described in the manufacturers protocol
- Take 25 µl of the supernatant of NP-exposed cells
- Add 25 µl of the freshly prepared substrate-solution
- Incubate 30 min (dark, RT)
- Stop the reaction with 25 µl stop-solution
- measure the OD at 492 nm

As positive control lysis buffer 15 of the Proteome Profiler™ Array, Human Apoptosis Array Kit (R&D, ARY009) was used 1:10 diluted in the respective cell culture medium simultaneously to NP incubation. Additionally, a volume control (lysis-buffer in cell culture medium without cells), a medium control (cell culture medium without cells) as well as NP controls (nanoparticle dilutions in cell culture medium without cells) were performed in parallel.

Equation 1: formula to calculate percentage LDH release

$$LHD\ release\ [\%] = \frac{exposed\ cells - medium\ control}{lysis\ control - volume\ control} \times 100$$

As a result of particle-dye interactions concentrations of 6000 µg/ml aSNP showed false positive results in the LDH assay for the coculture after 4h exposure (i.e. Ludox TM-40: 10±1.6%, NexSil20: 10±0.66% of the lysis control). Therefore, the percentage due to aSNP interference with the dye has been subtracted from the measurements.

2.2.3.5 Determination of the number of viable cells by cristal violet staining

A second quantification method for determination of the number of viable cells is cell staining with crystal violet [97]. Crystal violet (*N*-hexamethylpararosaniline) is a monochromatic dye which stains cell nuclei. After fixation of NP-exposed cells they were incubated with 50 µl/96er-well of a 0.1% crystal violet in $Aqua_{dest}$ solution for 20 minutes (RT, 70 rpm). Subsequently, the excessive dye was thoroughly washed away with tap water and dried over night at room temperature. Then, cell-bound dye crystals were

released with 100 µl 33% acetic acid for 10-15 minutes (RT, 70 rpm) and transferred to a new 96-well plate to measure the adsorbance at 600 nm.

2.2.3.6 Effect of NPs on apoptosis markers

The Caspase-Glo® 3/7 Assay: This test is used as a pre-test on monocultures to evaluate the sufficient aSNP concentration for further experiments on the coculture. The Caspase-Glo® 3/7 Assay measures the activity of Caspase 3 and 7 via an enzymatic reaction involving their substrate, DEVD, and luciferase, which generates a luminogenic signal. After incubation of cells with aSNPs in 100 µl on a 96-well plate an equal volume of the Caspase-Glo® 3/7 was added and incubated for 1h at room temperature. Cells were lysed and active Caspase 3 and 7 generate the luminogenic signal by cleaving the DEVD/luciferase complex which was measured by means of a plate reader (TECAN).

Proteome Profiler™ Array: To detect the production of 35 apoptosis-related proteins upon aSNP exposure the Human Apoptosis Array Kit (Proteome Profiler™ Array, ARY009 from R&D Systems®, Wiesbaden, Germany) was used. After 10 min, 1 hour and 4 hour exposure to 600 µg/ml NexSil20 the transwell filters were cut, transferred to the lysis buffer for 30min at 4°C and mixed at 60 rpm using the Intelli-Mixer (NeoLab, Heidelberg, Germany). Four filters with the same exposure conditions were mixed and for the array two similar experiments were pooled. Thus, eight identically treated cocultures were analyzed. After lysis, protein content was quantified using the BCA-Kit (Pierce, Schwerte, Germany). The absorption at 550nm was measured in a plate reader (TECAN). In the Human Apoptosis Array Kit 200 µg protein was used per sample. Further procedures were performed according to the manufacturer´s protocol. The resulting spots were visualized via chemoluminescence, detected by means of the Chemi-Smart 5100 (peqlab, Erlangen, Germany). A detailed evaluation of chemoluminescence intensity was conducted using the software Array-Pro Analyzer Version 4.5 from Media Cybernetics (Bethesda, USA).

2.2.3.7 Transbilayer Electrical Resistance Measurements

To evaluate the functional efficiency of an intact barrier of the coculture model of the alveolar-capillary barrier the transepithelial electrical resistance (TER) was measured with an EVOM voltohmmeter (World Precision Instruments, Berlin, Germany) equipped with a STX-2 chopstick electrode. HTS 24-Transwell® filter membranes without cells coated with rat tail collagen type-I were measured and set as blank (approximately 110 Ω). Barrier resistance readings (Ω) were obtained for each well individually and, after subtracting the resistance of the blank filter membrane, were multiplied by the membrane area (0.33 cm^2) to give Ωcm^2. In the experiments showing, for example, a time-dependent effect of aSNP exposure the TER is expressed as % of t0 (TER value before aSNP exposure).

2.2.4 Cell staining

2.2.4.1 Immunofluorescence (IF)

IF was performed to label respective cell proteins of interest such as cell-cell contacts (Table 12), endosomal markers (Table 11) or markers for alveolar macrophages (Table 13). After the experimental procedure cells were fixed either with methanol/ethanol (endosomal markers) in a ratio of 2:1 for 15 min at room temperature or with paraformaldehyde (3.7%) in CS buffer (PIPES 0.1M, EGTA 1mM, 4% polyethylene glycol 800, NaOH 0.1M) for 20 min at room temperature (cell-cell contacts or alveolar macrophage markers). PFA fixed cells require a permeabilisation with 0.5%-2%Triton X-100 in PBS for 10 minutes and washed three times with PBS. After fixation cells underwent the following staining procedure:

- Incubation with primary antibody for 1h (RT) or overnight (4°C)
    - Wash 3 x with PBS

Incubation with secondary antibody listed in Table 15 (1h, RT)

- Wash 3 x with PBS

- Nuclear staining with Hoechst 43222 (1:10000 in PBS), 5 minutes, RT
    - Wash 3 x with PBS

- Mounting with Fluoromount-G™ (Transwell-plates) or Mounting medium (IMM) for µ-slides

2.2.4.2 Organelle Lights

H441, ISO-HAS-1 were seeded on 8-well µ-slides reaching ca. 70-80% confluence after 24h. Subsequently, the transfection procedure using Organelle Lights Lysosomes-RFP (Cat.: 010100, Molecular Probes) was conducted as follows:

- 0.5 ml Component A + 0.875 ml PBS →250 µl/well
- incubate 2h at RT and 70 rpm
- 0.5 ml Medium + 0.5 µl Enhancer (Component B) → 250 µl/well
- Incubate 2h at 37°C and 5% CO_2
- Medium change with RPMI with 10% FCS, 1%P/S and 16 h further cultivation

2.2.4.3 Staining for F-actin

Staining for actin stress fibres was conducted by means of Alexa Fluor® 594 phalloidin (A12381, Invitrogen) according to the manufacture´s protocol. After fixation of the cells using PFA (3.7% in CS-Buffer) for 20 min, RT, cells were stained for 1h with phalloidin diluted 1:80 in 1% PBSA.

2.3 Co-localisation experiments of internalized NPs with endosomal markers

NCI H441, ISO-HAS-1 and PMA-stimulated THP-1 were incubated with nanoparticles such as Sicastar Red 30nm (6 µg/ml), AmorSil20 (300 µg/ml) and PEI (2.5 µg/ml) to reveal possible endocytosis mechanisms which may be involved in cellular uptake. The incubation times chosen were 20 minutes, 4h and 4h with subsequent 20 h recovery with fresh FCS-containing medium. After the individual incubation period the cells were fixed with Methanol/Ethanol in a ratio of 2:1 for 15 minutes (RT, dark). Then, the cells were washed three times with PBS and underwent the immunofluorescence staining procedure. (volume: 200 µl/well for ibidi coverslips, 50 µl/well for transwell-plates).

2.3.1 Comparison of inflammatory responses between conventional monocultures cocultures

50 µl of the supernatant taken after 4h NP exposure was analysed for soluble intercellular adhesion molecule-1 (sICAM-1) and inflammatory cytokine release (IL-6, IL-8) using Duoset ELISA Kits (R&D Systems®, Wiesbaden, Germany). Additionally, after removal of the unbound NPs, cells were cultured for further 20h in RPMI with 10% fetal calf serum and further tested for sICAM-1 and cytokine release. A list of consumables and a work flow of the ELISA procedure is depicted in Table 22.

Table 22: ELISA Kits for cytokine release

Cytokines		**company**
sICAM		DuoSet R&D,DY720
IL-6		DuoSet R&D,DY206
IL-8		DuoSet R&D,DY208
IL-10		DuoSet R&D,DY217B
IL-12		DuoSet R&D,DY1270
E-Selectin		DuoSet R&D,DY724
Material		NUNC Maxisorp 96 well plates
Chemicals	**PBSA 1%**	1.5 g BSA, Fraction V 7.5 g Sucrose 0.075 g NaN3 ad 150 ml with PBS
	TRISA 0.1%	1.211 g Trisma Base 4.38 g NaCl 0.5 g BSA, Fraktion V ad 500ml with Aqua ad injectabile, pH= 7,2-7,4 + 250 µl Tween 20
Streptavidin-HRP	**1:200**	R&D, 890803
Substrate solution		R&D, DY999
	Color Reagence A	H_2O_2
	Color Reagance B	3,5,3´,5´-tetramethylbenzidine (TMB) mix A and B (1:1) prior to use
Stop solution	**2 N = 1 M H_2SO_4**	1.5 ml 97% H_2SO_4 + 25.8 ml Aqua ad injectabile

Work flow for the DuoSet ELISA:

1. **Coating with capture antibody, 2 µg/ml in PBS: O.N., RT, 50 rpm**

   100/well (NUNC Maxisorp 96-well plate)

   - wash 3x with PBS + 0.025 % Tween 20, 400 µl

2. **Blocking with PBSA 1%: 2h, RT, 50 rpm**

   300 µl/well

   - wash 3x with PBS + 0.025 % Tween 20, 400 µl

3. **Application of the samples (supernatant): 2h, RT, 50 rpm**

   100 µl/well

Table 23: dilution of the samples (supernatants)for DuoSet ELISA

Cytokine	diluents	dilution
sICAM	PBSA 1%	1:25 monocultures 1:25 coculture, apical 1:3 coculture, basolateral
IL-6	PBSA 1%	1:10 monocultures 1:10 coculture, apical 1:3 coculture, basolateral
IL-8	TRISA 0.1%	1:10 monocultures 1:10 coculture, apical 1:3 coculture, basolateral
IL-10	PBSA 1%	1:10 coculture, apical 1:3 coculture, basolateral
IL-12	PBSA 1%	1:10 coculture, apical 1:3 coculture, basolateral

   - wash 3x with PBS + 0.025 % Tween 20, 400 µl

4. **Detection antibody, 200 ng/ml: 2h, RT, 50 rpm**

   100 µl/well

   - wash 3x with PBS + 0.025 % Tween 20, 400 µl

5. **Streptavidine-HRP, 200 ng/ml: 20 min, RT, 50 rpm**

   100 µl/well

- wash 3x with PBS + 0.025 % Tween 20, 400 µl

6. Substrate solution **20 min, RT, 50 rpm**

100 µl/well

7. Stop solution

Add 50 µl Stop solution and measure OD at 450 nm

2.3.2 Quantification of internalised nanoparticles

To compare uptake behaviour and to quantify NP uptake of H441, cells were kept in conventional monoculture and under coculture conditions. Thus, cells were incubated with fluorescence labelled NPs (Sicastar Red: 6 µg/ml, AmorSil: 300 µg/ml and PEI: 2.5 µg/ml) and observed with a fluorescence microscope (DeltaVision, Applied Precision). To allow comparisons the exposure time and intensity scale was adjusted equally for each sample. Subsequently, mean fluorescence intensity was measured via Fiji ((http://pacific.mpi-cbg.de).

To evaluate putative transcytosis events H441 in coculture with ISO-HAS-1) were incubated with Sicastar Red (60 µg/ml), AmorSil (300 µg/ml) and PEI (2.5 µg/ml) for 48h. Subsequently, ISO-HAS-1 were checked for internalized NPs via visual judgments of pictures made with a fluorescence microscope (DeltaVision, Applied Precision). Due to a high autofluorescence of the polycarbonate filter a quantification of fluorescence signal by measuring the intensity via Fiji was not suitable.

2.3.3 Cytotoxicity and membrane integrity after aSNP exposure on flotillin-1 and-2 depleted cells

Preparation of the siRNA for a 6/96 well plate:

- siRNAwas diluted in 100 µl serum-free Medium (concentration in the well with 2 ml: 50 nM)
- diluted siRNA was mixed with 100 µl Gencarrier-1 (GC) solution (GC: 4 µl Gencarrier-1 in 100 µl serumfree Medium)
- Incubation for 30 min at RT

Transfection of H441 with siRNA in a 6 (96) well plate:

In parallel to the seeding of cells on tissue culture plastic (TPP) the cells were transfected with siRNA:

1. The cells were washed with PBS, trypsinized with Trypsin/EDTA and resuspended in 10 ml fresh Medium.
2. 5 x 10^5 (3 x 10^4) cells were seeded in 800 µl (40 µl) of low-serum Medium (RPMI with 1% FCS) into a well and siRNA-tranfection mixture has been applied to the cells dropwise (volume: 1ml (50µl)) and mixed thoroughly
3. After 7h of incubation at 37°C and 5% CO_2, 1ml (50µl) of high-serum medium (20% FCS) was added and the cellculture has been continued for further 17h.
4. After 24 h the transfection medium was replaced by normal culture medium and the cells were cultured for further 48-72h to achieve the highest siRNA-inhibition efficiency. Inhibition efficiency of the siRNA was checked via real-time PCR.

Work flow of the RNA Isolation (RNeasy Micro Kit):

1. put 5 x 10^5 trypsinized cells in an Eppendorf tube and centrifuge, resuspend the pellet in 350 µl RLT (10ml RLT + 100 µl ß-Mercaptoethanol)
2. vortex the cells to homogenize the lysate
3. Put samples in a Qiashredder and centrifuge for 3 minutes at 12000 rpm, discard Qiashredder
4. Put 350 µl in the collection tube with the sample and pipette the sample into a RNeasy MinElute spin column and centrifuge for 15sec at 12000 rpm, discard flow though
5. Put 350 µl RW1-Buffer onto the columns, centrifuge for 15sec at 12000 rpm, discard flow through
6. Add 80 µl DNase onto the filter and incubate 15 minutes at room temperature,
7. Add 350 µl RW1 to the columns and centrifuge 15s at 12000 rpm, discard flow through
8. Put the columns in a new 2 ml tube, add 500 µl RPE-Buffer and centrifuge 15sec at 12000 rpm, buffer must not touch the columns!)
9. Put columns in a new 1.5 ml tube and wash the filter 2x with 50 µl RNase-free water, centrifuge 1 min at 12000 rpm

Work flow of the Reverse Transcription (Omniscript):

1. thaw RNA (50 ng-2µg), primer, 10x Buffer, dNTP Mix, RNase-free water and the reverse transcriptase on ice
2. dilute RNase inhibitor (40units/µl) with 1x Buffer (10x Buffer 1:10 with RNase-free water) to 10 units/µl), vortex and centrifuge
3. prepare mastermix as decribed in Table 24
4. add template RNA, vortex and centrifuge
5. incubate for 60 min at 37°C → ready for Real-Time PCR

Table 24: Mastermix of the Reverse Transcription

Master mix	Volume/reaction	Final concentration
RNase-free water	xx	
10x Buffer RT	2 µl	1x
RNase inhibitor (10units/µl)	1 µl	10 units (per 20 µl reaction)
dNTP Mix (5 mM eachdNTP)	2 µl	0.5 mM each dNTP
Oligo-dT primer (10 µM)†	2 µl	1 µM
Reverse Transcriptase	1 µl	4 units (per 20 µl reaction)
Template RNA	xx	Up to 2 µg (per 20 µl reaction)

Real-time PCR:

Following items were thawn on ice, mastermix (21 µl) was aliquoted on a MicroAmp™ Optical 96-well reaction plate (AB, Applied Biosystems, #N801-0560) and 4 µl cDNA was added.

Table 25: Mastermix of Real-time PCR

Water	8 µl
SybrGreen	12.5 µl
Primer forward	0.25 µl
Primer reverse	0.25 µl
cDNA	4 µl
	25 µl

2.3.4 Triple coculture model of the alveolar-capillary barrier

The previously described coculture model (NCI H441/ISO-HAS-1) of the alveolar-capillary barrier [79] was completed by the addition of alveolar macrophages. Therefore, THP-1, a human myeloid leukaemia cell line [88] was apically added to the H441 cells. First, the THP-1 were stimulated for 4 days with 8 nM Phorbol 12-myristate 13-acetate (PMA, Sigma) to induce differentiation of the monocytic cells to cells exhibiting macrophage features [98, 99]. Then, THP-1 were washed with PBS, trypsinized with Trypsin/EDTA for several minutes (visual control) and added to the coculture when the epithelial and endothelial cells have reached a polarized state (day 8) with a tight barrier. Several endpoints described below were checked to characterise the behaviour of the coculture upon addition of the macrophage-like THP-1: **1.** transbilayer electrical resistance (TER: see section 2.2.3.7) measurements have been performed to study the behaviour of the barrier functionality of the coculture model **2.** Furthermore, immunocytochemical staining (IF see section 2.2.4) of macrophage-like markers such as CD14 and CD11a (see Table 13) was conducted to detect macrophage-like THP-1 which were attached to the epithelial monolayer of the H441 in coculture with ISO-HAS-1.

2.3.5 Statistical analysis

From several independent measurements, means and standard deviations were calculated. Analyses are shown as mean ± S.D. from at least three separate experiments. Testing for significant differences between means was carried out using one-way ANOVA and Dunnett`s Multiple Comparison test at a probability of error of 5% (*), 1% (**) and 0.1% (***) or two-way ANOVA with Bonferronie´s post test using GraphPad Prism (Version 5.00 for Windows, GraphPad Software, San Diego California USA, www.graphpad.com).

3 Results

3.1 Nanoparticle characterisation

NexSil20 and Ludox TM-40: Experimental data, tables and draftings in this section were courtesy of Christoph Bantz (Institute of Physical Chemistry, Johannes Gutenberg University, Mainz) and described in Kasper et. al [95]: Prior to the experiments the stability of the nanoparticle dispersions in Milli-Q water, phosphate-buffered saline (PBS, 150 mM salt in total) and the cell culture medium RPMI 1640 (Table 26) was examined.

The size of the nanoparticles in the dry state (DTEM) was nearly the same as in solution, indicating that the effect of particle shrinkage during the preparation of the samples for TEM is minimal (See additional files, Figure 1 in Kasper et. al. [95]). In all media the hydrodynamic diameter of the particles remained at a value of about 33 nm (for both particle types) and the formation of aggregates was not observed in any case. No marked change in particle size was observed on measuring 20 min, 140 min, 260 min and 24 h after preparation. Even at different temperatures (20° and 37°C) only minor differences were determined. Applying the Ludox TM-40 sample to the cell culture medium, there was a doubling of the polydispersity after 24 hours at nearly constant size, pointing to a slightly increased tendency of the particles to aggregate. Within the given limitations of a ready-to-use instrument like the Zetasizer and for the investigated system, the results using the different DLS equipment were identical. Thus, the values of the Zetasizer (second column) could be confirmed by the more precise measurements.

With increasing concentration of salt and organic additives, the zeta potential of the particles became less negative – in contrast to the fact that the size remained stable. Even if the ionic strength was not yet high enough to affect the stabilisation through surface charges, this additionally indicates at least an increased tendency to form aggregates.

Table 26: characterisation of silica based nanoparticles. The measurements were performed 20 minutes after preparation of the samples at concentrations of 600 µg/mL (corresponding particle concentration: $4.4 \cdot 10^{13}$ particles per mL dispersion) and a temperature of 20°C. The first values from the light scattering measurements were determined with the fully equipped DLS setup, the second ones with the Zetasizer- The corresponding µ2 values diverge because of the different measuring angles

Diluent	**aSNP (10% + 90% diluent)**	
	Amorphous Silica	
	NexSil20	**Ludox TM-40**
$\langle D_{TEM} \rangle$ / nm	31.4 ± 3.8	31.2 ± 4.0
Milli-Q water:		
ζ / mV	-51.0	-57.3
$\langle D_h \rangle_z$ / nm	32.8 | 35.1	32.0 | 37.9
μ_2	0.12 | 0.04	0.06 | 0.03
PBS:		
ζ / mV	-18.2	-20.0
$\langle D_h \rangle_z$ / nm	36.8 | 37.2	34.2 | 32.6
μ_2	0.08 |0.17	0.04 | 0.01
Medium RPMI1640:		
ζ / mV	-19.8	-26.6
$\langle D_h \rangle_z$ / nm	35.4 | 33.4	32.2 | 32.6
μ_2	0.07 | 0.03	0.02 | 0.01

Fluorescence-labelled, silica-based nanoparticles: Sicastar Red with a size of 30 nm showed in solution of H_2O a hydrodynamic radius of 12.6 nm (diameter: 25.2 nm). In salt-containing buffer solution such as PBS and cell culture medium RPMI however, the 30 nm Sicastar Red dispersion got destabilized and the particles partly agglomerated; In PBS the hydrodynamic radii average around 66.2 nm and in RPMI 58.1 nm. The polydispersity index (µ2), which represents the width of the particle size distribution, was also increased. This leads to the conclusion, that there is still non-agglomerated material in the dispersion. Sicastar Red with a size of 70 nm and 300 nm show in all aquous solutions similar radii without the tendence to aggregate. According to the dynamic light scattering measurements, AmorSil with averaged radii of about 48.1 nm in RPMI medium appeared to be stable in all aquous solutions.

Table 27: characterisation of fluorescence-labelled, silica-based nanoparticles: Hydrodynamic radii (Rh / nm, with µ2 values as an estimate for the polydispersity) in different aquous dispersions (H_2O, phosphate buffered saline (PBS) and serumfree cell culture medium RPMI) obtained via dynamic light scattering

	H_2O		PBS		RPMI	
	R_h / nm	µ2(90°)	R_h / nm	µ2(90°)	R_h / nm	µ2(90°)
Sicastar Red 30 nm	12.6	0.10	66.2	0.16	58.1	0.17
Sicastar Red 70 nm	33.2	0.059	34.1	0.032	31.6	0.034
Sicastar Red 300 nm	157	0.016	151	0.012	151	0.013
AmorSil	52.9	0.17	47.9	0.09	48.1	0.11

Poly(ethyleneimine) (PEI): Branched polyethyleneimine-nanoparticles (PEI, MW: 25 000 g/mol) were delivered by Peter Dubruel (Polymer Chemistry & Biomaterials Research Group, Ghent University. Characterisation of green fluorescent PEI-OG (Oregon green, OG488-X succinimidylester) is described previously by Peter Dubruel [94]. PEI has a molecular weight of only 25 000 g/mol, thus the PEI particles have a size of only a few nanometer [100], which is too small to be detected via DLS.

3.2 Endotoxin remnants in NP dispersions

Prior to all following experiments aSNPs used in this study were checked for endotoxin contamination via ELISA and immunofluorescence for E-selectin induction on endothelial cells. None of the used particles induced an E-selectin signal in endothelial cells after 4 and 24 h exposure, whereas the TNF-α and LPS controls were positive (data not shown).

The induction of E-Selectin in endothelial cells is a highly sensitive method, similar to the classical Limulus amebocyte lysate test with a sensitivity of less than 3 pg/ml LPS. This means that there is no detectable endotoxin contamination in the used NPs samples which might interfere with all subsequent tests.

3.3 Effect of nanoparticles on cells of the alveolar-capillary barrier

3.3.1 Viability of cells in different culture systems after aSNP exposure

Organosiloxane nanoparticles (AmorSil) and polyethyleneimine (PEI) did not show significant cytotoxic effects (MTS and LDH) after 4h and 4h with 20h recovery (MTS after 4h for Amorsil (600 µg/ml): 102±18% compared to untreated control and PEI (2.5 µg/ml): 95±14%). However, aSNPs caused a significant cytotoxic effect and inflammatory response on lung epithelial and endothelial cells. Thus studies have been concentrated on NexSil20 and Ludox TM-40 (aSNPs) for the comparison of the different culture systems. Both particles NexSil20 and Ludox TM-40 at a concentration of 600 µg/ml (180µg/cm^2 cell layer) resulted in a cell viability of about 80% of the untreated control cells (Ludox TM-40: 85±8.4% and NexSil20: 80±7.9%) for the H441 cell line and about 40% (Ludox TM-40: 41±6.5% and NexSil20: 37±6%) for ISO-HAS-1 (Figure 9, A) in the conventional monoculture after 4h incubation. 300 µg/ml aSNP showed no significant effect on the viability of H441 (Ludox TM-40: 97±8.4% and NexSil20: 95±7%), whereas for the ISO-HAS-1 cells a reduced viability (Ludox TM-40: 32±1.3% and NexSil20: 40±3.5%) was still measurable. Thus, the endothelial cell line seems to be more sensitive to aSNP exposure than the epithelial cell line. After removal of the unattached aSNPs cell viability further decreased in a concentration-dependent fashion for both cell lines (see Figure 9 A: 4h exposure, 20 h recovery). A concentration of 60 µg/ml aSNPs or less did not show any effect on MTS conversion.

3.3.2 Membrane integrity upon aSNP-treatment

The LDH assay (lactate-dehydrogenase (LDH) release) provided corresponding results to the viability test of the monocultures (Figure 9B). H441 and ISO-HAS-1 cells showed a concentration-dependent release of LDH. After 4h exposure to 600 µg/ml aSNPs H441 cells released about 75% (Ludox TM-40: 78±14% and NexSil20: 74±17%) of their total LDH, whereas ISO-HAS-1 cells released less LDH (Ludox TM-40: 44±7% and NexSil20: 62±5%) into the supernatant. 300 µg/ml aSNPs also induced a significant loss of LDH in H441

(Ludox TM-40: 53±11% and NexSil20: 59±11%) and ISO-HAS-1 (Ludox TM-40: 37±9% and NexSil20: 47±4.5%). The lower LDH content of the supernatant measured for 300 and 600 µg/ml aSNP in H441 after 20 h recovery compared to 4h (Figure 9 B) is due to the fact that medium was replaced after 4h. Hence, following medium change a minor membrane leakage was observed for H441, whereas ISO-HAS-1 continuously released LDH into the culture supernatant during the 20h recovery in a concentration-dependent manner.

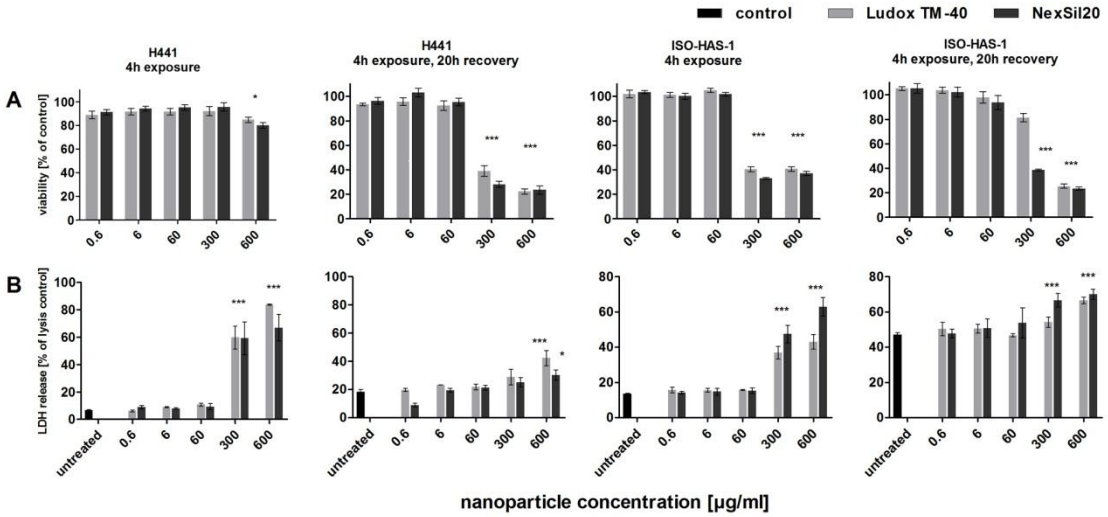

*Figure 9: Mitochondrial activity was measured using the MTS assay (A) and membrane integrity was determined by the LDH assay (B) for monocultures of H441 and ISO-HAS-1 on 96 well plates (conventional monoculture). Cells were incubated with aSNP (Ludox TM-40: light grey, NexSil20: dark grey) for 4h in serum-free medium. aSNPs were then removed and cells were cultivated for further 20h. The assays were conducted after both time points (4h exposure and 4h exposure with 20h recovery). Data are depicted as percentage of the untreated control (A: MTS) or as percentage of the total LDH amount of the cells (B: LDH, lysis control). Results are shown as means ± S.D. (n=6-9) of 2-3 independent experiments. *P <0.05, **P<0.01 and ***P<0.001 compared to the untreated control*

LDH leakage was measured after 4h apical (upper well) exposure and also after 20h recovery of the coculture (Figure 10). After 4h a concentration of 600 µg/ml aSNPs caused a non-significant release of LDH (Ludox TM-40: 19±10% and NexSil20: 15±5%), whereas after 20h recovery a significant, but much lower release compared to the monoculture, was detected for 600 µg/ml aSNPs, apically exposed (Ludox TM-40: 53±11% and NexSil20: 35±5%). Incubation with 6000 µg/ml, however, showed a considerable LDH release at 4

h (Ludox TM-40: 72±0.85% and NexSil20: 90±11%) as well as after 20 h recovery (Ludox TM-40: 97±3.5% and NexSil20: 95±0.24%). The coculture revealed a lower responsiveness towards aSNP exposure concerning LDH release. Compared to the conventional monocultures the response towards aSNP exposure was shifted by about a factor of 10 with respect to aSNP concentration (from 600 µg/ml to 6000 µg/ml).

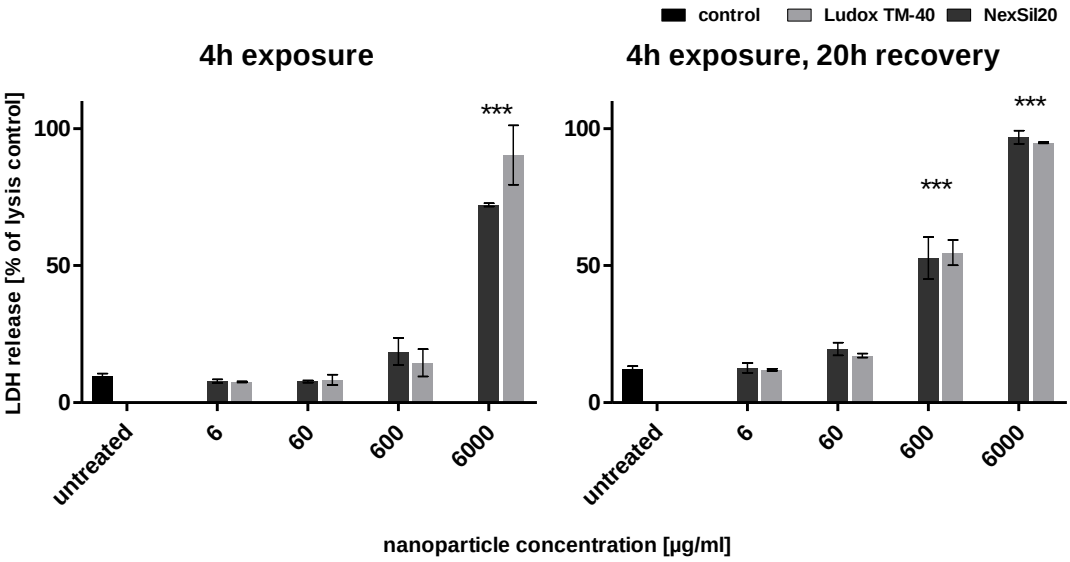

*Figure 10: Membrane integrity was determined by the LDH assay for H441 in coculture. The H441 of the coculture were incubated with aSNP (Ludox TM-40: light grey, NexSil20: dark grey) for 4h in serum-free medium. aSNPs were then removed and cells were cultivated for further 20h. The assays were conducted after both time points (4h exposure and 4h exposure with 20h recovery). Data are depicted as percentage of the total LDH amount of the cells (lysis control). Results are shown as means ± S.D. (n=6-9) of 2-3 independent experiments. *P <0.05, **P<0.01 and ***P<0.001 compared to the untreated control*

3.4 Morphological evaluation of aSNP treated cells

3.4.1 aSNP effect on conventional monoculture and coculture in comparison

Using immunofluorescence, comparisons of the response of H441 in conventional monoculture and in coculture (with ISO-HAS-1) have been drawn regarding the development of tight junctional TJ (ZO-1) and adherens junctional structures (β-catenin and E-cadherin). Under conventional tissue culture conditions monocultures of H441 show a fragmented immunostaining of tight

junction (TJ) and adherens junction (AJ) proteins, whereas polarized cells in coculture establish a functional TJ and AJ network (see Figure 11). Visual examination was conducted by means of a fluorescent microscope (personalDV, Applied Precision, Issaquah, USA).

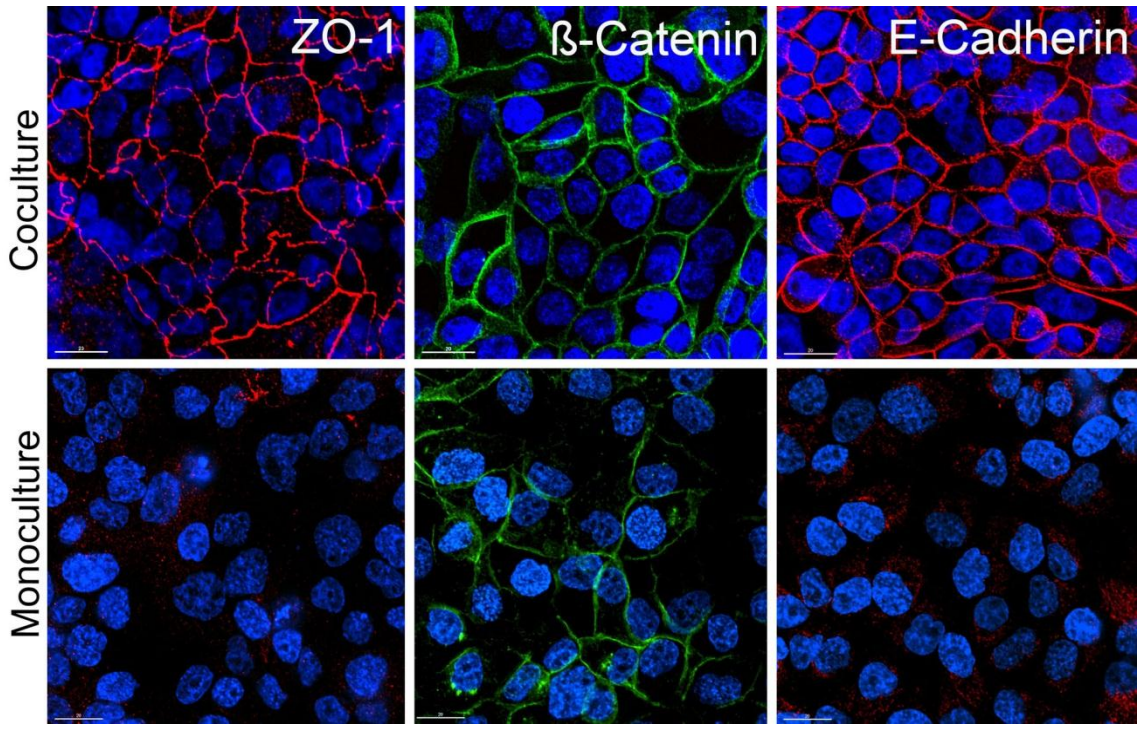

Figure 11: Comparison of H441 in conventional monoculture and in coculture (with ISO-HAS-1) regarding the development of tight junctional TJ (ZO-1) and adherens junctional structures (β-catenin and E-cadherin). Nuclei are stained using Hoechst 33342 (blue), scale bar=20 µm

3.4.2 Morphological alterations in conventional monocultures and coculture after aSNP treatment

In conventional monoculture morphological alterations were observed at an aSNP concentration of 600 µg/ml for both cell lines H441 and ISO-HAS-1 (see Figure 12 and Figure 13). 60 µg/ml aSNP did not cause any changes in cellular morphology. H441 in conventional monoculture show a diffuse F-actin staining in general. Together with the results from junctional staining H441 in conventional monoculture do not show a differentiated, polarized epithelial phenotype. Therefore, the same experimental procedure was conducted for the coculture, in which the H441 develop a polarized, barrier-forming epithelial layer.

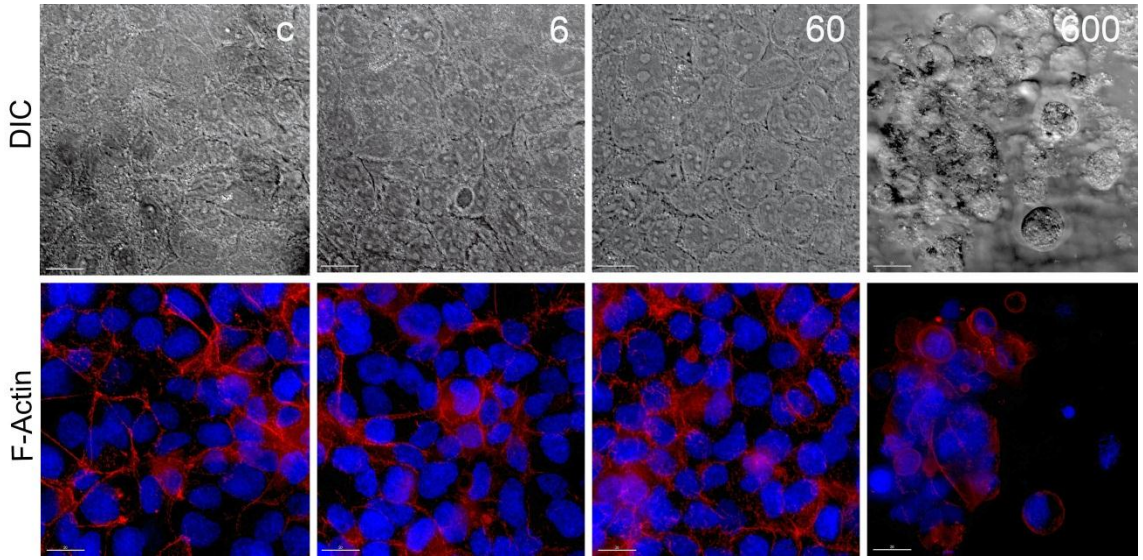

Figure 12: After aSNP exposure, H441 cells in conventional monoculture were checked for morphological alterations. The cells were incubated with aSNP (NexSil20: concentration range 0.6 – 6000 µg/ml, c: untreated control) for 4h in serum-free medium. aSNPs were then removed and cells were cultivated for further 20h. Additionally, cells were counterstained for F-actin with Phalloidin-TRITC. Visual examination was conducted by means of a fluorescent microscope (personalDV, Applied Precision, Issaquah, USA). Nuclei are stained using Hoechst 33342 (blue), scale bar=20 µm

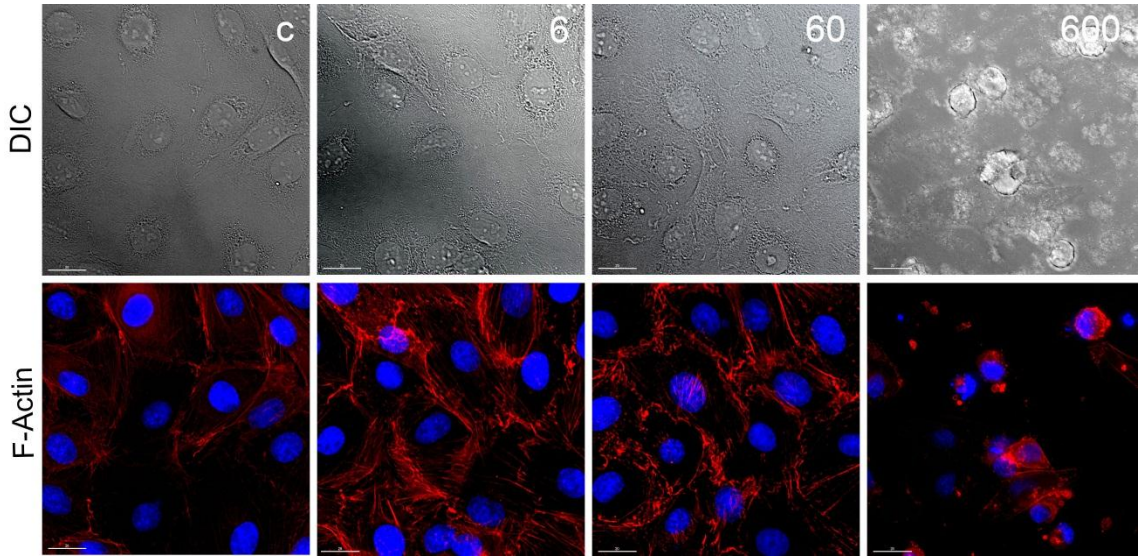

Figure 13: After aSNP exposure, ISO-HAS-1 in conventional monoculture were studied for morphological alterations. The cells were incubated with aSNP (NexSil20: concentration range 0.6 – 6000 µg/ml, c: untreated control) for 4h in serum-free medium. aSNPs were then removed and cells were cultivated for further 20h. Additionally, cells were counterstained for F-actin with Phalloidin-TRITC. Visual examination was conducted by means of a fluorescent microscope with DIC (personalDV, Applied Precision, Issaquah, USA). Nuclei are stained using Hoechst 33342 (blue), scale bar=20 µm

Conventional monoculture of ISO-HAS-1 showed a better developed cortical F-actin ring (Figure 13), compared to the H441 epithelial cells (Figure 12). Low concentrations of aSNP (6 µg/ml), induced a stress response of the endothelial cells to aSNPs, although no cytotoxicity (MTS and LDH) could be observed.

Up to a concentration of 600 µg/ml aSNP the E-cadherin staining pattern of H441 in coculture showed no difference compared to the untreated control (Figure 14). A concentration of 6000 µg/ml aSNPs, a factor 10 x higher than in monoculture, caused visible changes in the assembly of cell-cell junctions and first signs of cell detachment. The indirectly exposed ISO-HAS-1 (PECAM-1 counterstaining) in coculture did not show any morphological alterations even at a concentration of 6000 µg/ml.

Figure 14: After aSNP exposure layer integrity of H441 and ISO-HAS-1 in coculture was examined by immunofluorescent localization of junction-associated proteins. The H441 cells of the coculture were incubated with aSNP (NexSil20: concentration range 0.6 – 6000 µg/ml, c: untreated control) for 4h in serum-free medium. aSNPs were then removed and cells were cultivated for further 20h. The H441 were labelled for E-cadherin, the ISO-HAS-1 were counterstained for PECAM-1. Nuclei are stained using Hoechst 33342 (blue), scale bar=20 µm

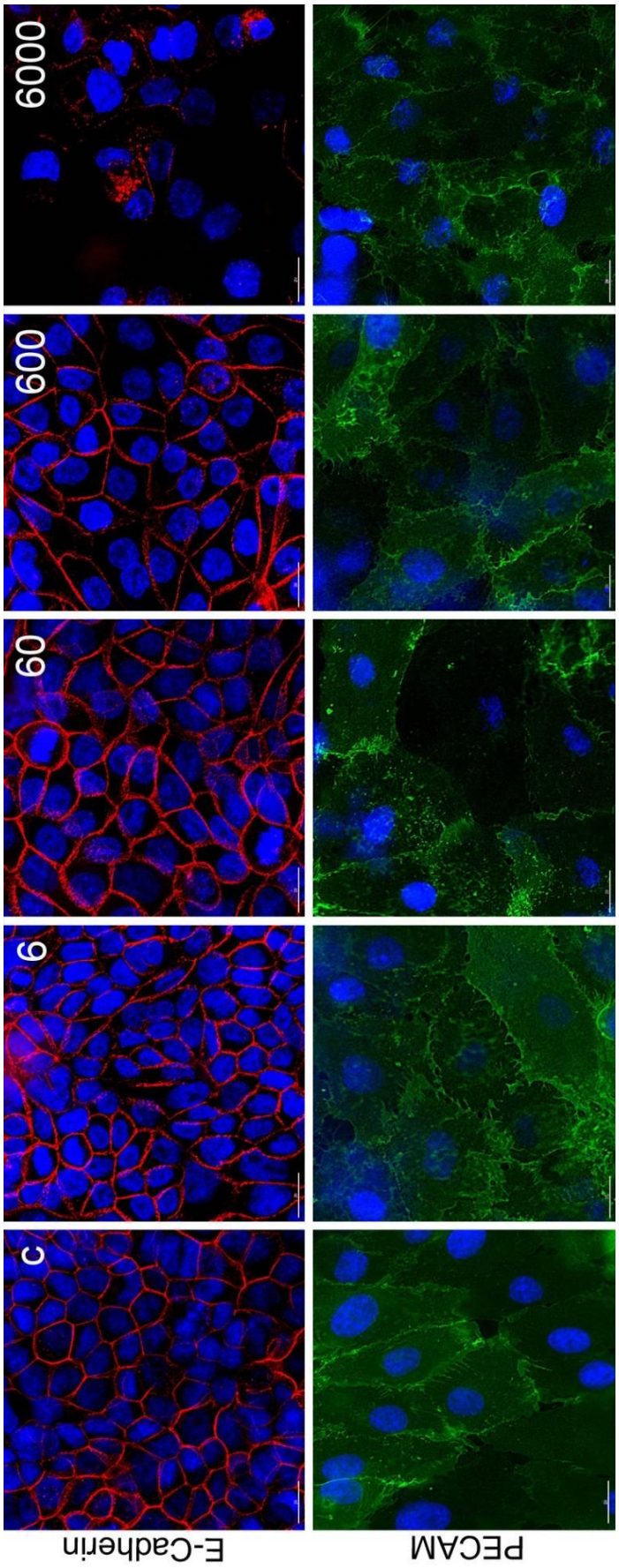
6000
600
60
6
c
E-Cadherin
PECAM

Morphological alterations could be observed when tight junctional markers were studied. Whereas ZO-1 did not show alterations at a concentration of 600 µg/ml (see Figure 16), claudin-5 immunostaining did show an effect following nanoparticle treatment with 600 µg/ml (Figure 15), with marked fragmentation of the signal.

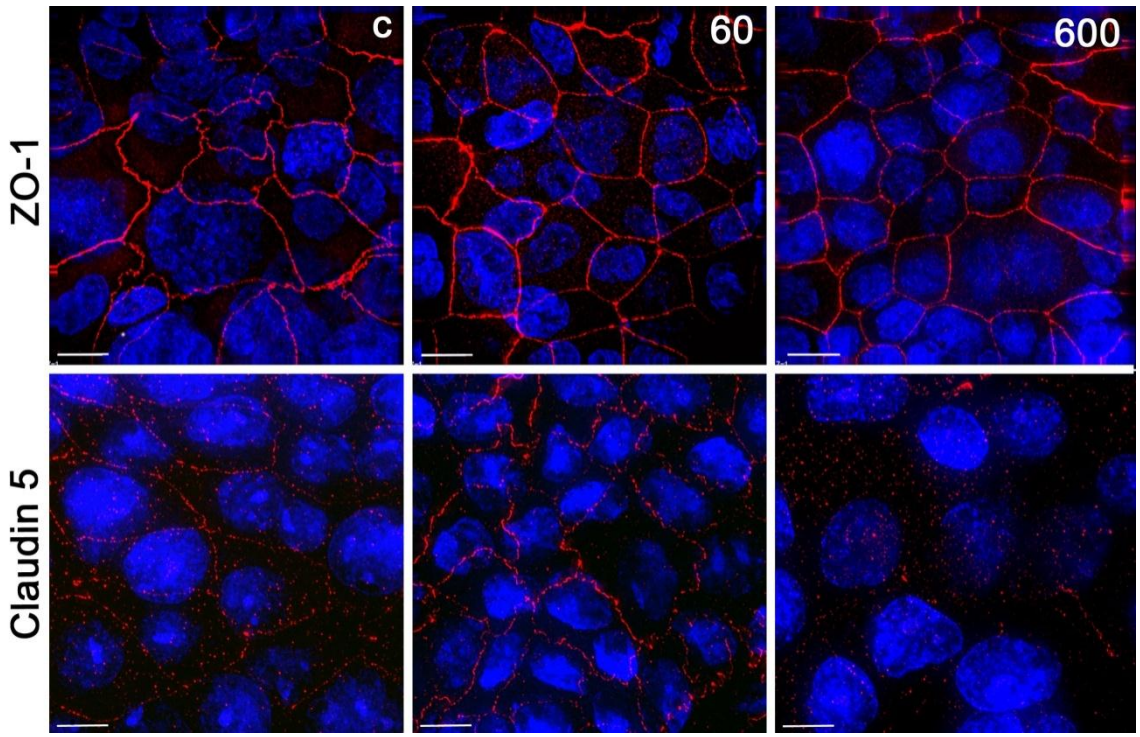

Figure 15: After aSNP exposure layer integrity of H441 in coculture with ISO-HAS-1 was determined by immunofluorescent localization of junction-associated proteins. The H441 cells of the coculture were incubated with aSNP (NexSil20: concentration range 0.6 – 6000 µg/ml, c: untreated control: only depicted: c, 60 and 600 µg/ml)) for 4h in serum-free medium. aSNPs were then removed and cells were cultivated for further 20h. The H441 were labelled for ZO-1 and claudin 5 (red), nuclei are stained using Hoechst 33342 (blue), scale bar: 5 µm

3.5 Comparison of inflammatory responses on aSNPs in different culture systems

The release of inflammatory mediators measured after aSNP exposure of conventional monocultures on 96-well plates is shown in Figure 16 for H441 and ISO-HAS-1 cells. For H441 cells even a concentration of 60 µg/ml NexSil20 induced a maximum release of sICAM-1 (Figure 16A). Concentrations of 300-600 µg/ml of both aSNPs show a 2fold increase of sICAM-1 for both cell lines, compared to untreated controls. Both aSNPs induced a maximum IL-6 release at concentrations of 60 µg/ml for H441 (Ludox TM-40: 1.4fold, NexSil20: 2fold) and 300 µg/ml for ISO-HAS-1 (2fold increase compared to untreated control) (Figure 16B). For both cell lines IL-8 release was seen at similar aSNP concentrations as for IL-6 (Figure 16C).

Due to the different compartments that are formed by growing barrier-forming cells on transwells, not only an apical/basolateral differentiated coculture but also polarized monocultures were grown on transwells (see Figure 17). These transwell-monocultures of H441 and ISO-HAS-1 with the same culture conditions and seeding surface served as a control for the effects of an upper well aSNP exposure of the individual cell types.

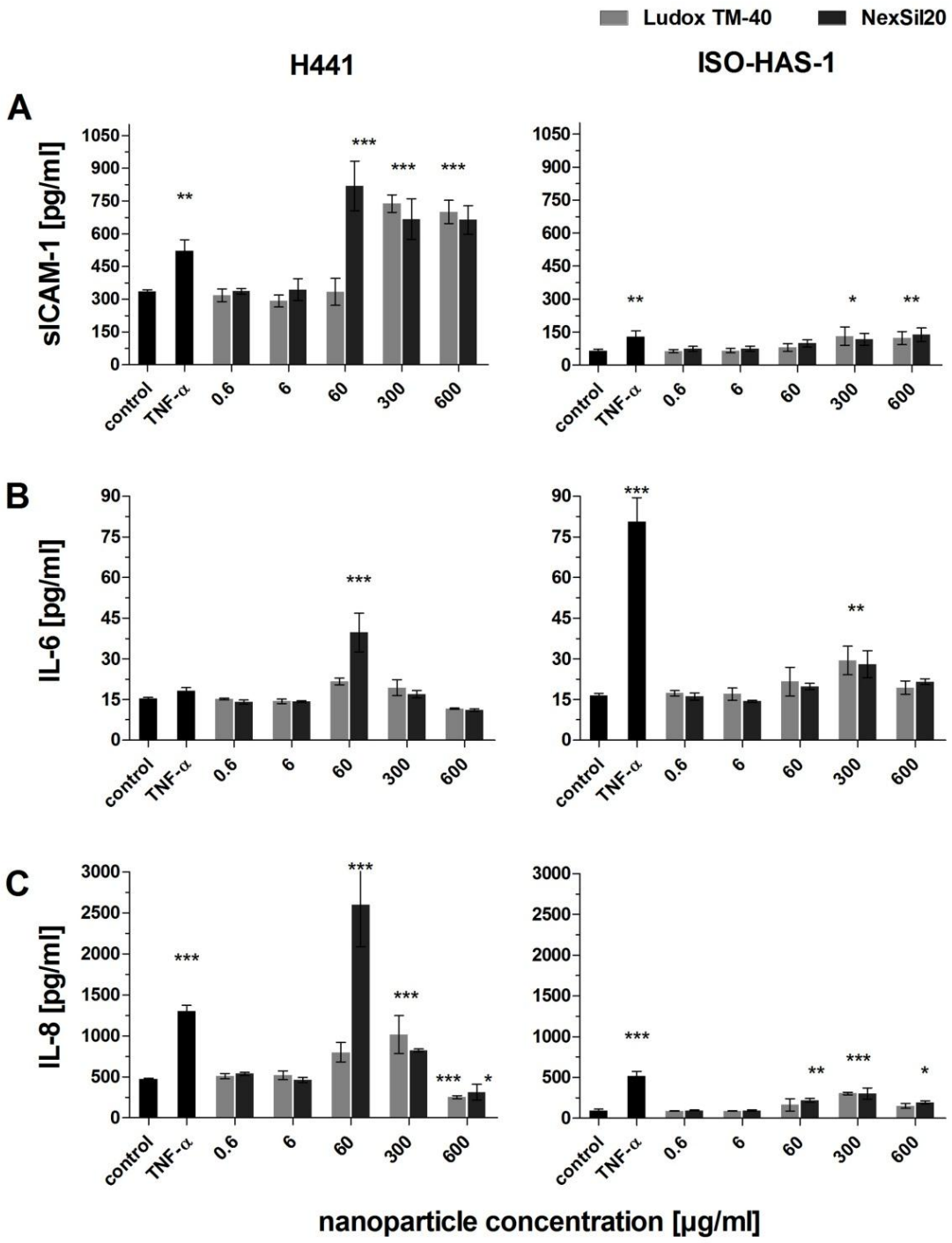

*Figure 16: The release of inflammatory mediators was measured after aSNP (Ludox TM-40: light grey, NexSil20: dark grey) exposure of monocultures of H441 and ISO-HAS-1 on 96-well plates (conventional monoculture). After 4h incubation, aSNPs were removed and the cells were cultivated for further 20h to detect sICAM-1, IL-6 and IL-8 release. Data are depicted as means ±S.D. of one representative experiment out of three independent experiments with n=3 samples for each treatment. All independent experiments showed a comparable reaction following aSNP treatment. *P <0.05, ** P <0.01 and *** P <0.001 compared to the untreated control*

The analysis of sICAM-1 in the untreated controls of the three approaches (H441/ISO-HAS-1 (upper/lower surface), H441 (upper surface) and ISO-HAS-1 (lower surface) yielded significantly different basic levels of sICAM-1. The transwell-monoculture of H441 released in total 19fold more sICAM-1 compared to the coculture in total. The sICAM-1 response of the cocultures and transwell-monocultures of H441 to aSNPs was most intense (30fold in total) at a concentration of 6 µg/ml and decreased with increasing aSNP concentration. At concentrations from 6-600 µg/ml aSNPs there was no significant release of sICAM-1 into the lower compartment. With 6000 µg/ml aSNP sICAM-1 increased significantly in the lower well for the cocultures and the transwell-monocultures of H441. sICAM-1 response of the cocultures behaved in a similar fashion to the H441 monoculture. Monocultures of ISO-HAS-1 growing at the lower surface of the transwell filter showed no sICAM release upon upper well exposure.

In coculture the IL-6 level rose slightly with increasing aSNP concentration, whereas the transwell-monocultures did not show a clear response. In the lower well (basoloateral compartment) increased IL- 6 and IL-8 amounts were already detectable at low concentrations of aSNPs (6 µg/ml). The H441 in transwell-monoculture showed no basolateral release of either IL-6 or IL-8 at this concentration. In addition, the ISO-HAS-1 in transwell-monoculture were not affected by aSNPs concentrations of 6 µg/ml. At concentrations of 600 µg/ml aSNPs an IL-8 release (in total approx. 1.6fold of untreated control) into both compartments was detected for H441 in transwell-monoculture. The transwell-monoculture of ISO-HAS-1 showed no significant reaction to aSNP exposure from the upper well (basolateral exposure for the endothelial cells on the lower surface of the transwell) regarding IL-6 release. Not until concentrations of 6000 µg/ml aSNPs were reached was there a slightly increased IL-8 release in the upper and lower well of ISO-HAS-1 in transwell monoculture.

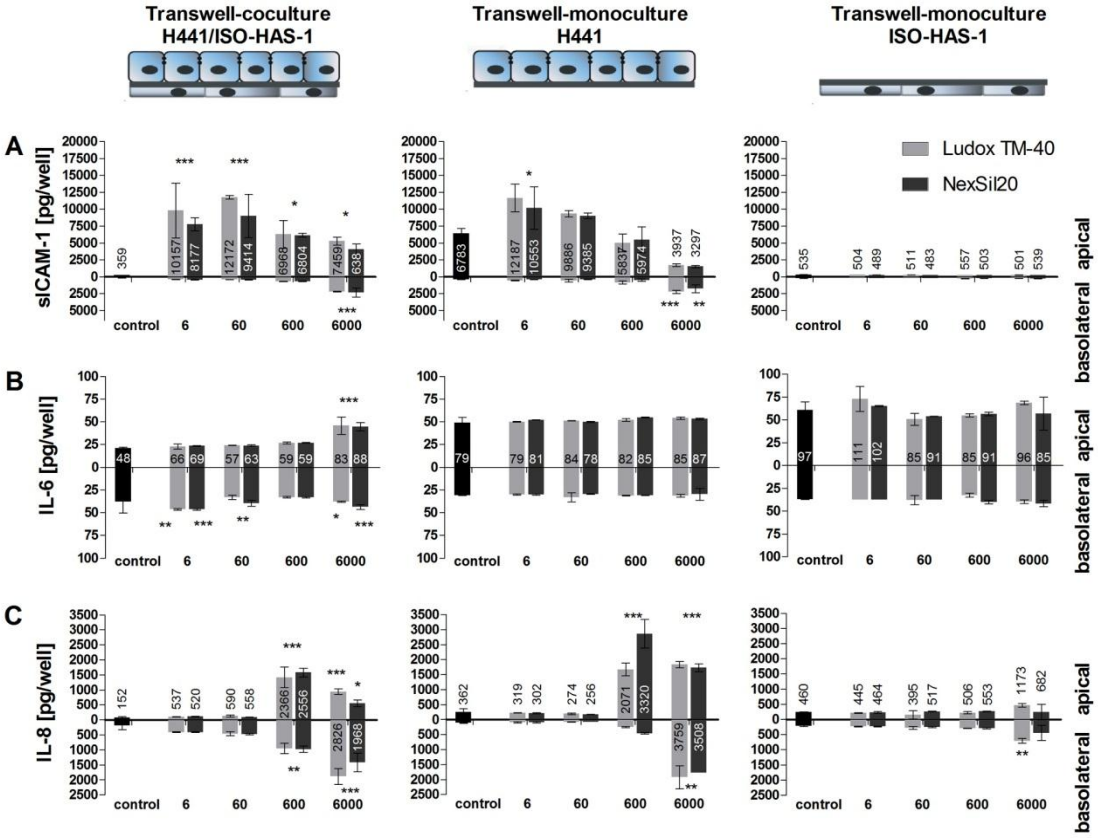

*Figure 17: The release of inflammatory mediators (sICAM-1, IL-6 and IL-8) is shown after aSNP (Ludox TM-40: light grey, NexSil20: dark grey) incubation on apical/basolateral differentiated cocultures of H441 and ISO-HAS-1, as well as on their appropriate monocultures grown on HTS 24-Transwell® filters. Cells were exposed to aSNPs from the apical side of the filter membrane to mimic an inhalative exposure to aSNPs. After 4h serum-free incubation, aSNPs were removed and the cells were cultivated for further 20h. Subsequently, medium supernatant of both compartments (apical: upper well, basolateral: lower well) was examined. Data are depicted as means ± S.D. of one representative (of three independent) experiment with n=3 samples for each treatment. All independent experiments showed a comparable reaction following aSNP treatment. Exclusively in coculture, an apical exposure of 6 and 60 µg/ml aSNP caused an increased IL-6 and IL-8 release into the lower well (basolateral/endothelial side). For both monocultures increased amounts of sICAM-1, IL-6 and IL-8 in the lower well were not detected below concentrations of 600 µg/ml aSNP. *P <0.05, ** P <0.01 and *** P <0.001 compared to the untreated control*

Preliminary experiments regarding inflammatory responses to aSNPs have been conducted for the primary coculture model (ATII/HPMEC) with the same experimental procedure as described for the cell line-coculture (H441/ISO-HAS-1). Compared to the cell line model (H441/ISO-HAS-1), the primary coculture as well as the transwell-monocultures did not appear to respond to low concentrations of aSNP (6-60 µg/ml) concerning sICAM, IL-6 and IL-8 release (Figure 18).

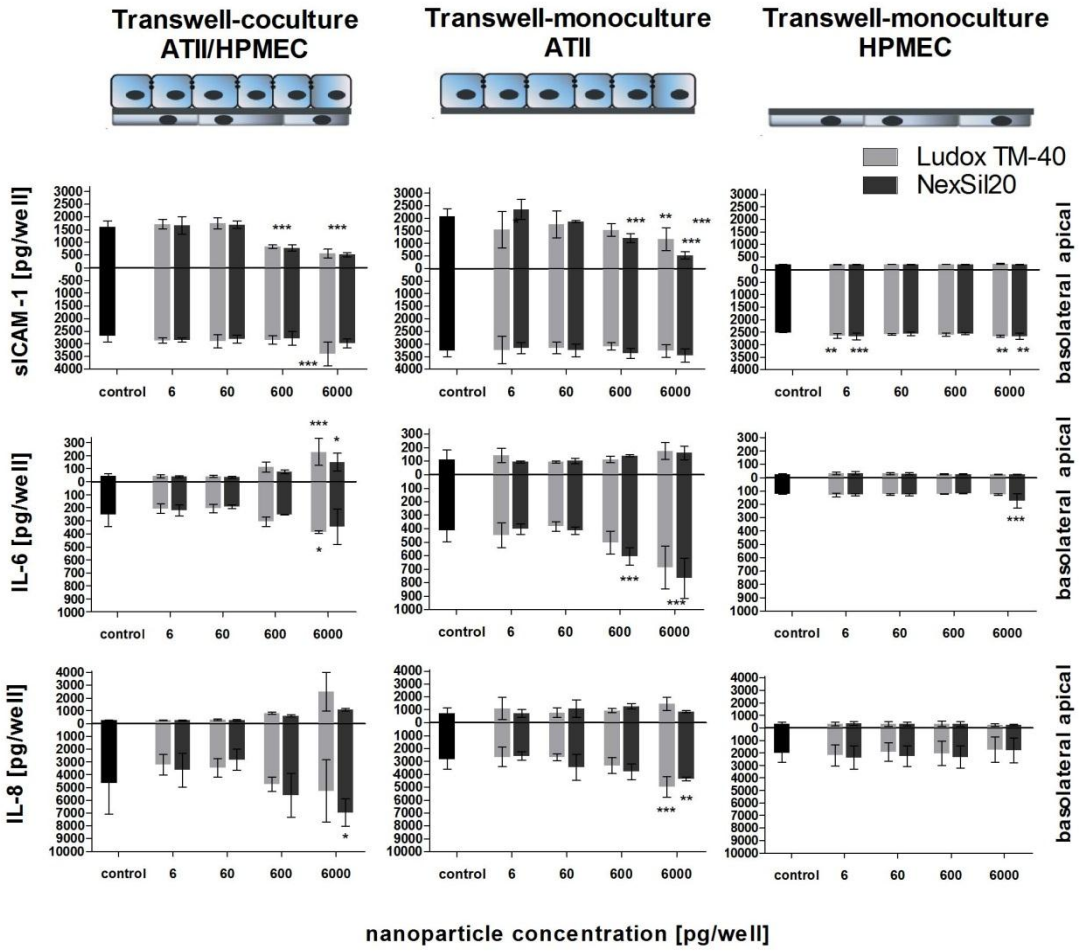

*Figure 18: The release of inflammatory mediators (sICAM-1, IL-6 and IL-8) is shown after aSNP (Ludox TM-40: light grey, NexSil20: dark grey) incubation on apical/basolateral differentiated cocultures of ATII and HPMEC, as well as on their appropriate monocultures grown on HTS 24-Transwell® filters. Cells were exposed to aSNPs from the apical side of the filter membrane to mimic an inhalative exposure to aSNPs. After 4h serum-free incubation, aSNPs were removed and the cells were cultivated for further 20h. Subsequently, medium supernatant of both compartments (apical: upper well, basolateral: lower well) was examined. Data are depicted as means ± S.D. of twoindependentexperiments with n=2 samples for each treatment.*P <0.05, ** P <0.01 and *** P <0.001 compared to the untreated control*

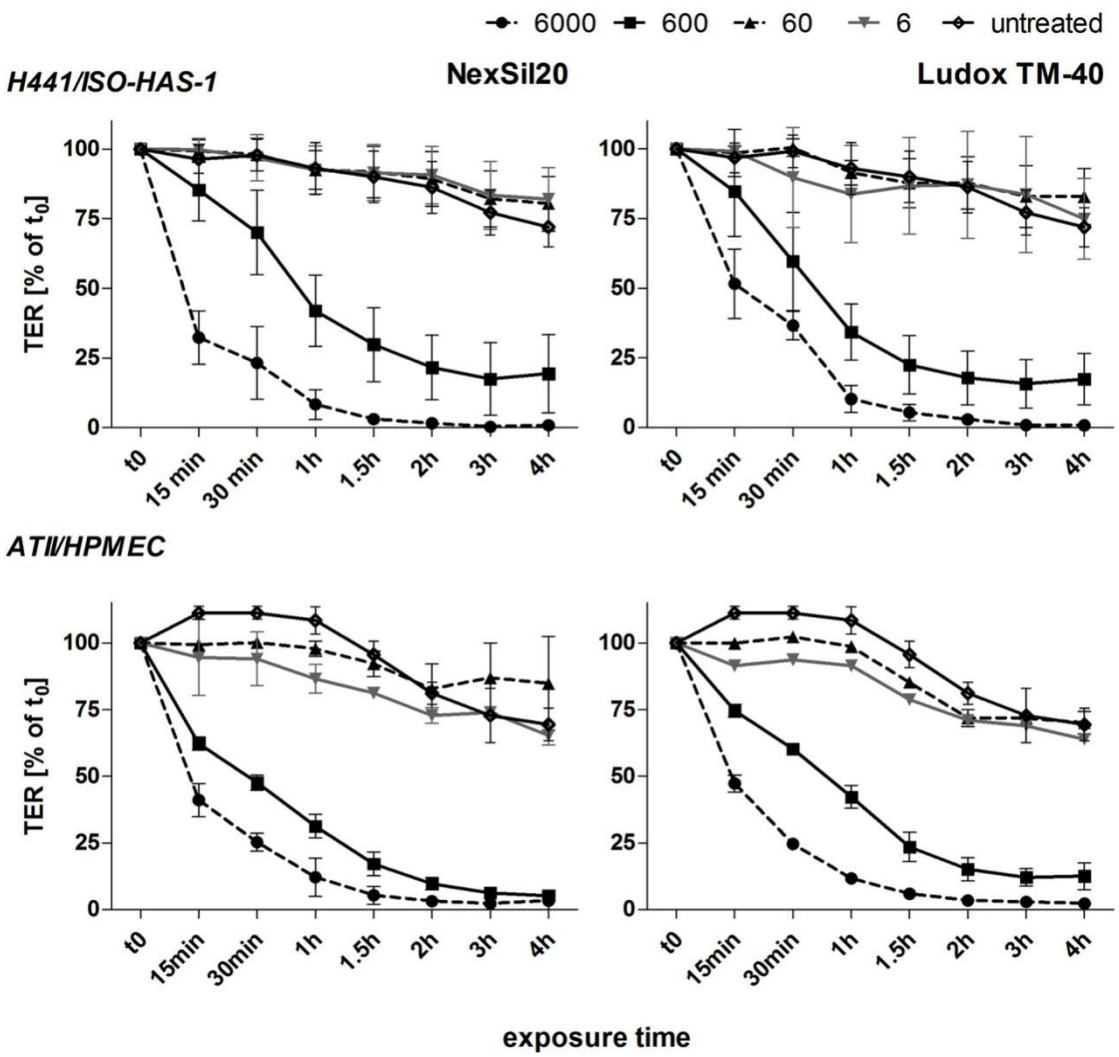

*Figure 19: Transmembrane electrical resistance was measured for cocultures of H441 with ISO-HAS-1 (H441/ISO-HAS-1) as well as for cocultures of primary isolated cells (alveolar type II and HPMEC (ATII/HPMEC)). During 4h incubation with aSNPs (NexSil20, Ludox TM-40 at concentrations of 6, 60, 600, and 6000, µg/ml) TER-values are depicted as % of time-point t0 (TER-value prior to aSNP treatment). Results are shown as means ± S.D. of 3 independent experiments with n=2 samples for each treatment. For statistical analysis using Dunnett´s Multiple Analyzing test, the 4h value of the untreated samples was used as control. Treatment with 600 and 6000 µg/ml of both aSNP revealed a time-dependent decrease of TER after 4h incubation. *P <0.05, ** P <0.01 and *** P <0.001 compared to the untreated control*

As higher concentrations (600-6000 µg/ml) sICAM level decreases significantly at the upper well, while a slight increase was observed at the basolateral side. These observations correlate with a decrease in TER which is depicted in Figure 19. Similar results were obtained for the transwell-monoculture of ATII for the apical side, but it did not show an increase of sICAM at the basolateral side. However, a slight increase of sICAM release was detected for the HPMEC transwell-monoculture. Concerning IL-6 and IL-8, increased levels were

detected for high concentrations (6000 µg/ml) apically as well as basolaterally, which is accompanied by decreased TER values at those high concentrations. In summary, the primary coculture appears to respond less sensitively regarding cytokine release upon aSNP stimuli at low concentrations, but shows similar release patterns at high concentrations compared to the cell line model.

3.6 Effect of aSNPs on apoptosis markers in conventional mono- and coculture

Tests using the Caspase-Glo® 3/7 Assay (Promega) were conducted to study apoptosis induction following aSNP (NexSil20) exposure on conventional monocultures by measuring active caspase 3/7. NP controls without cells revealed no interferences of NPs with the Caspase-Glo® 3/7 assay reagent. In both cell lines H441 and ISO-HAS-1 an increase of caspase 3/7 activity could only be observed for aSNP (NexSil20) at a concentration of 600µg/ml (see Figure 20).

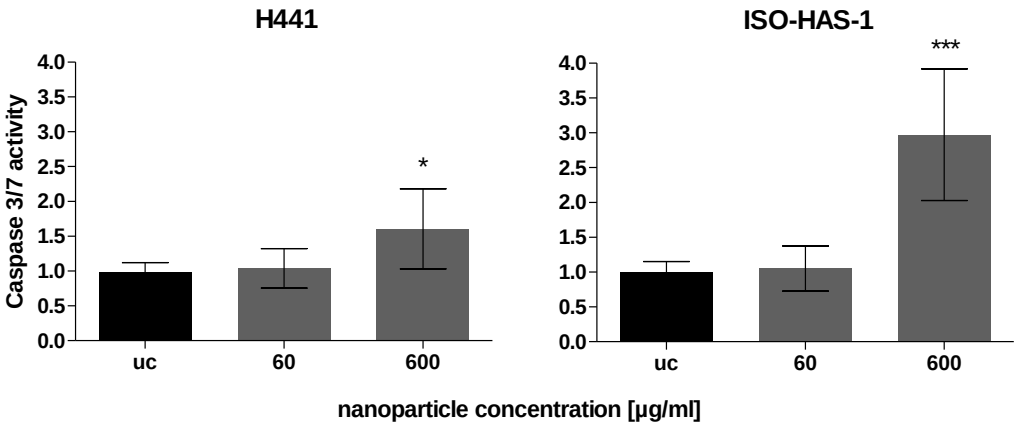

*Figure 20: Measurement of caspase 3/7 activity via the CaspGlo-assay on conventional monocultures of H441 and ISO-HAS-1 after aSNP treatment (NexSil20) for 4h. Results are depicted as means ± S.D. of four independent experiments with n=2 samples. *P <0.05, ** P <0.01 and *** P <0.001 compared to the untreated control.*

The protein array for apoptosis markers demonstrated for the coculture that the expression of a number of intrinsic apoptosis markers was elevated in a time-dependent way after exposure to 600 µg/ml NexSil20 (data for 10 min and

1 h exposure are not shown). Figure 21 shows the percentage change of apoptosis marker protein content related to the non-treated control after 4h exposure. The assay revealed phosphorylation of the p53-protein at Ser15, Ser46 and Ser392 (Ser15: 151±7%, Ser46: 143±7%, Ser392: 161±9%). An increase of pro-apoptotic markers such as bad (126±1.4%) and bax (144±20.5%) and its ligands was also detected. In addition, the assay detected cytochrome c release (110±0.9%) into the cytosol. Further major apoptotic markers, such as Fas (113±0.6%), DR4 (174±0.4%) and DR5 (164±2.4%) were also upregulated. Concerning hypoxia, HIF-1α (140±23%), an hypoxia inducible factor, showed a 1.4 fold increased level compared to the untreated control. On average, a 1.8 fold higher amount of cell cycle and proliferation regulator proteins p21 (174±10%) as well as p27 (181±13.8%) was observed compared to the untreated control. However, elevated levels of apoptosis inhibitory factors such as XIAP (X-linked Inhibitor of apoptosis Protein: 158±10.8%) and survivin (153±3.6%) were also established by this array following NexSil20 exposure. The increase of paraoxonase-2 (Pon2: 145±0.4%), which has a reducing function on reactive oxygen species, is an indication that the cells of the coculture are in a stressed condition after 4 h apical exposure to 600 µg/ml NexSil20.

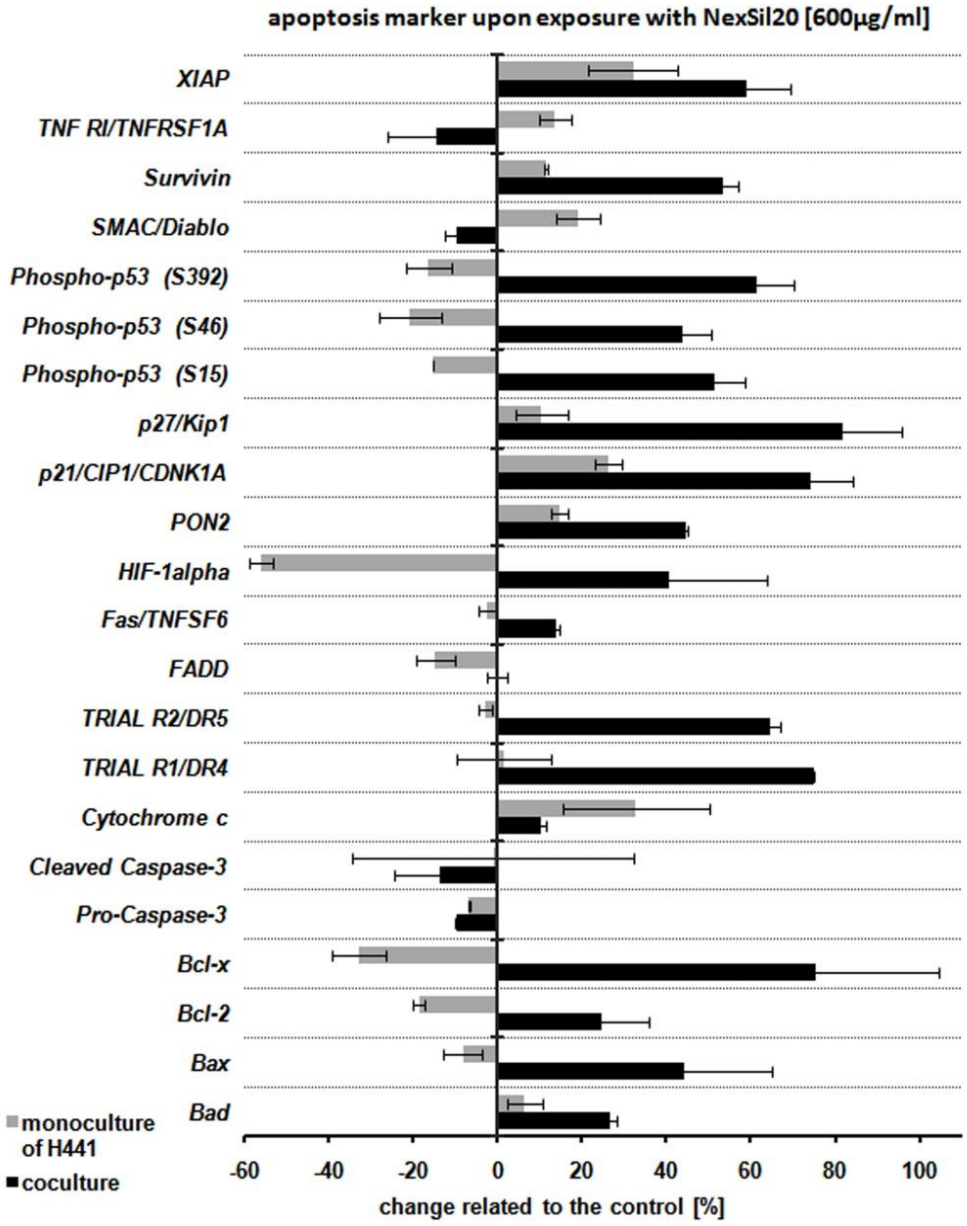

Figure 21: Protein expression of cell death regulators was analysed after apical exposure of differentiated cocultures with aSNPs (NexSil20: 600µg/ml) to mimic the situation after accidental inhalation of aSNPs. After 4h incubation with aSNPs filter membranes were excised, lysed for 30 min and an apoptosis protein array was performed. Data are depicted as means ± S.D. from 2 independent experiments with n = 4 samples for each treatment. Quantitative analysis of the array revealed increased levels of a number of apoptosis markers, especially of the intrinsic pathway

3.7 Quantification of internalized nanoparticles (aSNP, AmorSil, PEI

3.7.1 NP uptake by conventional monoculture and coculture of the alveolar-capillary barrier

Figure 22 depicts the quantification of internalized fluorescence-labelled NPs (Sicastar Red: 6 µg/ml, AmorSil: 300 µg/ml, PEI: 2.5 µg/ml) exposed for 4h to H441 with further 20 h cultivation in conventional monoculture and coculture with ISO-HAS-1. Concentrations have been chosen to obtain adequate fluorescence intensities which can be compared for mono- and cocultures. For all three NPs used in this study (aSNP (Sicastar Red), AmorSil and PEI), a significant increase of fluorescence intensity was observed for NP-exposed H441 in conventional monoculture (Figure 22: Sicastar Red: 1.6±0.5, AmorSil: 2.7±0.3, PEI: 9.8±1.4 fold of untreated control). For the H441 in coculture, however, an uptake via fluorescence intensity measurement could not be detected. According to visual judgments of the pictures taken, uptake of all three NP-types in H441 in coculture is extremely low compared to the conventional monoculture (data not shown)

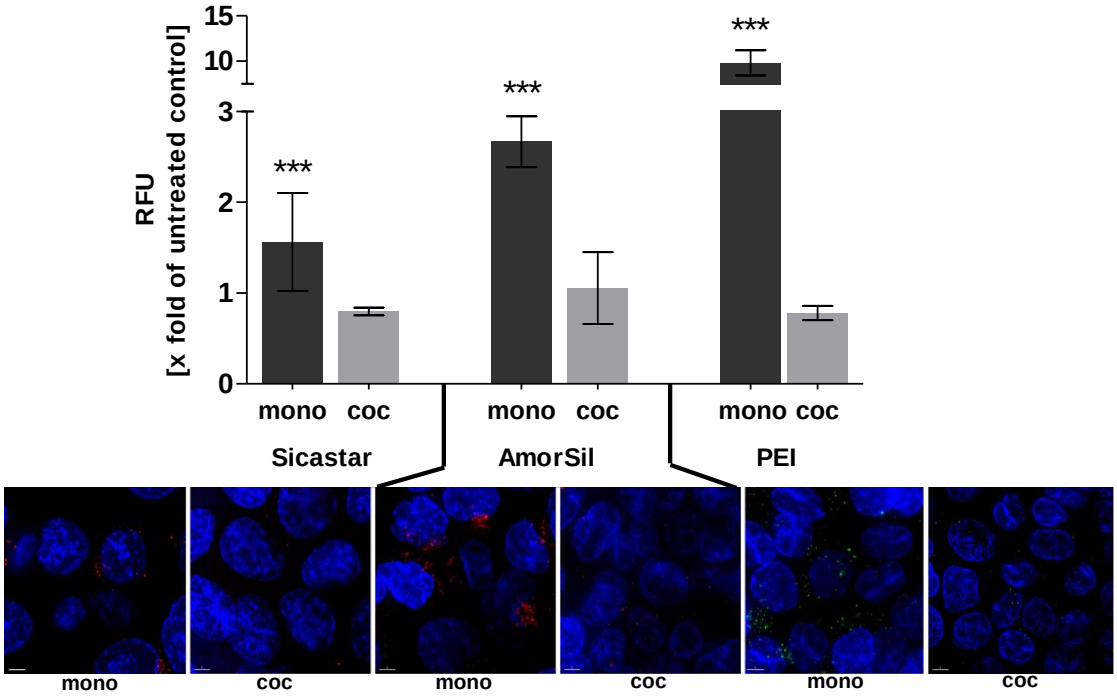

*Figure 22: Comparison of uptake behavior of H441 kept under different culture conditions (**mono**: conventional monoculture, **coc**: differentiated coculture with ISO-HAS-1) regarding different nanoparticles. Images were taken by means of a fluorescence microscope (DeltaVision, Applied Precision), Intensity scales were aligned for untreated and treated samples and mean fluorescence intensity was measured via Fiji. RFU = relative fluorescent unit. Data are depicted as means ± S.D. from 9 images. For statistical analysis the unpaired t-test was chosen (*P <0.05, ** P <0.01 and *** P <0.001 compared to the untreated control) Images: Sicastar Red and AmorSil: red, PEI: green, nuclei are stained using Hoechst 33342: blue, scale bar: 5 µm*

3.7.2 Transport of NPs across the alveolar-capillary barrier *in vitro*

Uptake studies with microscopical visualisation were conducted to evaluate transport of NPs, which were apically applied (on the epithelial monolayer of H441), across the epithelial layer and subsequent internalization by the endothelial layer of the ISO-HAS-1 on the lower surface. For this purpose, concentrations of NPs and exposure time were adjusted as required to obtain a sufficient uptake amount of NPs in H441. After 48h of permanent incubation of NPs (Sicastar Red: 60 µg/ml, AmorSil: 300 µg/ml and PEI: 2.5 µg/ml), a distinct uptake was detected via visual judgement in H441 kept under coculture conditions (see Figure 23).

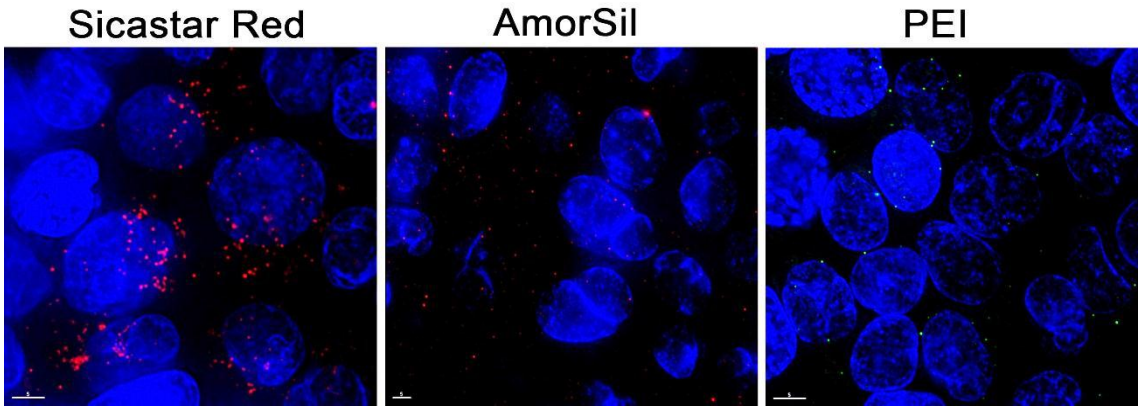

Figure 23: uptake of Sicastar Red (60 µg/ml), AmorSil (300 µg/ml) and PEI (2.5 µg/ml) in H441 in coculture with ISO-HAS-1, nuclei are stained using Hoechst 33342 (blue), scale bar: 5 µm

To verify the test setup for transport experiments, ISO-HAS-1 were cultured under various conditions: A. as monoculture according to the conventional seeding procedures with direct exposure to NPs B. As monoculture under coculture conditions, seeded on the lower side of the filtermembrane and cultured for 10 days with subsequent indirect (apically) NP-application and finally C. under coculture conditions with H441 on the upper-side of the filter membrane and apical exposure of NPs. The conventional monoculture of ISO-HAS-1, with an exposure time of NPs for 4h and further 20h cultivation as described for the colocalisation studies, revealed a sufficient uptake of NPs such as Sicastar Red (6 µg/ml), AmorSil (300 µg/ml) and PEI (2.5 µg/ml) (see Figure 24, left column). The ISO-HAS-1 monoculture under coculture conditions (seeded on the lower side of the filter membrane and cultivated for 10 days) also revealed an uptake of all NPs when apically applied to the filter membrane. However, compared to the conventional monoculture, a lower amount of NPs was taken up by the coculture (see Figure 24, middle column). These findings verify that the test setup is functional and particles that are applied apically (on top of the filter membrane) are able to diffuse through the collagen-1 coated filter membrane and reach the endothelial monolayer. In coculture with H441 however, although a sufficient uptake was seen after 48h exposure on the apical side of the filter membrane, no uptake of Sicastar Red, AmorSil and PEI could be verified in the endothelial layer (see Figure 24, right column).

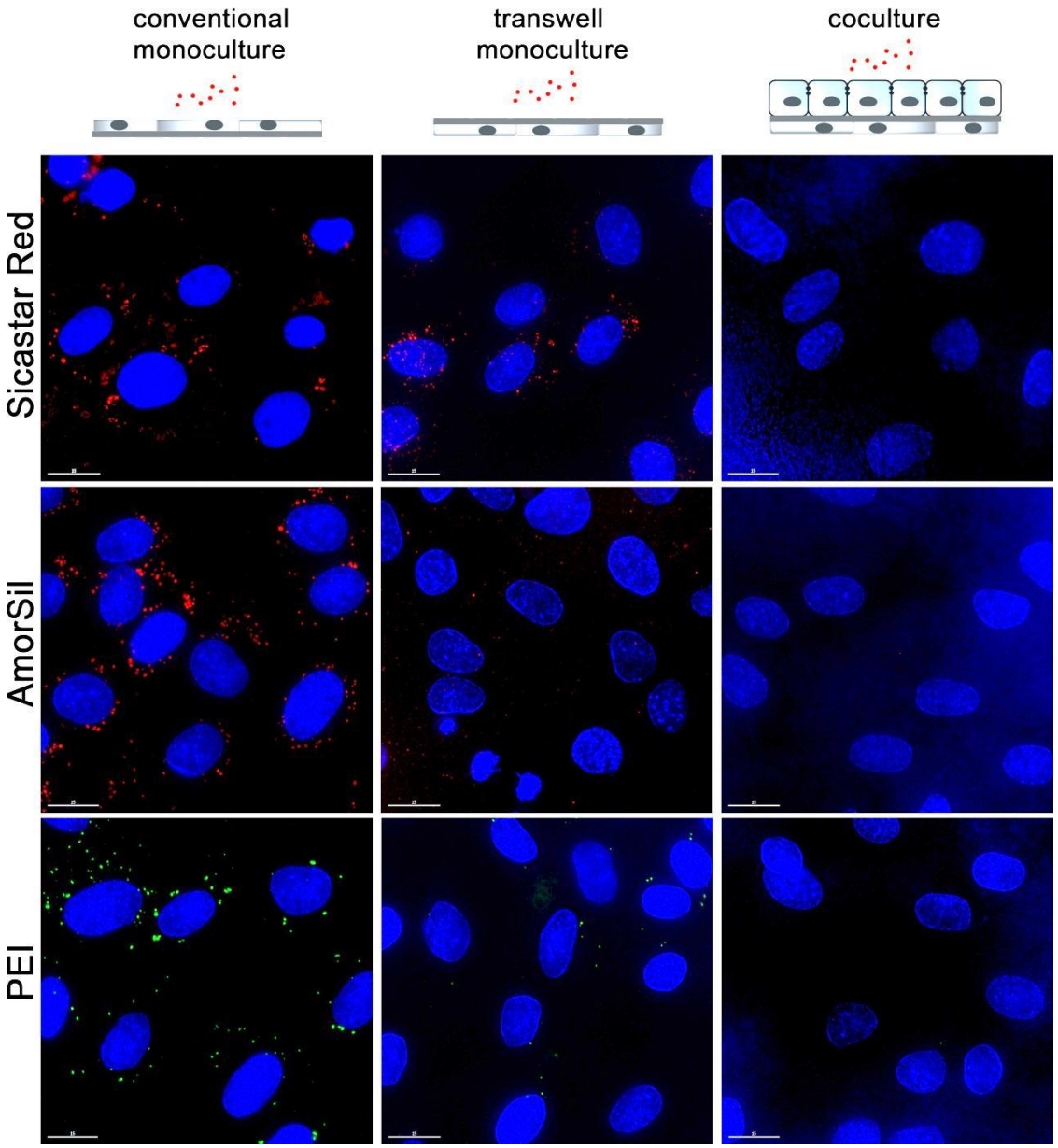

Figure 24: Evaluation of uptake of apically applied NPs (Sicastar Red: 60 µg/ml), AmorSil: 300 µg/ml and PEI: 2.5 µg/ml) ***Left column:*** *ISOHAS-1 under conventional monoculture conditions (Incubation for 4h with 20h further cultivation in fresh medium, Sicastar Red: 6 µg/ml, AmorSil: 300 µg/ml and PEI: 2.5 µg/ml),* ***middle and right column:*** *ISO-HAS-1 under different coculture conditions (Incubation time: 48h, Sicastar Red: 60 µg/ml, AmorSil: 300 µg/ml and PEI: 2.5 µg/ml, left column: ISO-HAS-1 in conventional monoculture, middle column: ISO-HAS -1 as monoculture under coculture conditions, right column: ISO-HAS-1 in coculture with H441). Images were taken by means of a fluorescent microscope (DeltaVision, Applied Precision), nuclei are stained using Hoechst 33342 (blue), scale bar: 10 µm*

3.8 Examination of endosomal uptake routes of NPs

To examine endosomal uptake, three different fluorescence-labelled nanomarteials were used: 1. aSNP: Sicastar Red (6µg/ml), 2. organosiloxane: AmorSil (100 µg/ml) and 3. polyethyleneimine: PEI-OG (2.5 µg/ml) using three relevant cell types of the alveolar-capillary barrier (H441, ISO-HAS-1, THP-1).

Colocalisation studies of NPs with endosomal marker proteins belonging to the clathrin-mediated or caveolae-mediated endocytosis pathways were performed by means of immunofluorescence staining procedures.

After 20 min of exposure to **aSNP (Sicastar Red)** no definite uptake in endosomes could be observed for all three cell types. The fluorescence signals of the NPs scattered diffusely over the cell, indicating an attachment of the NPs on the cell membrane before initial uptake events may occur (see Figure 25: H441, Figure 28: ISO-HAS-1 and Figure 31: THP-1). After 4h of incubation the Sicastar Red nanoparticles showed a perinuclar distribution (scattered around the nucleus), thus indicating an internalisation of NPs (see Figure 26: H441, Figure 29: ISO-HAS-1 and Figure 32: THP-1). At this time point, endothelial cells (ISO-HAS-1) seem to take up aSNPs to a greater extent than epithelial cells (H441). After 20h of further cultivation a progressive perinuclear accumulation occurred (see Figure 27: H441, Figure 30: ISO-HAS-1 and Figure 33: THP-1). For H441 no colocalisation with endosomal markers after 4h could be observed. By contrast, after 20h of further cultivation the Sicastar Red nanoparticles were clearly enclosed by flotillin-1- and -2-containing vesicles. In the endothelial cell line, ISO-HAS-1, a colocalisation with flotillin-1 and -2 was already visible after 4h (Figure 29), indicating a faster upkake procedure then in epithelial cells. From a morphological viewpoint, the phagocyte cell type, THP-1, took up Sicastar Red aSNP to the greatest and fastest extent (see Figure 31 - Figure 33). Sicastar Red aSNPs could already be detected in flotillin-1- and-2-marked vesicles after 4h in THP-1 (see Figure 32). In fact, after an incubation time of 4h (Figure 32) and 4h with further 20h cultivation (Figure 33) Sicastar Red was found in Cathepsin-D-labelled vesicles of THP-1 cells, which is a marker for late endosomes or lysosomes.

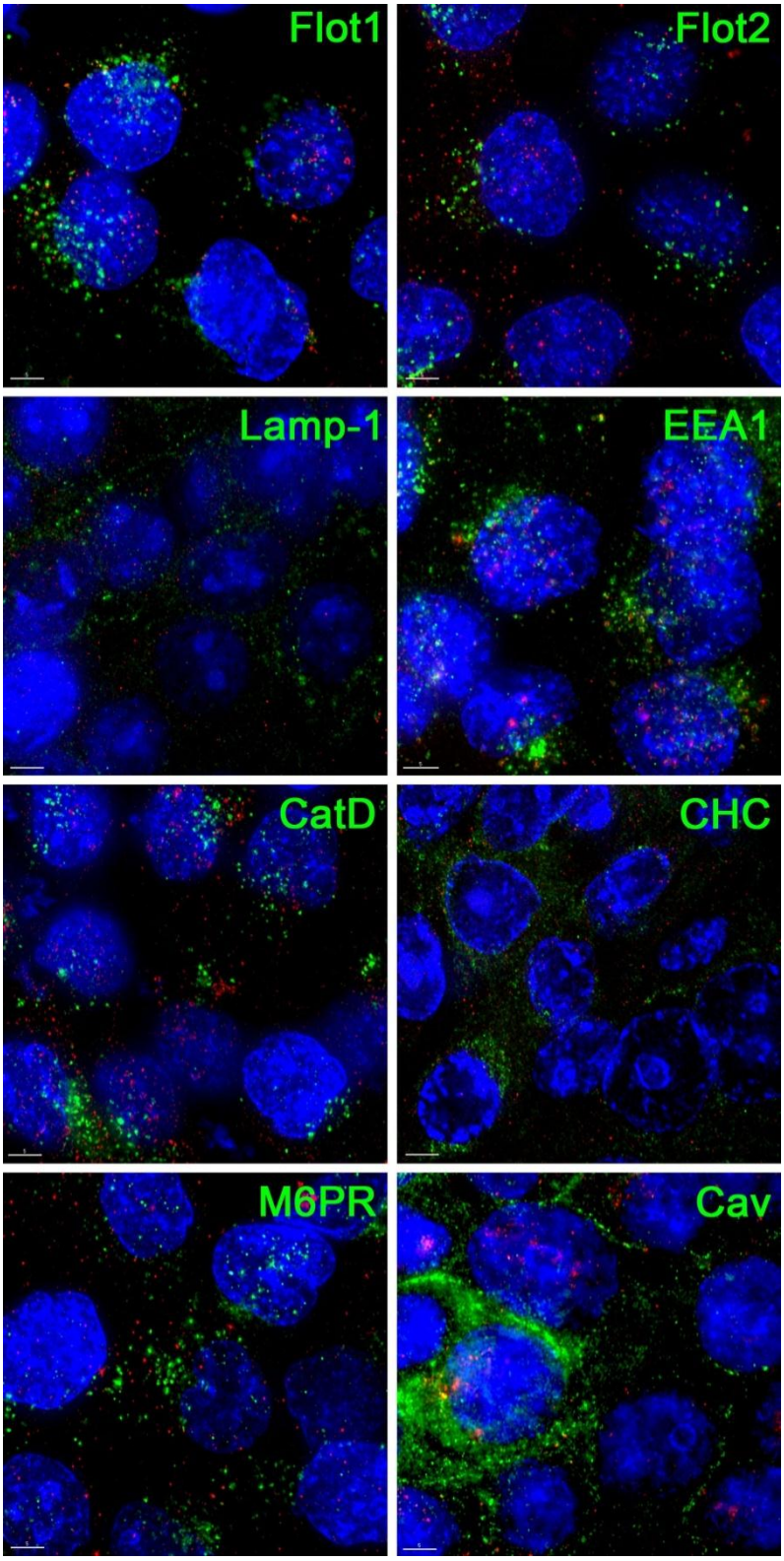

*Figure 25: **H441** incubated with **Sicastar Red** (30 nm) for **20 min** (red). H441 were stained for several endosomal marker proteins (green): Flot1/2: flotillin1/2, Lamp-1: lysosomal-associated membrane protein 1, EEA1: early endosome antigen 1, CatD: cathepsin D, CHC: clathrin heavy chain, M6PR: mannose-6-phosphate receptor, Cav: caveolin-1. No definite uptake in endosomes could be observed for this timepoint. Nuclei are stained using Hoechst 33342 (blue), scale bar: 5 µm*

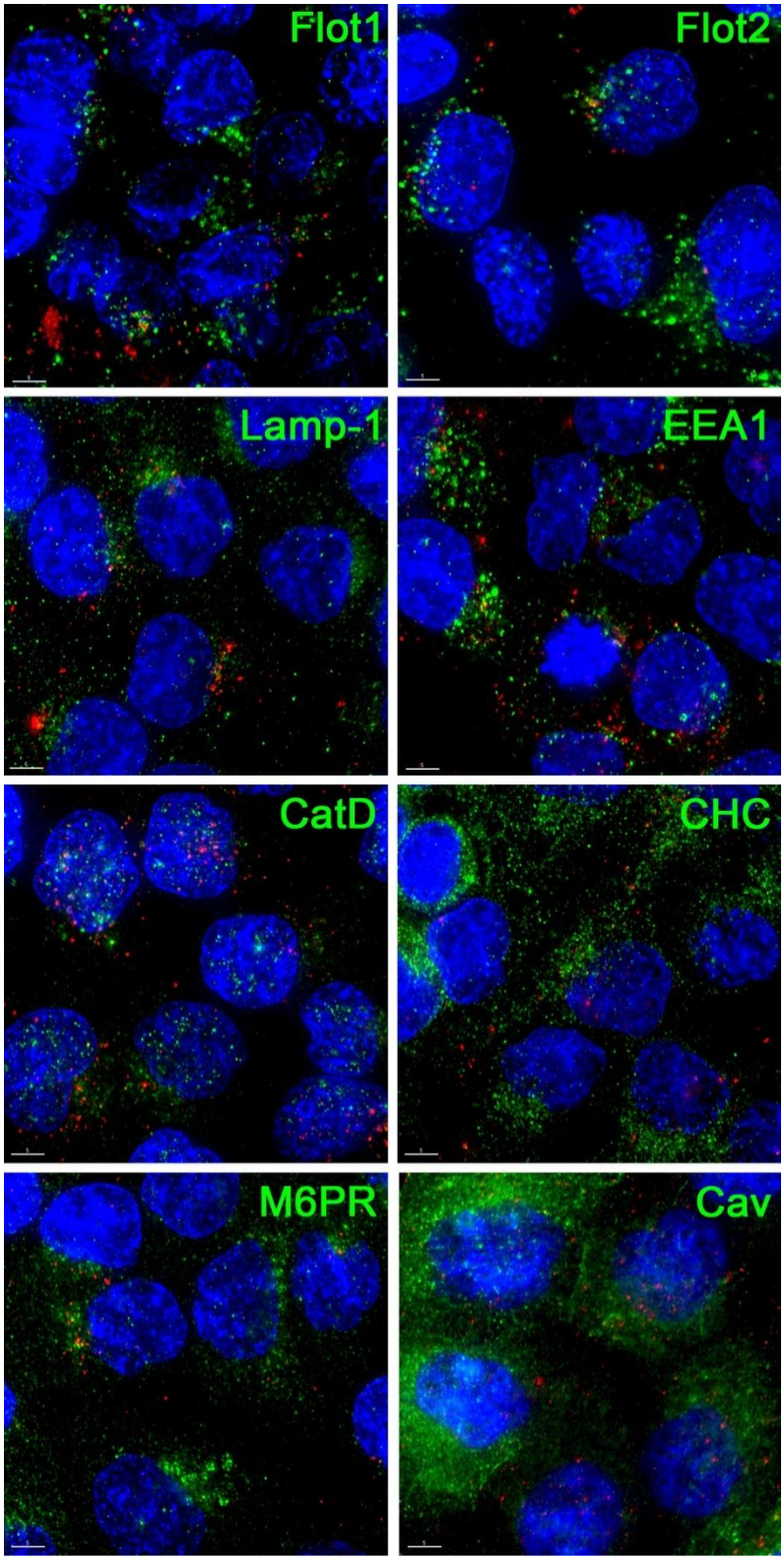

*Figure 26: **H441** incubated with **Sicastar Red** (30 nm) for **4h** (red). H441 were stained for several endosomal marker proteins (green): Flot1/2: flotillin1/2, Lamp-1: lysosomal-associated membrane protein 1, EEA1: early endosome antigen 1, CatD: cathepsin D, CHC: clathrin heavy chain, M6PR: mannose-6-phosphate receptor, Cav: caveolin-1. NPs show a perinuclar distribution, but no definite uptake in endosomes could be observed. Nuclei are stained using Hoechst 33342 (blue), scale bar: 5 µm*

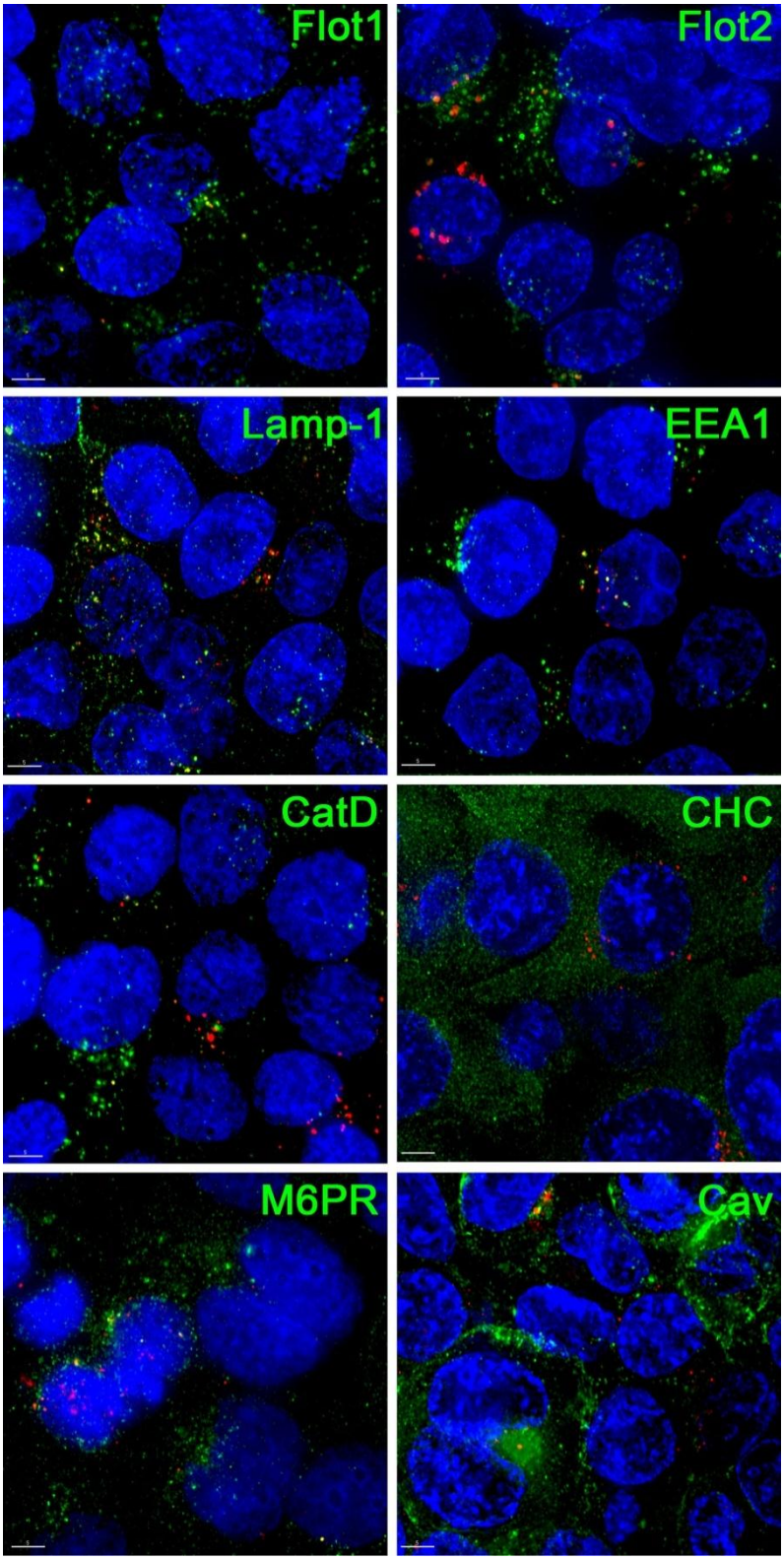

*Figure 27: **H441** incubated with **Sicastar Red** (30 nm) for **4h** and further cultivation of **20h** (red). H441 were stained for several endosomal marker proteins (green): Flot1/2: flotillin1/2, Lamp-1: lysosomal-associated membrane protein 1, EEA1: early endosome antigen 1, CatD: cathepsin D, CHC: clathrin heavy chain, M6PR: mannose-6-phosphate receptor, Cav: caveolin-1. NPs are clearly enclosed by flotillin-1- and -2-containing vesicles. Nuclei are stained using Hoechst 33342 (blue), scale bar: 5 µm*

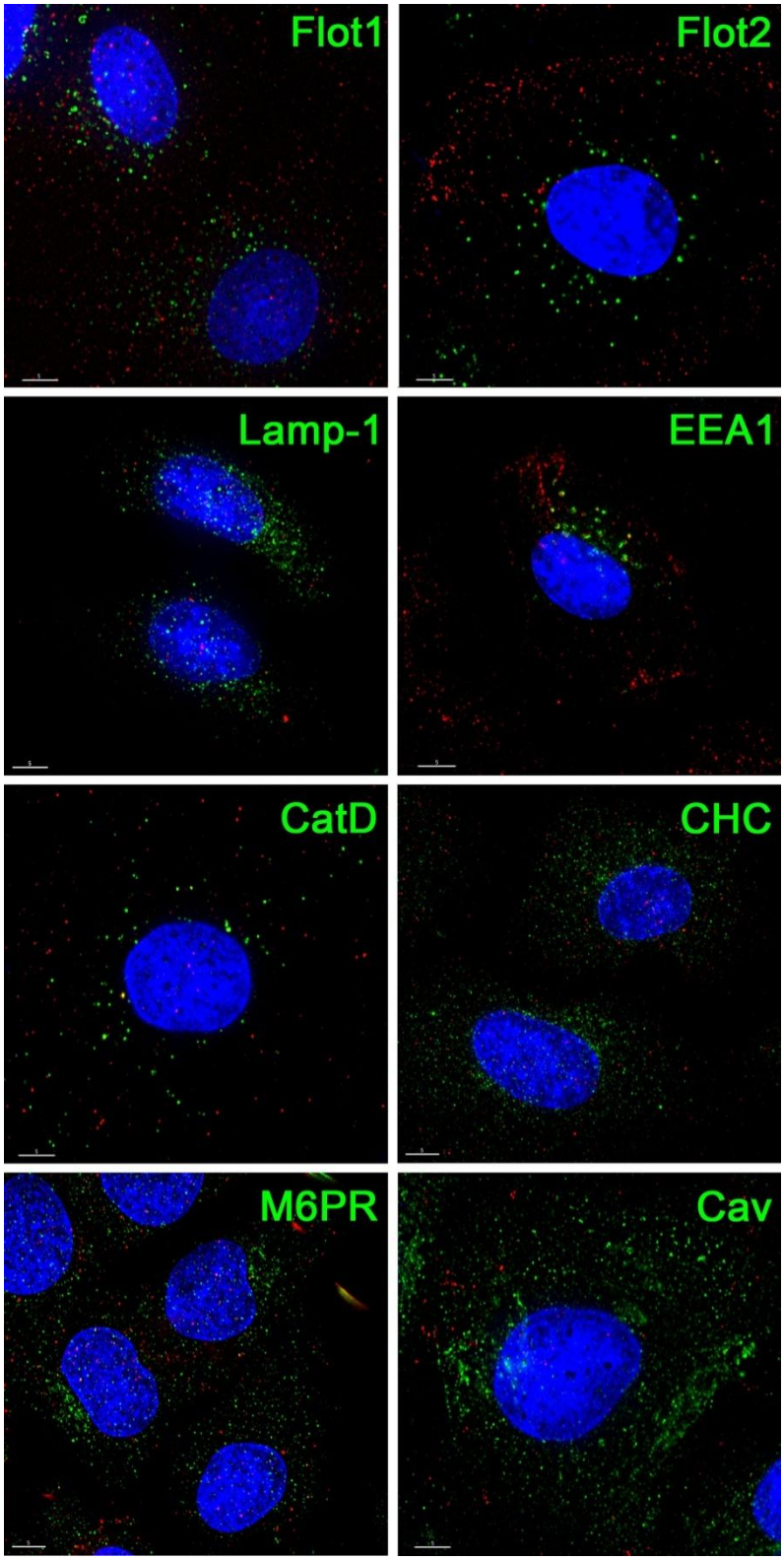

Figure 28: ***ISO-HAS-1*** *incubated with* ***Sicastar Red*** *(30 nm) for* ***20 min*** *(red). Cells were stained for several endosomal marker proteins (green): Flot1/2: flotillin1/2, Lamp-1: lysosomal-associated membrane protein 1, EEA1: early endosome antigen 1, CatD: cathepsin D, CHC: clathrin heavy chain, M6PR: mannose-6-phosphate receptor, Cav: caveolin-1. No definite uptake in endosomes could be observed for this timepoint. Nuclei are stained using Hoechst 33342 (blue), scale bar: 5 µm*

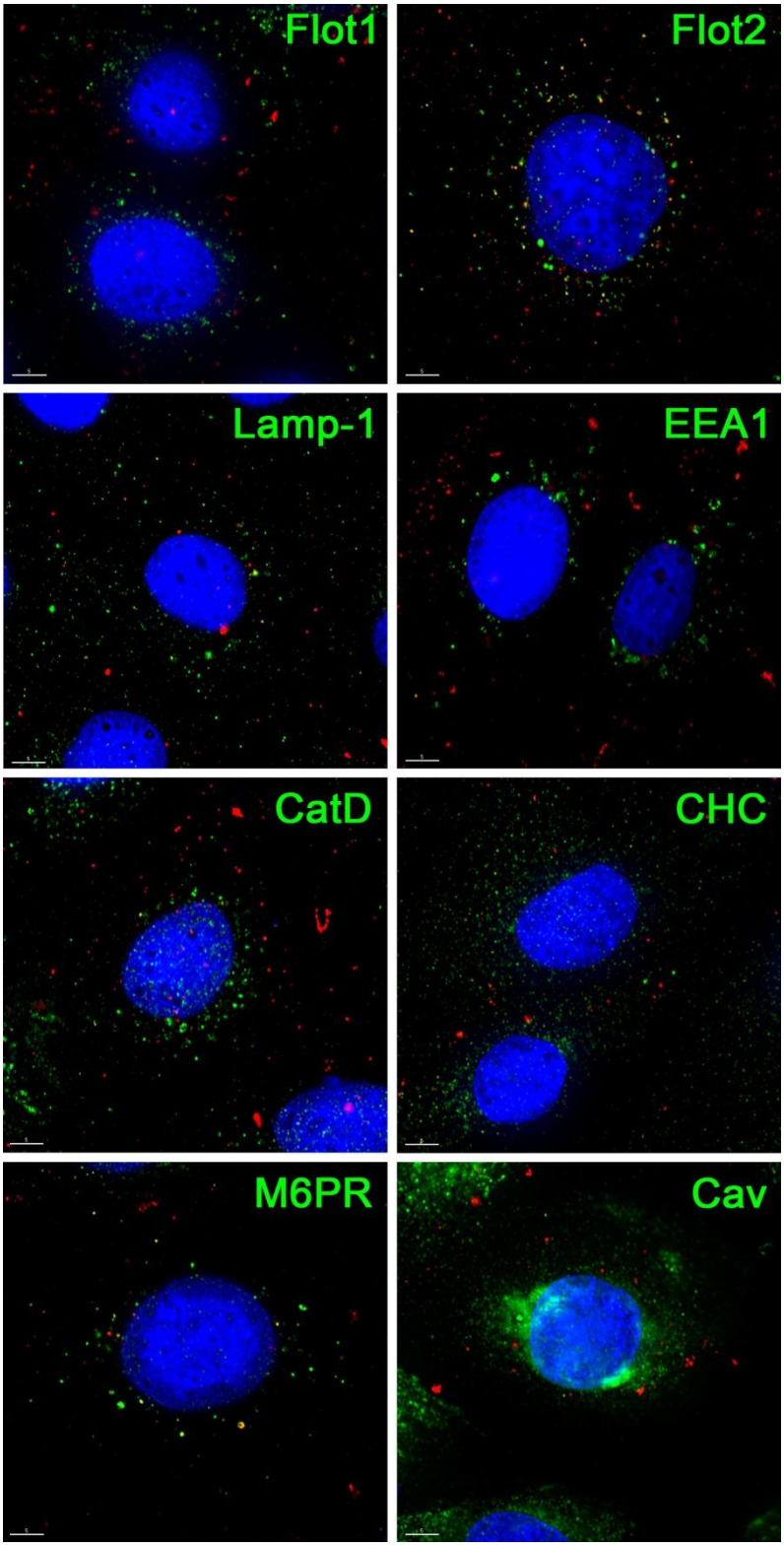

*Figure 29: **ISO-HAS-1** incubated with **Sicastar Red** (30 nm) for **4h** (red). Cells were stained for several endosomal marker proteins (green): Flot1/2: flotillin1/2, Lamp-1: lysosomal-associated membrane protein 1, EEA1: early endosome antigen 1, CatD: cathepsin D, CHC: clathrin heavy chain, M6PR: mannose-6-phosphate receptor, Cav: caveolin-1. Colocalisation with flotillin-1 and particularly -2 is observed. Nuclei are stained using Hoechst 33342 (blue), scale bar: 5 µm*

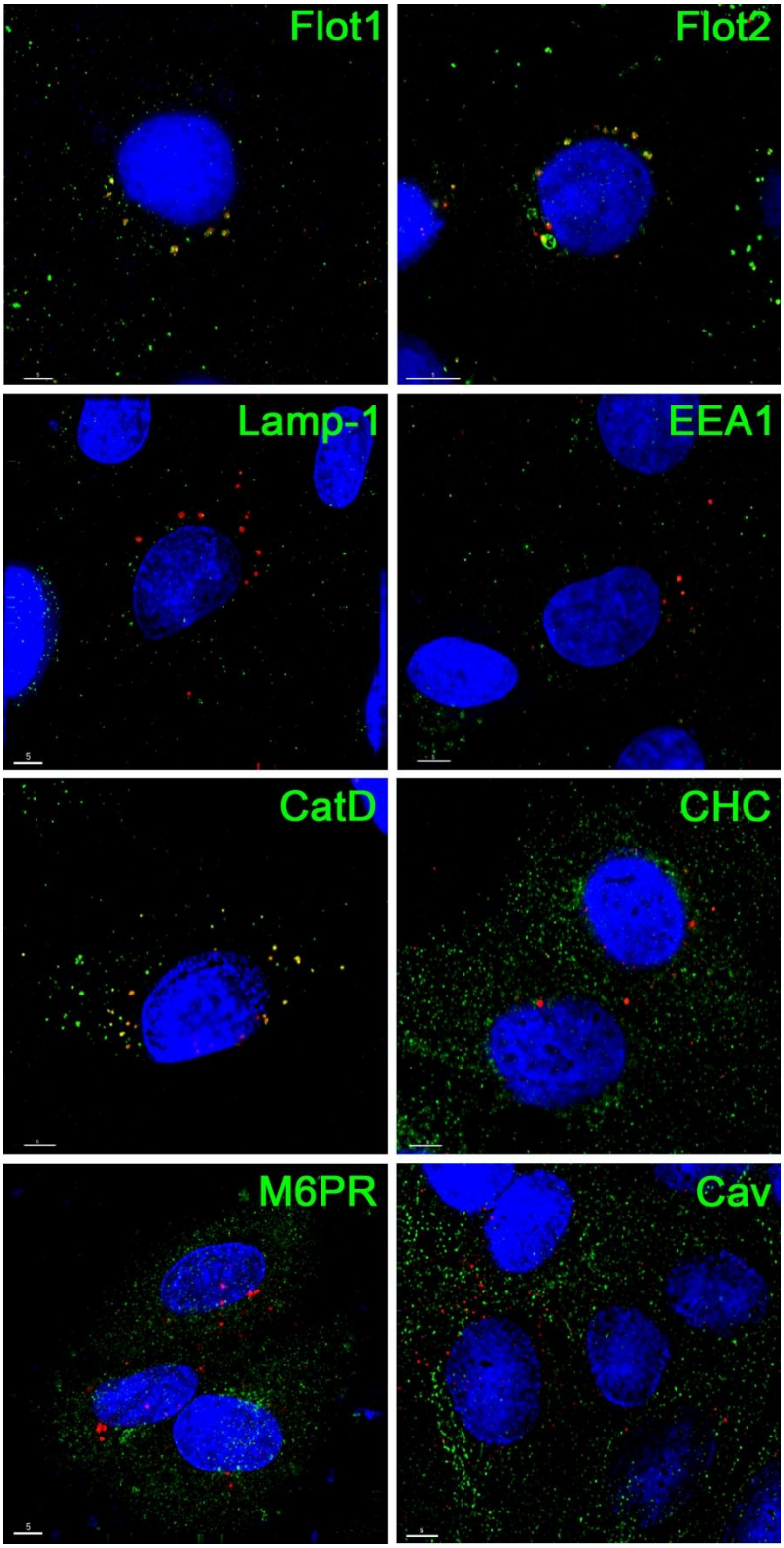

*Figure 30: **ISO-HAS-1** incubated with **Sicastar Red** (30 nm) for **4h** and further cultivation of **20h** (red). Cells were stained for several endosomal marker proteins (green): Flot1/2: flotillin1/2, Lamp-1: lysosomal-associated membrane protein 1, EEA1: early endosome antigen 1, CatD: cathepsin D, CHC: clathrin heavy chain, M6PR: mannose-6-phosphate receptor, Cav: caveolin-1. Cocolalisation clearly occurred with flotillin-1/2 and cathepsin D-containing vesicles. Nuclei are stained using Hoechst 33342 (blue), scale bar: 5 µm*

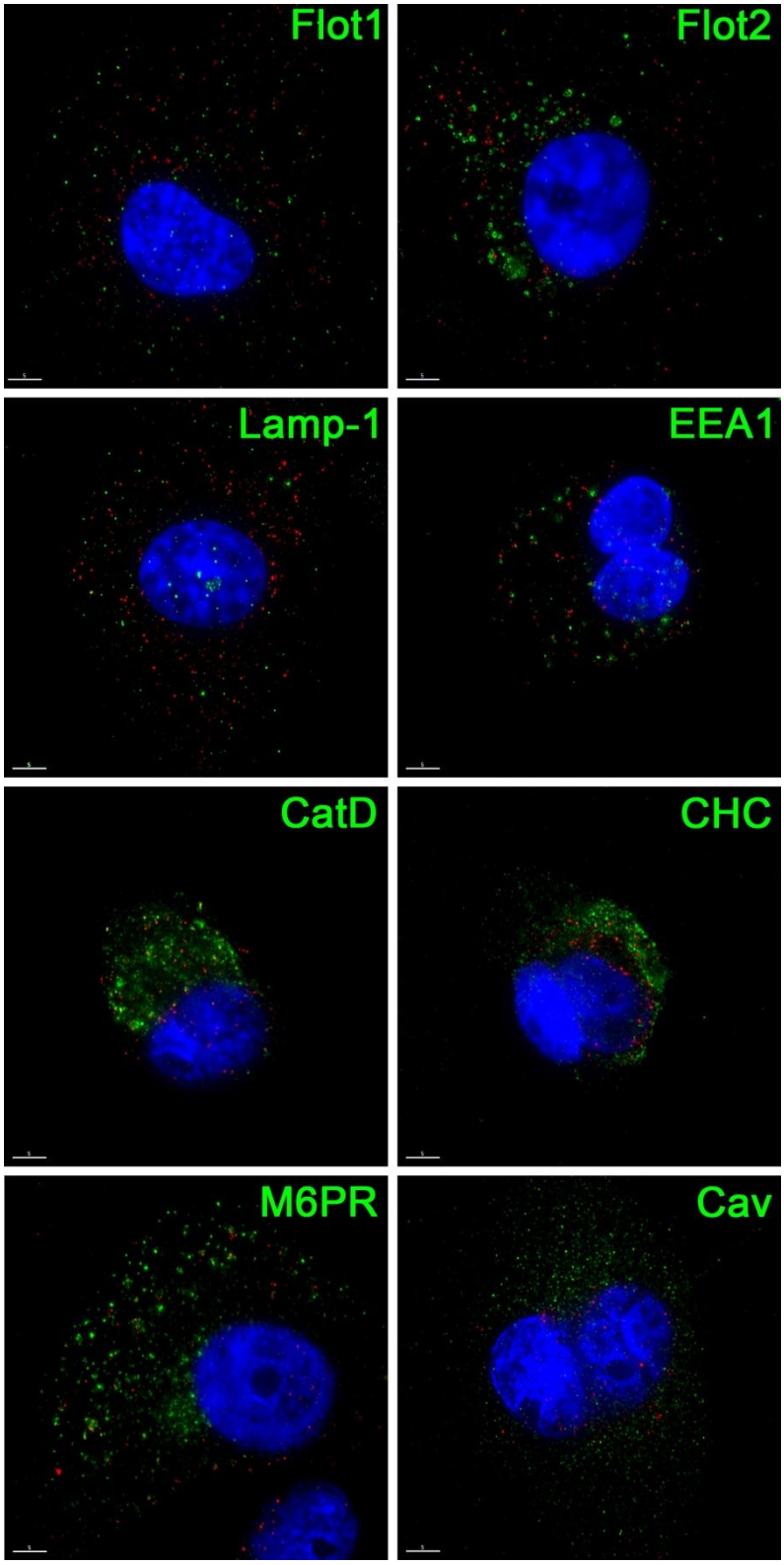

*Figure 31: **THP-1** incubated with **Sicastar Red** (30 nm) for **20min** (red). Cells were stained for several endosomal marker proteins (green): Flot1/2: flotillin1/2, Lamp-1: lysosomal-associated membrane protein 1, EEA1: early endosome antigen 1, CatD: cathepsin D, CHC: clathrin heavy chain, M6PR: mannose-6-phosphate receptor, Cav: caveolin-1. Sicastar Red was partly colocalised with cathepsin-D-labelled vesicles of THP-1 cells, which is a marker for late endosomes or lysosomes. Nuclei are stained using Hoechst 33342 (blue), scale bar: 5 µm*

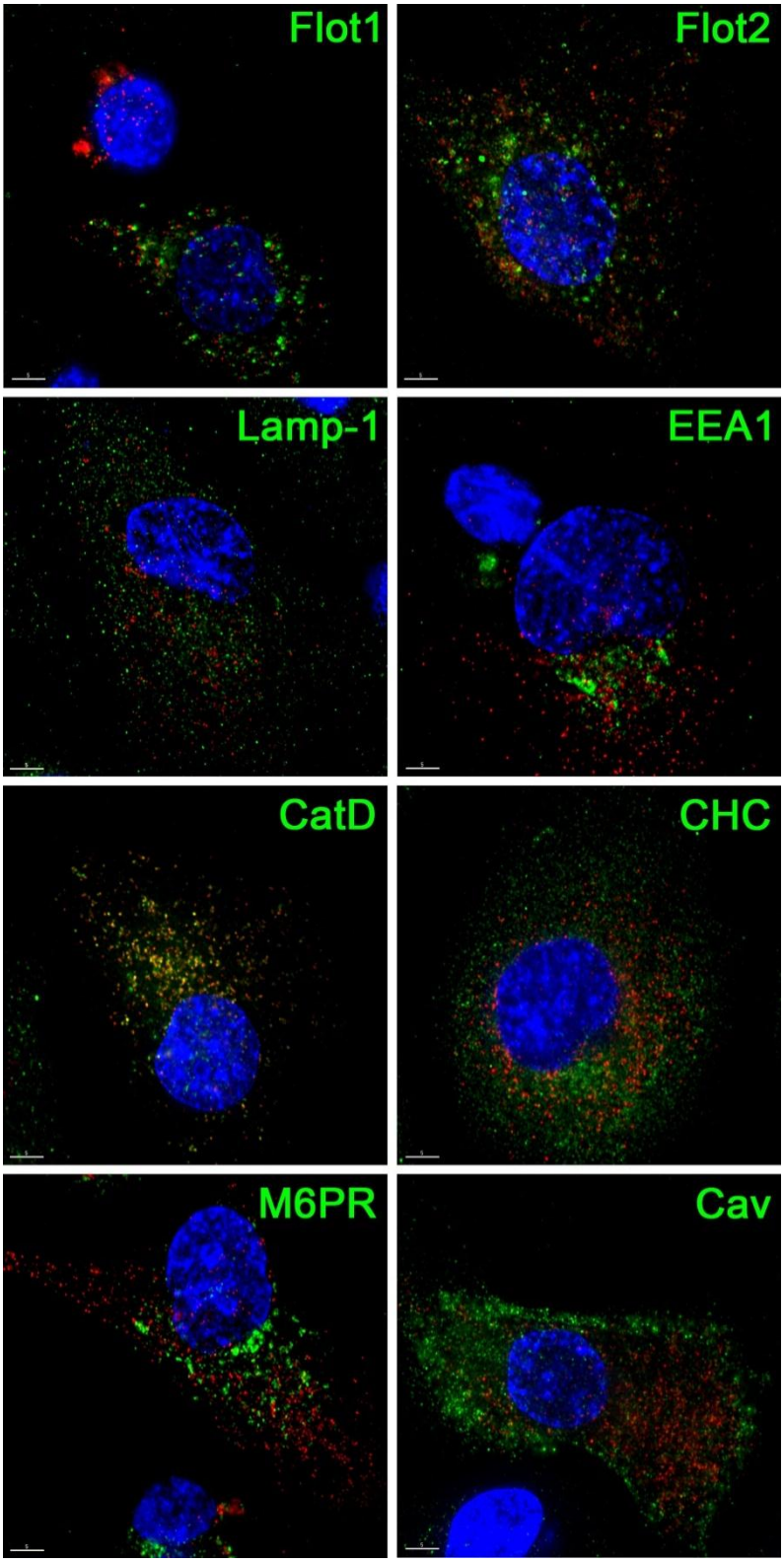

Figure 32: ***THP-1*** *incubated with* ***Sicastar Red*** *(30 nm) for* ***4h*** *(red). Cells were stained for several endosomal marker proteins (green): Flot1/2: flotillin1/2, Lamp-1: lysosomal-associated membrane protein 1, EEA1: early endosome antigen 1, CatD: cathepsin D, CHC: clathrin heavy chain, M6PR: mannose-6-phosphate receptor, Cav: caveolin-1. Sicastar Red was clearly found in cathepsin-D-labelled vesicles of THP-1 cells, which is a marker for late endosomes or lysosomes. Nuclei are stained using Hoechst 33342 (blue), scale bar: 5 µm*

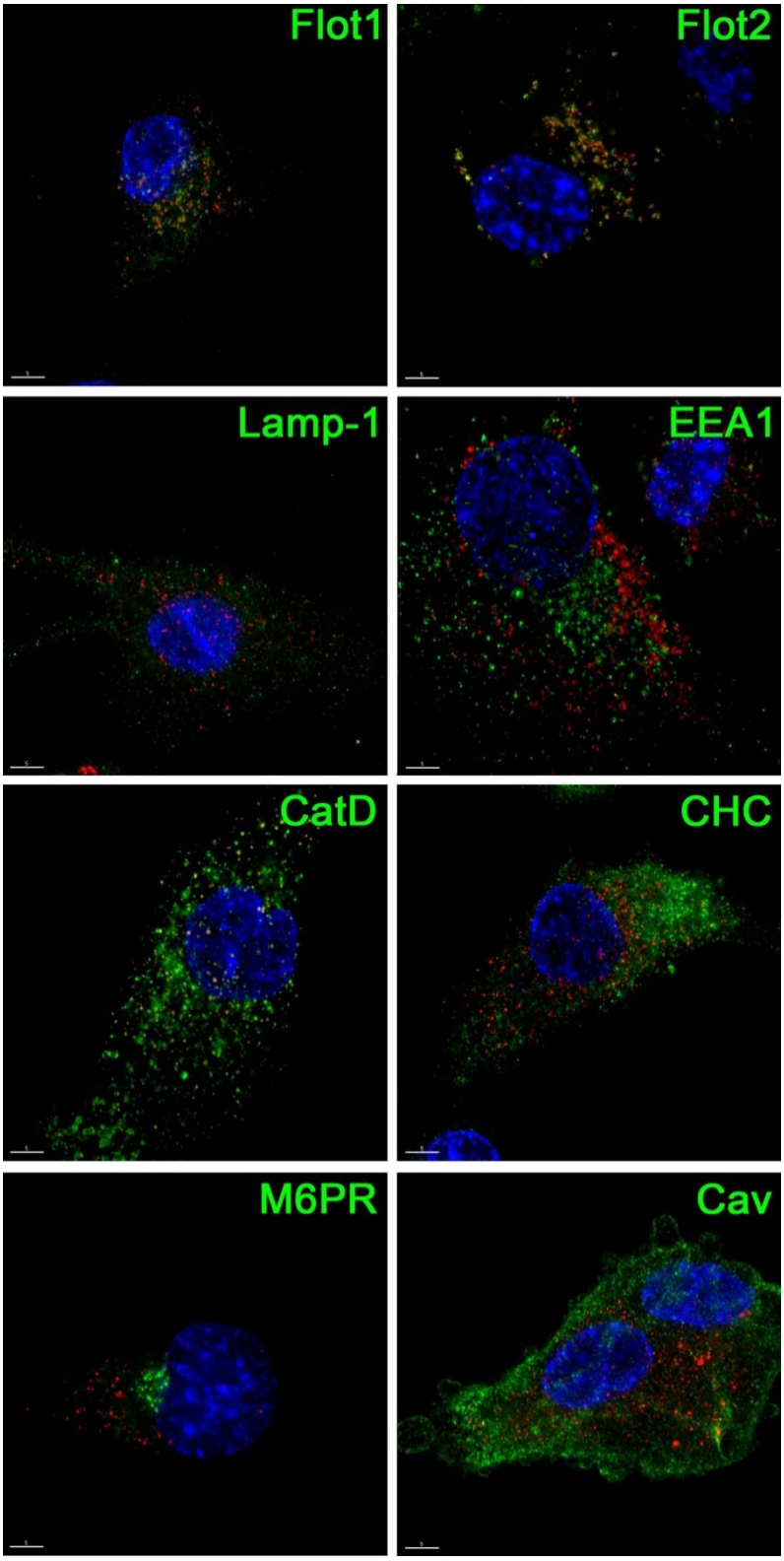

*Figure 33: **THP-1** incubated with **Sicastar Red** (30 nm) for **4h** and further cultivation of **20h** (red). Cells were stained for several endosomal marker proteins (green): Flot1/2: Flotillin1/2, Lamp-1: lysosomal-associated membrane protein 1, EEA1: early endosome antigen 1, CatD: cathepsin D, CHC: clathrin heavy chain, M6PR: mannose-6-phosphate receptor, Cav: caveolin-1. Sicastar Red clearly colocalized with flotillin-1/2- and cathepsin-D-labelled vesicles. Nuclei are stained using Hoechst 33342 (blue), scale bar: 5 µm*

Uptake studies with organosiloxane-NPs (AmorSil) and polyethyleneimine (PEI) revealed similar results to those obtained for Sicastar Red nanoparticles.

For **AmorSil** no colocalisation with endosomal markers for clathrin- and caveolae-mediated pathways could be observed. After 20 min exposure in H441, ISO-HAS-1 and THP-1 the fluorescent signals of AmorSil scatters diffusely throughout the cells, no clear internalisation occurred at that time point (data not shown). After 4h exposure a perinuclear distribution was observed in all cell types. Furthermore, an incorporation of AmorSil NPs in flotillin-1- and -2-bearing vesicles of H441, ISO-HAS-1 and THP-1 was detected. After 20h of further cultivation Amorsil is found in flotillin-1 and -2 vesicles of all three examined cell types with progressive perinuclear accumulation (Figure 34). Additionally, for H441 and THP-1 a cocolalisation with cathepsin-D labelled vesicles was detected. For THP-1 AmorSil nanoparticles were also colocalized with the late endosomal marker, lamp-1.

After 20 min of exposure Oregon-Green-labelled **polyethyleneimine (PEI)** nanoparticles distributed in the same manner as Sicastar Red and AmorSil, with no colocalisation being detected with the endosomal markers chosen (data not shown). After 4h incubation as well as for the further 20h cultivation, the PEI nanoparticles were localised in the cells in a similar fashion to Sicastar Red and AmorSil nanoparticles, that is, primarily distributed in flotillin-1- and -2-labelled endosomes (Figure 34).

These findings show that independent of the different composition of the NPs (silica, organosiloxane or cationic polymers) and the cell types (epithelium, endothelium, phagocytes) used in this study, all NPs target flotillin-1- and -2-containing vesicles in a cell-specific, time-dependent manner. It is important to note that endocytosis via classical uptake mechanisms (clathrin- or caveolae-mediated) could not be verified by means of immunofluorescent labelling of the endosomal marker proteins, clathrin heavy chain or caveolin-1.

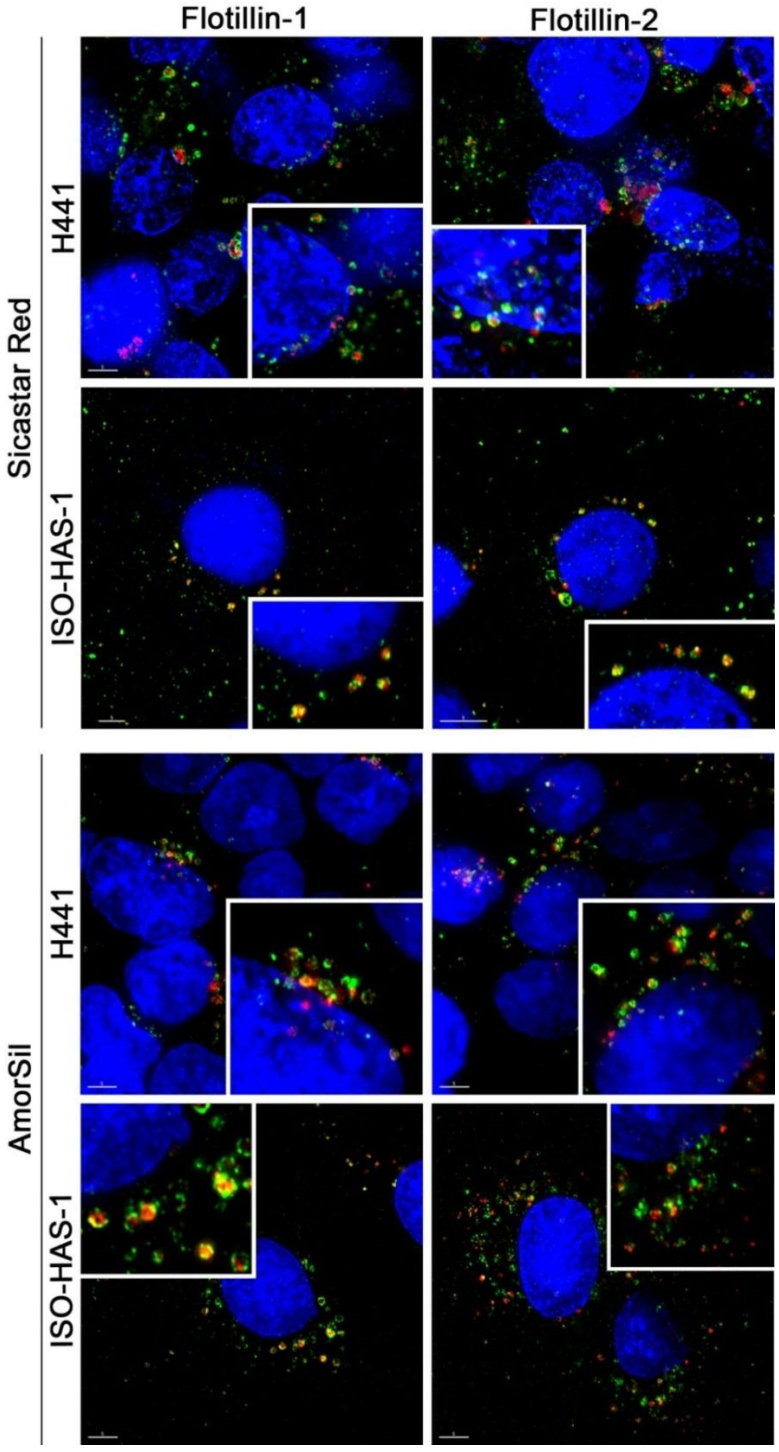

Figure 34: Uptake studies of immunofluorescently stained H441 and ISO-HAS-1 kept in conventional monoculture and exposed to Sicastar Red (6 µg/ml) and AmorSil (100 µg/ml) for 4h and further 20 h cultivation (red signal). A clear incorporation of NPs in flotillin-1- and -2-containing vesicles (green signal) could be detected. Nuclei are stained using Hoechst 33342 (blue), scale bar: 5 µm

To reveal any differences in nanoparticle uptake or trafficking behaviour from conventional monocultures of H441, the same exposure and staining procedures were accomplished with H441 grown in coculture with ISO-HAS-1. As described previously in section 3.7, H441 in coculture internalize NPs to a much lower extent compared to the H441 in monoculture. Therefore, increased exposure times are needed to detect any NP uptake in differentiated cocultures. Colocalisation studies with endosomal marker proteins revealed in principle a similar uptake behaviour for barrier forming H441 as for H441 in conventional monoculture. Although the monoculture of H441 already showed fluorescent signals inside the cells after 4h of incubation, this time period yielded no uptake in cocultures with all three NP types studied. Similar to the findings in the conventional monoculture, no clear uptake in early endosomes (EEA-1, Caveolin-1) was detected in the coculture at all time points chosen. Corresponding to the monocultures, accumulation of Sicastar Red and PEI in flotillin-1- and -2-bearing vesicles occurred after 20 h following the 4h incubation period (Figure 35). AmorSil, however, did not show any colocalisation with endosomal markers in H441 in coculture for all time points chosen.

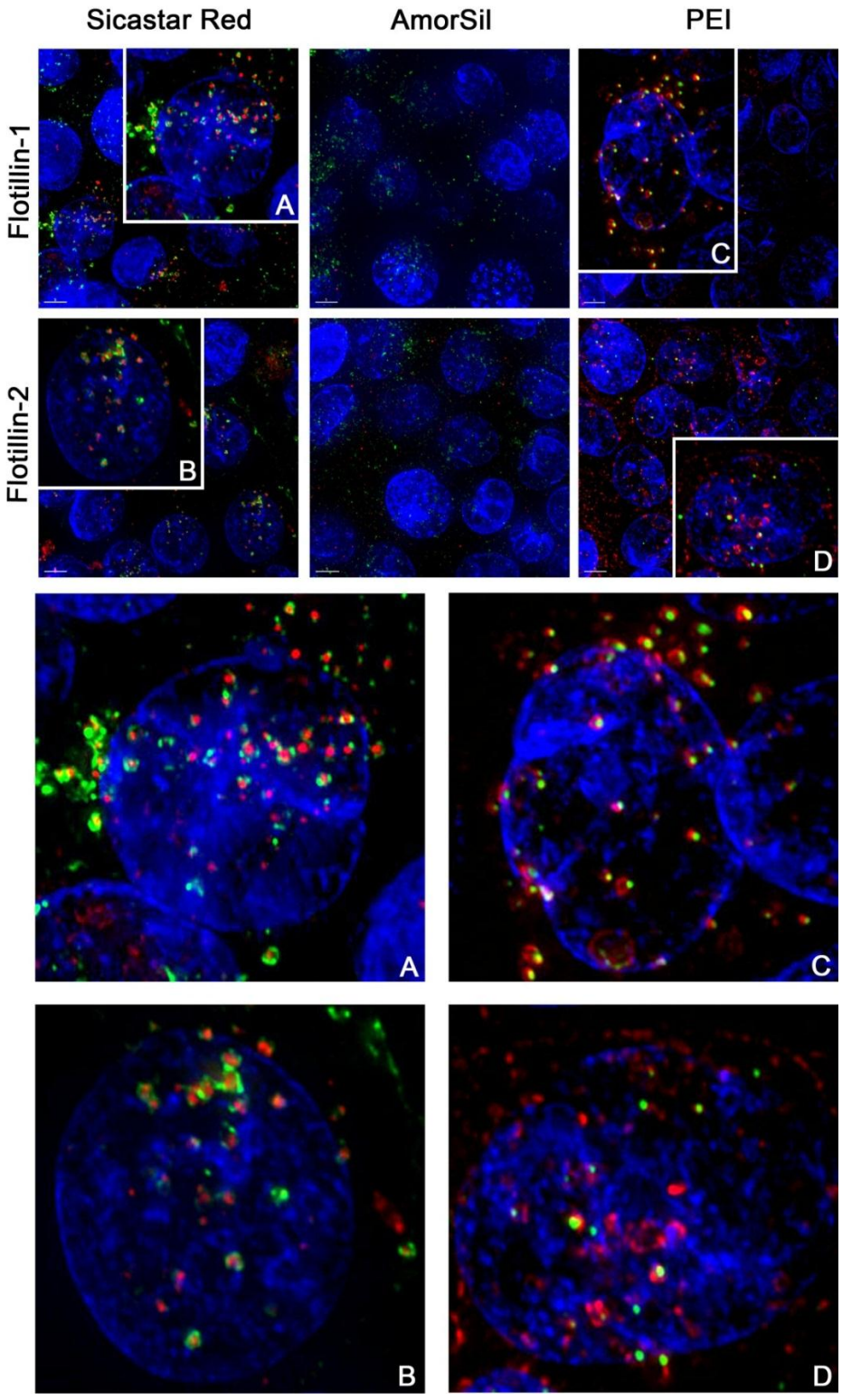

*Figure 35: Uptake studies of IF-stained H441 kept in coculture with ISO-HAS-1 exposed to different nanoparticles (vertical columns: Sicastar Red: 60 µg/ml (red signal), AmorSil: 300 µg/ml (red signal) and PEI: 2.5 µg/ml (green signal) for 4h and further 20 h cultivation). **A**: Sicastar Red (red), flotillin-1 (green), **B**: Sicastar Red (red), flotillin-2 (green), **C**: PEI (green), flotillin-1 (red), **D**: PEI (green), flotillin-2 (red). A clear incorporation of Sicastar Red (Red) and PEI (Green) in flotillin-1 and -2 (green or red) containing vesicles could be detected. Nuclei are stained using Hoechst 33342 (blue), scale bar: 5 µm*

Furthermore as depicted in Figure 36, a counterstaining for flotillin-1 and-2 in Organelle-Lights transfected H441 and ISO-HAS-1 revealed a colocalisation of both flotillins with lysosomes (LAMP-1). This indicates that flotillin-1/2 containing vesicles are a marker for late endosomal structures. A colocalisation with early endosomal structures (small Rho-GTPase Rab5) was not observed (Data not shown).

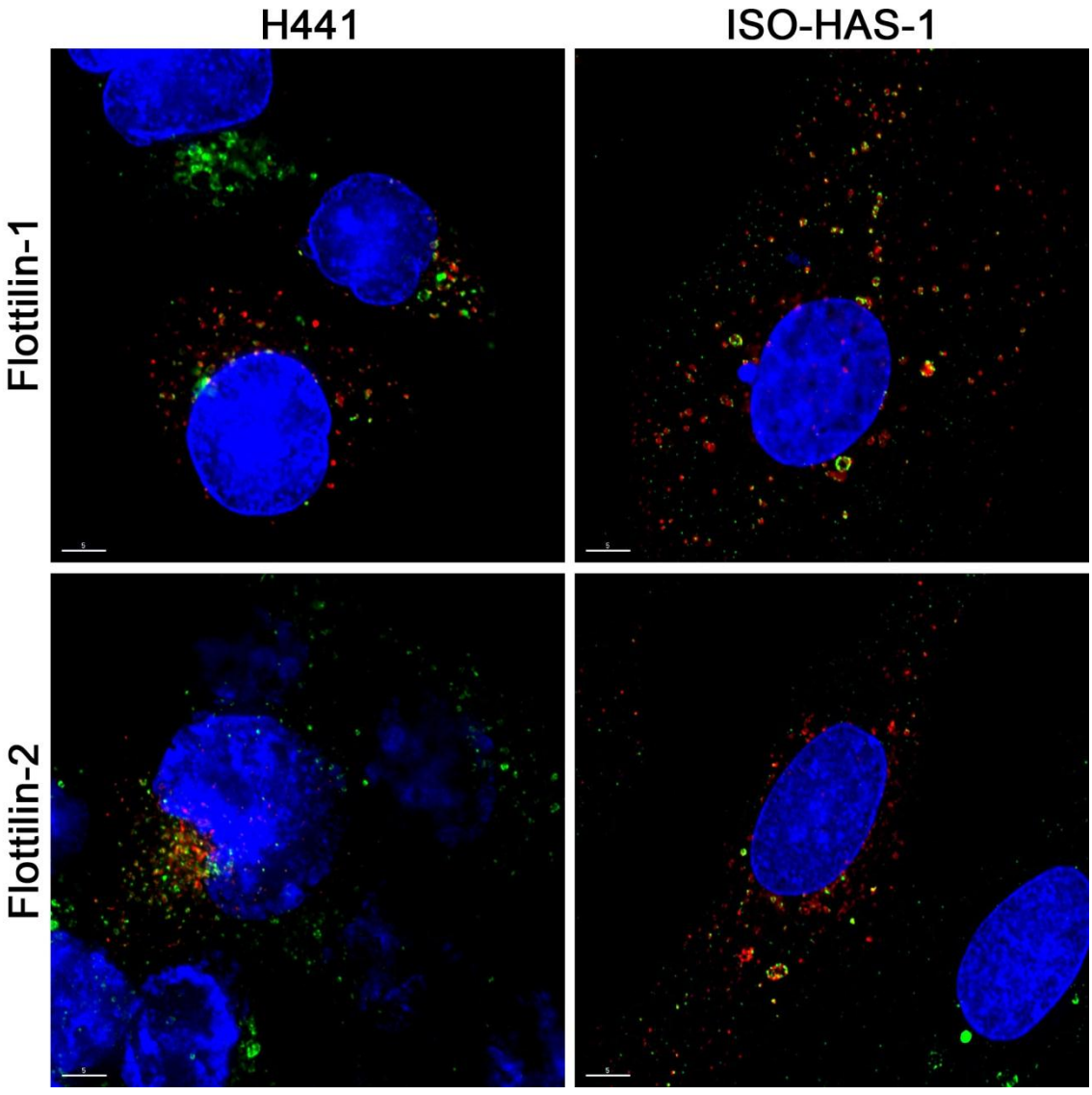

Figure 36: Organelle Lights (lysosomes: red) transfected H441 and ISO-HAS-1 counterstained via immunofluorescence for flotillin1/2 (green). Colocalisation of lysosomes with flotillin-1/2 antibodies is observed in both cell lines H441 and ISO-HAS-1. Nuclei are stained using Hoechst 33342 (blue), scale bar: 5 µm

3.9 Cytotoxicity and uptake of different sized aSNPs

Figure 37 depicts the viability of H441 in conventional monoculture after exposure to different sized aSNPs (Sicastar Red 30 nm, 70 nm, 300 nm) with an incubation period of 4h (Figure 37 A) and 4h followed by 20h recovery in fresh serum-containing media (Figure 37 B). After 4h of incubation, significant differences in cytotoxic effects between the three different sized aSNP were observed (concentration of NPs 150 µg/ml). 30 nm sized aSNPs caused a reduced viability in H441 (77±13% of untreated control) compared to the larger sized aSNPs of 70 nm and 300 nm, which did not show a significant cytotoxic effect (70 nm: 90±15%, 300 nm: 96±10% of untreated control). Higher concentrations (300 µg/ml and 600 µg/ml) illustrate a clearly increased toxicity of the smaller sized aSNPs of 30 nm (300 µg/ml: 23±6%, 600 µg/ml 6.5±2%) compared to the larger sized aSNPs of 70nm (300 µg/ml: 88±18%, 600 µg/ml: 82±20%) and 300 nm (300 µg/ml: 102±7, 600 µg/ml: 102±11%). After a recovery period of 20h in fresh medium the size-dependent differences in cytotoxicity appeared comparable to the 4h incubation. A concentration of 150 µg/ml of 30 nm sized aSNP caused a decreased viability to 32±6% of untreated control, whereas 70 nm (91±14%) and 300 nm (103±7%) did not show a reduced viability. Higher concentrations of aSNPs (300 µg/ml and 600 µg/ml) caused further reduction of viability of H441 cells.

Figure 38 illustrates the LDH release after exposure to different sized aSNPs (Sicastar Red 30 nm, 70 nm, 300 nm) with an incubation period of 4h (Figure 38 A) and 4h followed by 20h recovery in fresh serum-containing media (Figure 38 B). After an incubation of 4h, LDH leakage occurred for the 30 nm aSNP at a concentration of 60 µg/ml (41±12% of lysis control) and reached a peak value at an aSNP concentration of 150 µg/ml (128±16% of lysis control). For 70 nm aSNPs however, a marginal but still significant LDH leakage was observed at a concentration of 150 µg/ml (32±14% of lysis control) and the leakage increased with augmented aSNP concentration and reached a total value at 600 µg/ml (119±11% of lysis control). Incubation with 300 nm aSNPs resulted in a marginal LDH release at a concentration of 600 µg/ml (35±9% of lysis control).

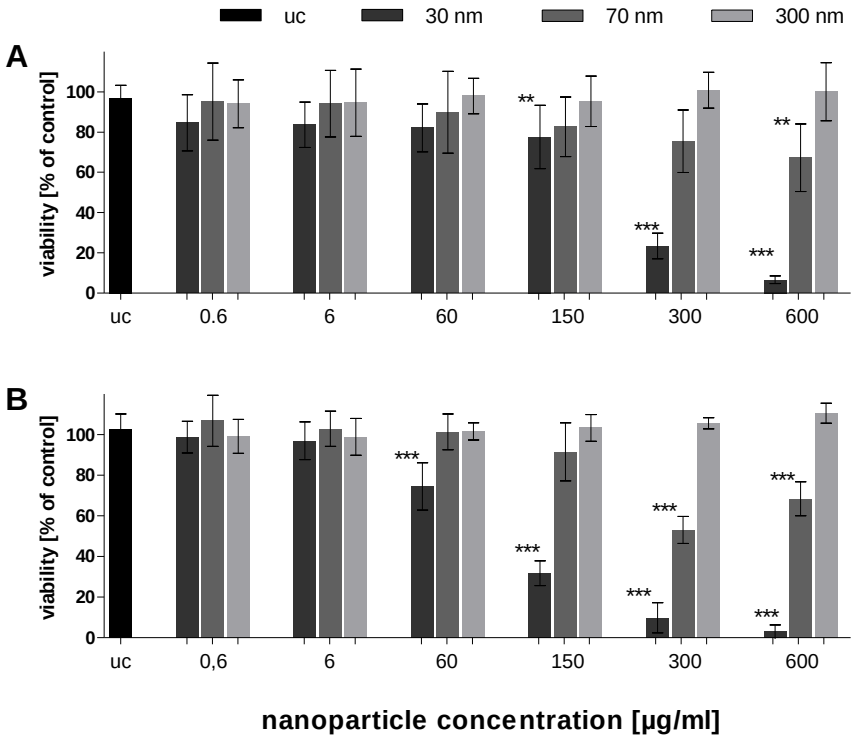

*Figure 37: Viability (MTS assay) of H441 following aSNP treatment with different sized **Sicastar Red** (30 nm, 70 nm, 300 nm). **A:** 4h incubation, **B:** 4h incubation with subsequent cultivation for 20h in fresh medium. Data are depicted as means ± S.D. of 3 independent experiments with n=3 samples for each treatment. For statistical analysis two-way-anova with Bonferroni´s post test was applied. *P <0.05, ** P <0.01 and *** P <0.001 compared to the untreated control (uc). 30 nm sized aSNPs caused a reduced viability in H441 compared to the larger sized aSNPs of 70 nm and 300 nm*

Lower concentrations (300 µg/ml – 0.6 µg/ml) did not have an effect on membrane integrity. Similar results were obtained after the 20h recovery that followed the 4h incubation (Figure 38 B). A concentration of 60 µg/ml of the 30 nm aSNP resulted in a total LDH release (126±7% of lysis control). LDH leakage decreased with increasing aSNP concentration, which is due to cell loss and medium change after the 4h incubation. 70 nm aSNP caused a total LDH release at a concentration of 150 µg/ml (120±9% of lysis control), whereas 300 nm aSNPs merely caused a LDH release of 70±13% (of lysis control) at the highest concentration tested, 600 µg/ml.

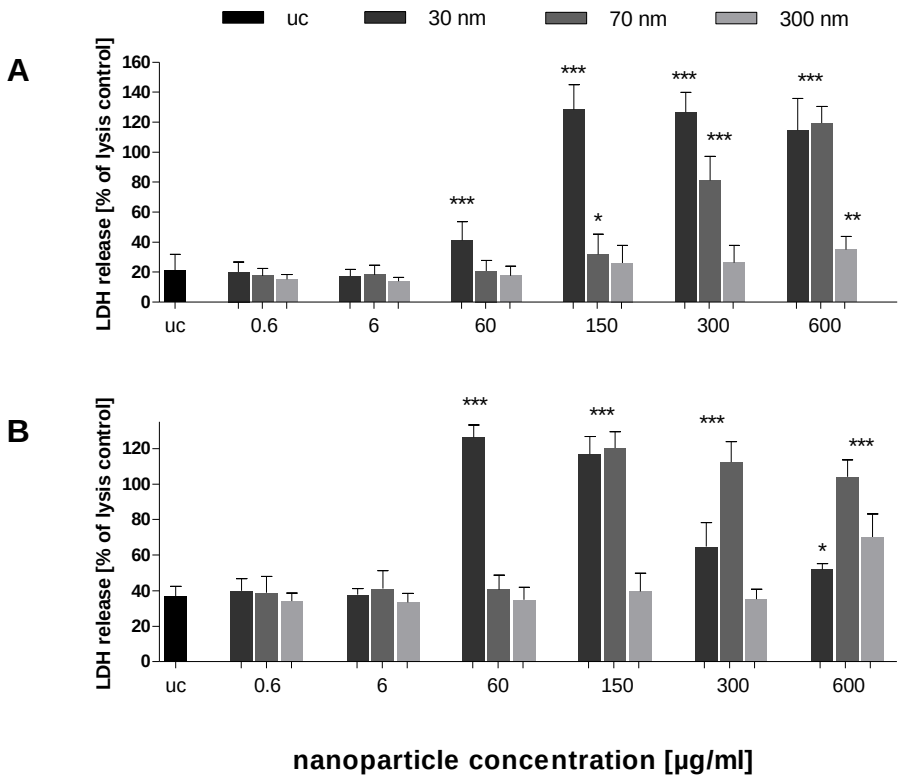

Figure 38: Lactate dehydrogenase release of H441 following aSNP treatment with different sized ***Sicastar Red*** *(30 nm, 70 nm, 300 nm).* ***A:*** *4h incubation,* ***B:*** *4h incubation with subsequent cultivation for 20h in fresh medium. Data are depicted as means ± S.D. of 3 independent experiments with n=3 samples for each treatment. For statistical analysis two-way-anova with Bonferroni´s post test was applied. *P <0.05, ** P <0.01 and *** P <0.001 compared to the untreated control (uc). 30 nm sized aSNPs induce a higher LDH leakage in H441 compared to the larger sized aSNPs of 70 nm and 300 nm*

Figure 39 depicts the uptake and colocalisation with flotillin-1/2-containing vesicles of different-sized aSNPs (30nm, 70 nm, 300 nm). All sizes are incorporated in flotillin-1/2-vesicles.

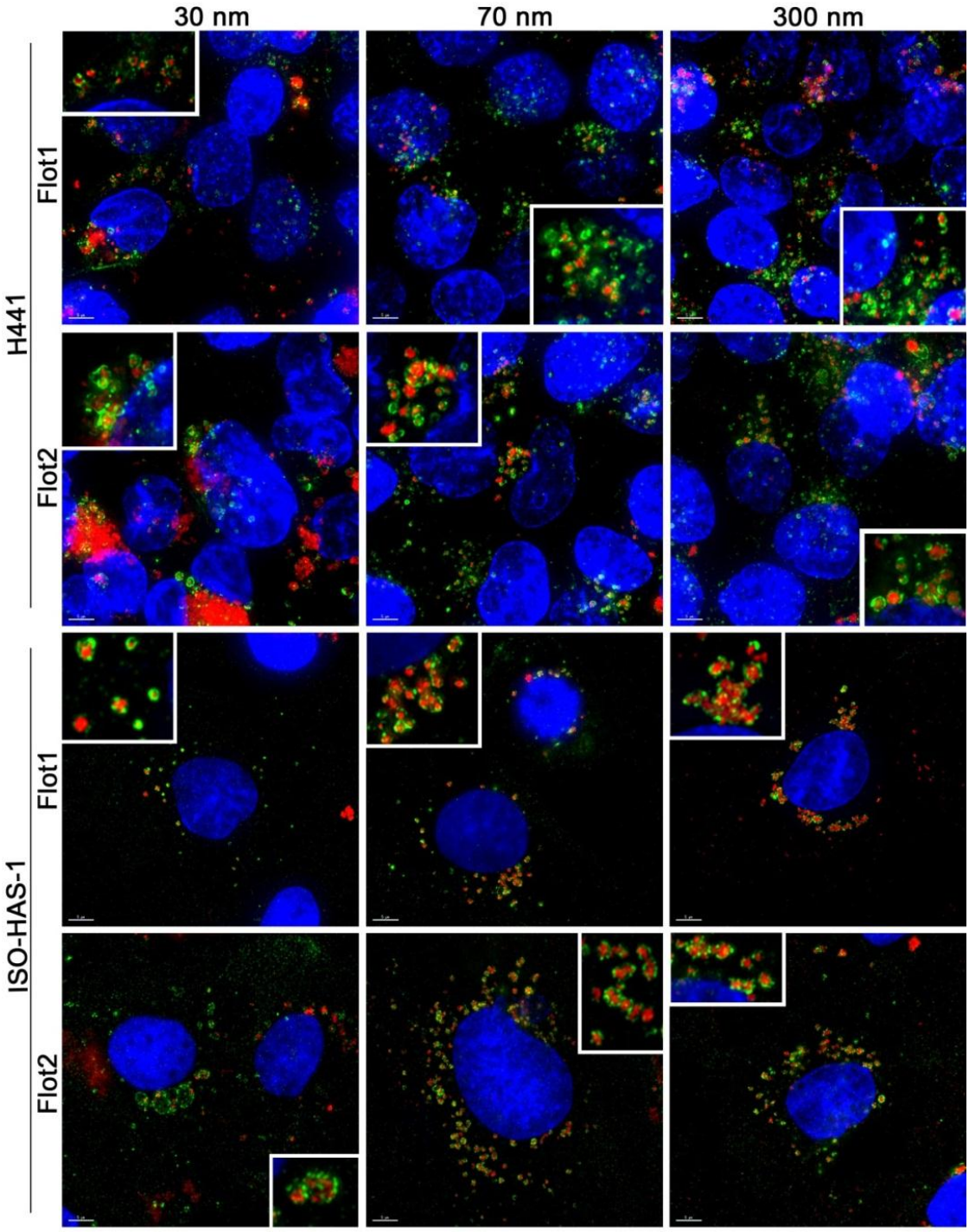

Figure 39: Uptake studies of immunofluorescently (green signal: flotillin1/2) stained H441 and ISO-HAS-1 kept in conventional monoculture and exposed to Sicastar Red (30nm, 70nm, 300nm) for 4h and further 20 h cultivation (red signal). A clear incorporation of NPs in flotillin-1- and -2-containing vesicles (green signal) could be detected for all NP-sizes. Nuclei are stained using Hoechst 33342 (blue). Colocalisation of different-sized aSNPs in flotillin-1/2.-containing vesicles occurred for all NP-sizes. Nuclei are stained using Hoechst 33342 (blue), scale bar: 5 µm

3.10 aSNP exposure on flotillin-1- and-2-depleted cells

To deplete flotillin-1 and -2 in H441, cells were incubated as described in chapter 2.3.3 with siRNA for Silencer® Negative Control #1 which served as a negative control siRNA (neg: non-trageted siRNA) and with Silencer®Select siRNA for flotillin-1 and -2 in combination (F12-depleted). Transfection efficiency was determined via real time-PCR. After 4d the flotillin-1 and-2 RNA amount was determined. Real time-PCR revealed a flotillin-1/2-RNA reduction to 32±9% p<0.01) for flotillin-1 and 31±6% (P<0.01) for flotillin-2 (compared to untransfected control), whereas the negative control (neg) remained unaffected (Flotillin-1: 126±17% and Flotillin-2: 93±15%, p>0.05). Additionally, the fluorescence signal of immunofluorescently labelled flotillin-1/2 decreases in flotillin-1/2-depleted cells compared to untransfected cells (see fluorescence signals in Figure 42). Subsequently and prior to experiments with NPs, cytotoxicity of the transfection procedure was determined via MTS. The viability of cells was not significantly affected after negative (92±16% of untransfected control uc) and flotillin-1/2 (90±18% of untransfected control) siRNA treatment (Figure 40).

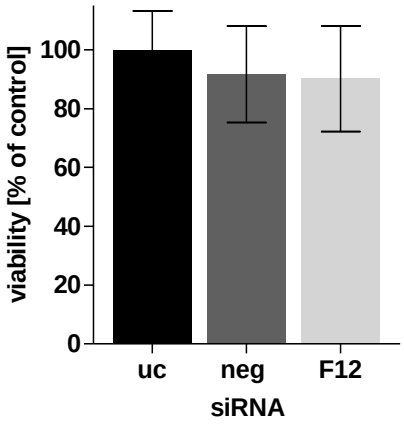

*Figure 40: Cytotoxicity evaluation (MTS assay) of transfected H441 using transfection reagent Genecarrier-1 with siRNAs **neg:** Silencer® Negative Control #1 siRNA and **F12:** Silencer®Select siRNA for flotillin-1 and -2 in combination (siRNA concentration: 50 nM) in comparison to **uc:** untreated control. Data are depicted as means ± S.D. of 2 independent experiments with n=3 samples for each treatment. For statistical analysis one-way-anova with Bonferroni´s post test was applied. *P <0.05, ** P <0.01 and *** P <0.001 compared to the untreated control. No significant cytotoxicity of siRNA tranfected cells could be observed*

After 4 days of *siRNA* transfection of H441 on 96-well plates, cells reached a confluent growth and aSNPs (Sicastar Red) were applied to the cells for 4h in serum-free medium and 4h followed by 20h recovery in fresh FCS-containing medium. Concentrations of aSNP ranged from 6 µg/ml to 300 µg/ml.

After 4h of aSNP exposure, untransfected H441 showed a significantly decreased viability (78±6.8% of untreated control) following Sicastar Red (30 nm) exposure at a concentration of 60 µg/ml (see Figure 41). Viability further decreased with increasing concentration and reached at a concentration of 300 µg/ml a viability of 66±5.5%, compared to the untreated control. After a 20h recovery period with fresh FCS-containing medium, the H441 exposed to 60 µg/ml aSNP recovered and a significant toxic effect (95±14%) was not detected. Concentrations of 100 µg/ml aSNP displayed a similar effect compared to 4h exposure (76±13% vs. 73±9.9%), whereas 300 µg/ml aSNP elicited a further decline in viability (28±8.8%).

Comparing viability of untransfected and transfected cells upon Sicastar Red exposure differences have been detected in a concentration range of 6-300 µg/ml. The non-targeted *siRNA* (neg) did not show any alterations compared to the untransfected cells concerning cytotoxicity after aSNP exposure. Moreover, after an incubation time of 4h, no significant differences between untransfected and flotillin-1/2-depleted aSNP-exposed cells were found. Nevertheless, after the 20h recovery period low, subtoxic concentrations of aSNPs, 6 µg/ml and 60 µg/ml, showed significant variances displaying a reduced viability of flotillin-1/2-depleted cells compared to untransfected cells (see red asterisks in Figure 41).

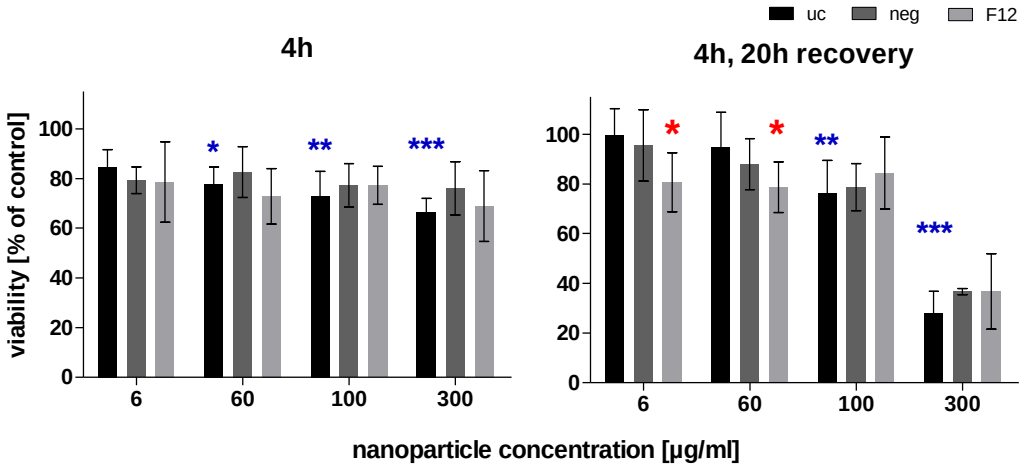

Figure 41: Cytotoxicity (MTS) of flotillin-1- and -2-depleted H441 following aSNP treatment with 6-300 µg/ml ***Sicastar Red*** *(30 nm).* ***uc****: untransfected control (no siRNA treatment),* ***neg:****Silencer® Negative Control #1 siRNA and* ***F12:****Silencer®Select siRNA for flotillin-1 and -2 in combination (siRNA concentration: 50 nM). Data are depicted as means ± S.D. of 3 independent experiments with n=3 samples for each treatment. For statistical analysis two-way-anova with Bonferroni´s post test was applied. *P <0.05, ** P <0.01 and *** P <0.001 compared to the untreated control of the respective siRNA pretreatment. Blue asterisks: "one-way-anova: within the untransfected control", red asterisks: "two-way-anova: within a concentration of aSNP". After 4h exposure and 20h recovery, subtoxic concentrations of 6 µg/ml and 60 µg/ml Sicastar Red showed a significantly reduced viability of flotillin-1/2-depleted cells compared to untransfected cells*

Surprisingly, flotillin-1/2-depleted cells take up less aSNP (Sicastar Red) than untransfected cells according to visual assessment of images taken by a fluorescence microscope (Figure 42). In order to obtain more specific evidence of these findings, uptake of Sicastar Red requires to be quantified. Due to the fact that concentrations of 6 and 60 µg/ml were too low to determine spectrophotometrically the amount of aSNPs taken up by H441, the quantification of internalized aSNP by H441 was conducted by means of intensity measurements of images made by a wide-field fluorescence microscope (personalDV, Applied Precision, Issaquah, USA).

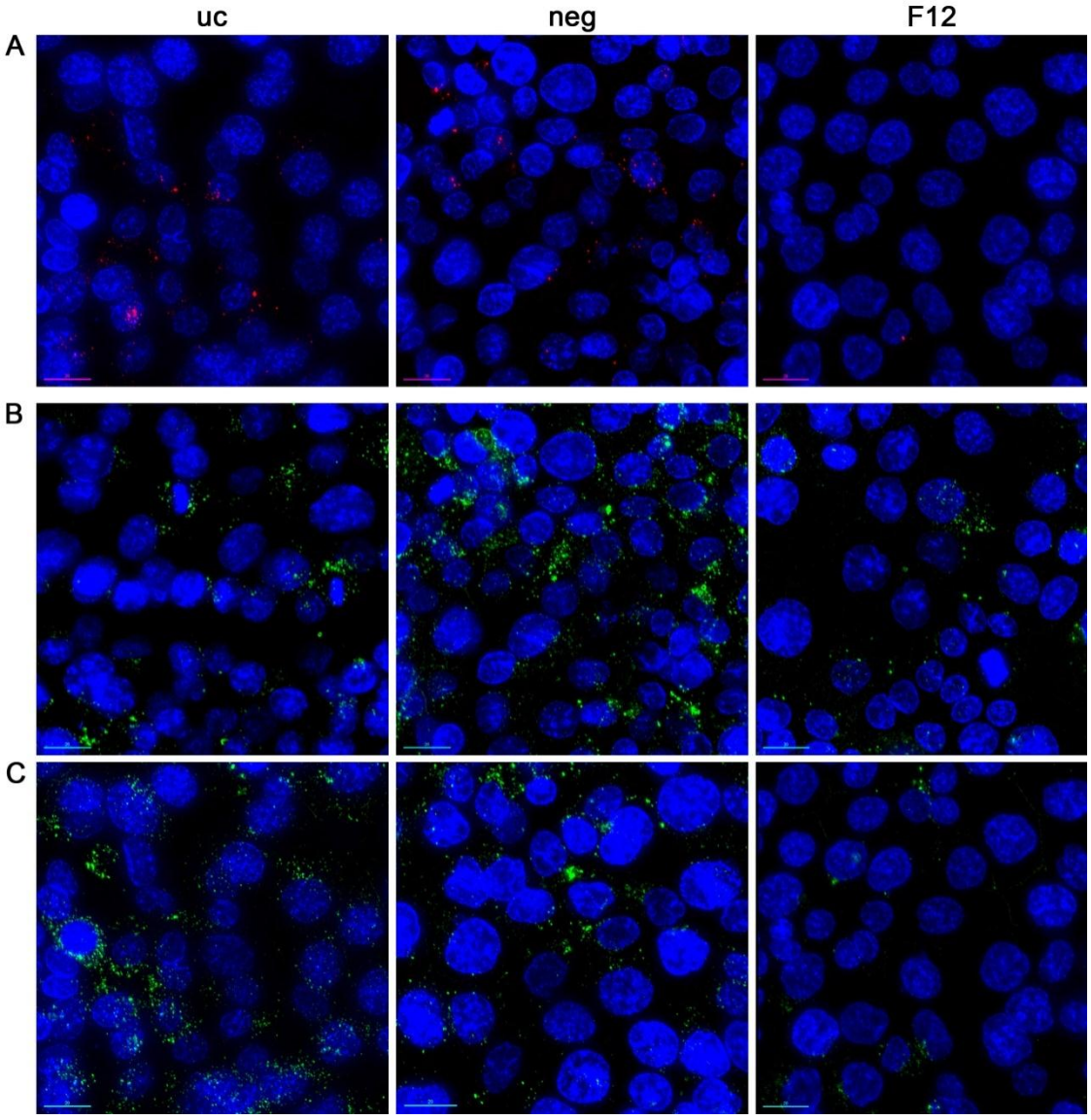

Figure 42: ***A:*** *Fluorescence signal of Sicastar Red (6 µg/ml) exposed to H441 (****uc:*** *untransfected,* ***neg:*** *non-targeted siRNA,* ***F12:*** *siRNA against flotillin-1/2) in conventional monoculture for 4h with further 20 h cultivation in fresh medium. Furthermore, transfected H441 were stained via immunofluorescence for flotillin-1 (****B****) and flotillin-2 (****C****). Pictures were taken by means of an fluorescence microscope (DeltaVision, Applied Precision). For appropriate comparison, exposure time and intensitiy scale was equally adjusted. Flotillin-1/2-depleted cells take up less Sicastar Red than non-targeted siRNA and untransfected cells. Nuclei are stained using Hoechst 33342 (blue), scale bar: 5 µm*

In Figure 43 A the relative fluorescent unit (RFU: related to the untreated control = 1) was determined for the fluorescence signal of Sicastar Red, which was incubated at a concentration of 6 µg/ml with H441 in conventional monoculture. Non-targeted siRNA showed a minor, non-significant reduction of fluorescence intensity (neg: 0.64±0.17%) of incorporated Sicastar incubated for 4h followed by 20h recovery in fresh medium. Flotillin-1/2-depleted cells, however, showed a significant decrease of internalized aSNPs according to RFU-measurements (Flot 12: 0.38±0.13%). Furthermore, quantification studies have been conducted via immunofluorescent staining for flotillin-1/2. RFU measurements of immunofluorescent staining against flotillin-1/2 revealed a significant reduction of flotillin-1 (0.45±0.15%) and flotillin-2 (0.39 ±0.2%) fluorescence signal in flotillin-1/2-depleted H441 cells (Figure 43 B). Non-targeted siRNA transfection resulted in a minor but non-significant reduction of fluorescence intensity of flotillin-1 (0.96±0.2%) and flotillin-2 (0.81±0.13%). In summary, flotillin-1/2 depletion results in a reduction of flotillin-1/2 and a decreased uptake of aSNP. Furthermore, although a decreased uptake of aSNPs in flotillin-1/2-depleted cells was detected an increased toxicity of aSNPs in flotillin-1/2 depleted cells was found.

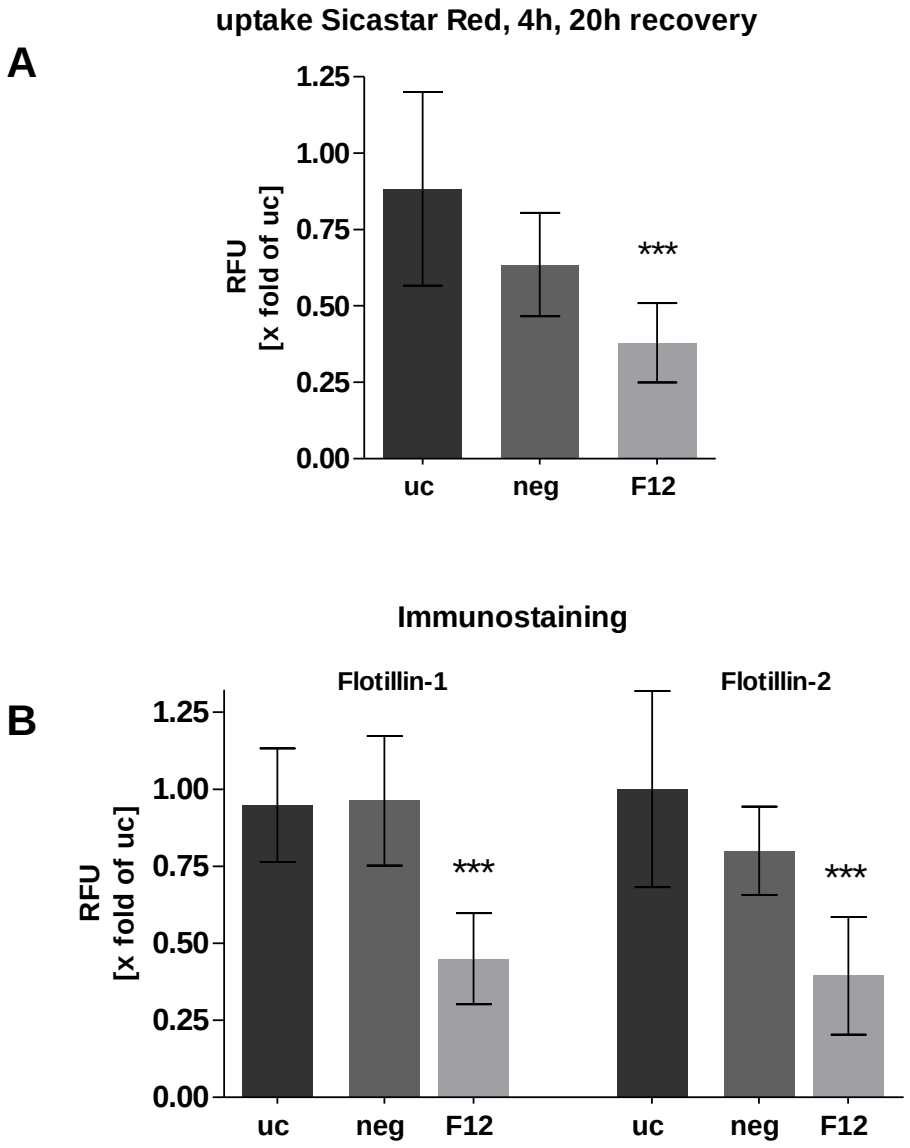

Figure 43: Determination of RFU (relative fluorescent unit related to untranfected control cells) ***A:*** *uptake quantification of aSNP Sicastar Red (6 µg/ml) in H441 (uc: untransfected, neg: treated with non-targeted siRNA, F12: Flotillin-1/2-depleted cells). Exposure time: 4h with further cultivation for 20h in fresh medium.* ***B:*** *Immunofluorescent staining (IF) for flotillin-1/2 and subsequent RFU measurement. Data are depicted as means ± S.D. of 2 independent experiments with n=5-9 images. For statistical analysis one-way-anova with Dunnett´s multiple comparison test was applied with*P <0.05, ** P <0.01 and *** P <0.00. Flotillin-1/2-depleted cells showed a significant reduction of flotillin-1 and flotillin-2 fluorescence signal and a decreased internalization of Sicastar Red compared to non-targeted siRNA and untransfected cells*

3.11 Development of a triple coculture model of the alveolar-capillary barrier

In order to differentiate the monocyte cell line, THP-1, to cells with macrophage features, cells were incubated with PMA (phorbol 12-myristate 13-acetate) at concentrations of 8 nM and 100 nM for 4d. Morphological evaluation of the PMA-treated THP-1 was conducted with a phase contrast microscope (Leica DMI 6000 B). PMA incubation induced cell adherence and spreading (Figure 44).

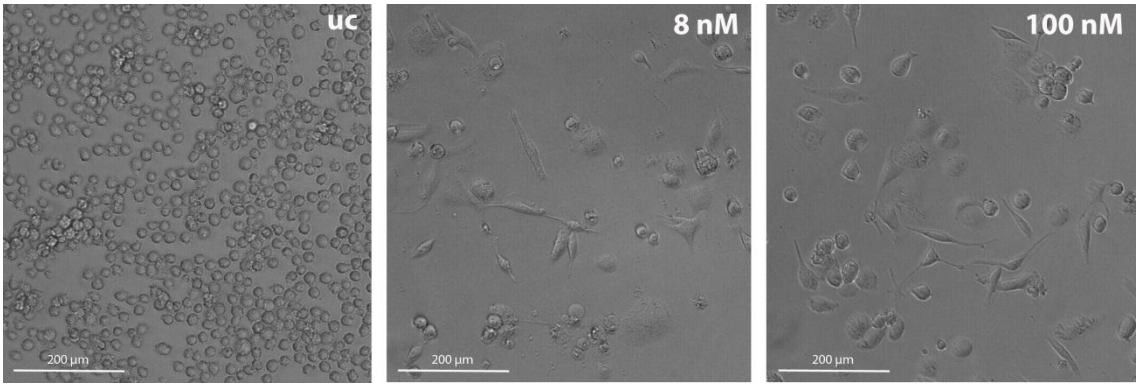

Figure 44: THP-1 monocytes were incubated with 8 nM and 100 nM PMA (phorbol 12-myristate 13-acetate) for 4 days. PMA induced cell adhesion and spreading which indicated the macrophage-like character. The untreated control cells (uc) remained unaltered.

After 4 days of PMA stimulation cells were washed, trypsinized and seeded with varying cell number (2.000, 10.000 and 20.000 THP-1 per coculture-transwell) onto an 8 day-old coculture of H441 and ISO-HAS-1. The coculture of H441/ISO-HAS-1 reaches efficient barrier properties around day 10 of coculture. From day 8 until day 10 (within 2 days of triple coculture), macrophages showed adherence to the epithelial layer. TER (Transepithelial resistance) was measured on day 10 of coculture (= day 2 of triple-coculture). Untreated THP-1 did not affect TER in any case (see Figure 45). Also 8 nM PMA-stimulated THP-1 did not influence the barrier properties of the triple-coculture. TER-values after addition of 20.000 untreated THP-1 cells and THP-1 cells treated with 8 nM PMA remained stable (342±42.8Ω*cm^2 compared to 349±34Ω*cm^2 for controls without THP-1). THP-1 which were pre-stimulated with 100 nM PMA showed a drastic decrease of TER after 48h (2000 THP-1

cells: 259±58.5Ω*cm^2, 10.000 THP-1 cells: 34±8.3Ω*cm^2 and 20.000 THP-1 cells: 18.5±7.8 Ω*cm^2).

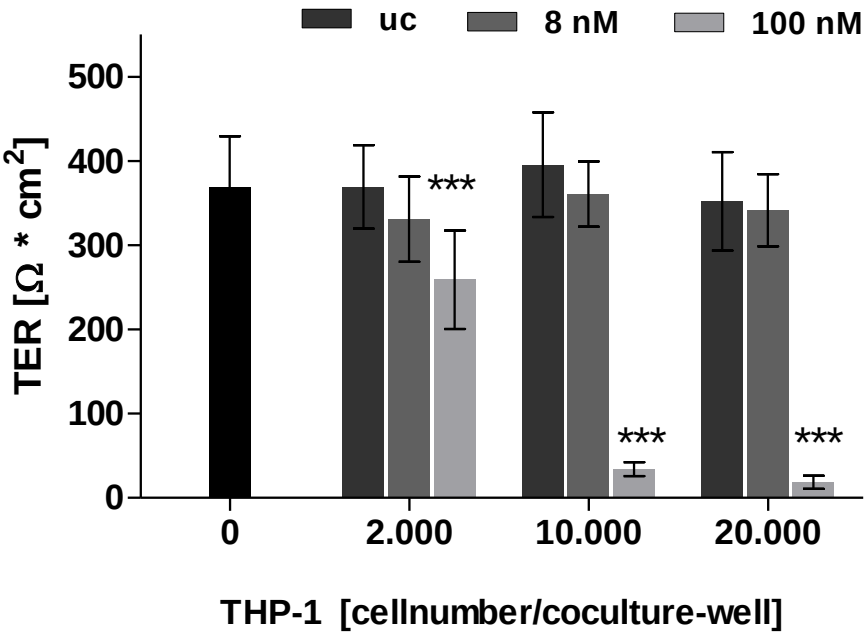

*Figure 45: Transmembrane electrical resistance (TER) was measured for cocultures of H441 with ISO-HAS-1 (H441/ISO-HAS-1) 48h (day 10 for the coculture) after addition of PMA-stimulated THP-1 (0, 2.000, 10.000 and 20.000 cells per coculture-well). THP-1 were stimulated with 8nM and 100nM 4 d prior to seeding on the coculture. Results are shown as means ± S.D. of 2 independent experiments with n=4-6 samples for each treatment. For statistical analysis using two-way-anova with Bonferroni´s post test, the values of the untreated coculture (without THP-1) was used as control. *P <0.05, ** P <0.01 and *** P <0.001. After addition of the highest number of THP-1 cells (20.000 cells) untreated THP-1 and THP-1 cells treated with 8 nM PMA still comparable TER-Values to the controls without THP-1. Treatment with 100nM stimulated THP-1 revealed a cell number-dependent decrease of TER.*

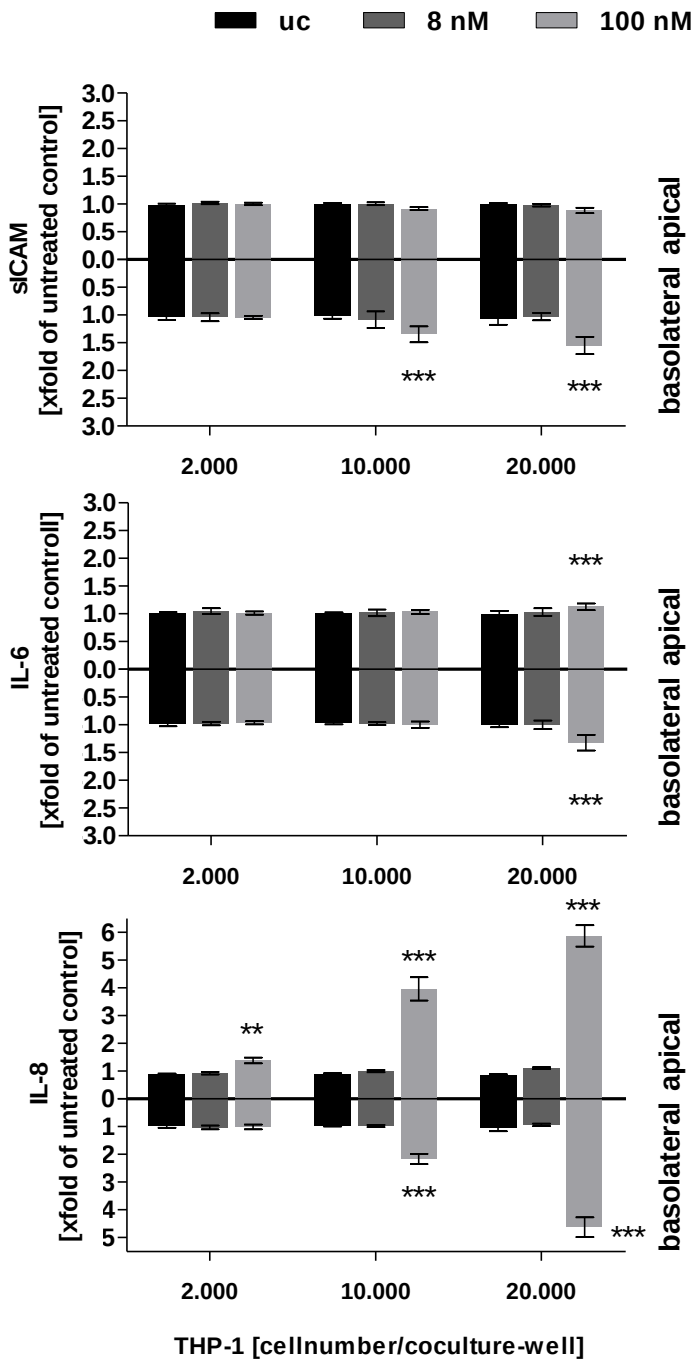

*Figure 46: Soluble intercellular adhesion molecule sICAM-1 and cytokine release (IL-6, IL-8) were measured for cocultures of H441 with ISO-HAS-1 (H441/ISO-HAS-1) (day 10 for the coculture) 48h after addition of PMA-stimulated THP-1 (0, 2.000, 10.000 and 20.000 cells per coculture-well). THP-1 were stimulated with 8nM and 100nM PMA 4d prior to seeding on the coculture. Results are shown as means ± S.D. of 2 independent experiments with n=4 samples for each treatment. For statistical analysis using two-way-anova with Bonferroni´s post test, the values of the untreated coculture (without THP-1) was used as control. *P <0.05, ** P <0.01 and *** P <0.001. Treatment with 100nM stimulated THP-1 revealed a cell number-dependent increase of cytokine release*

Figure 46 shows the release of sICAM-1 and cytokines, such as IL-6 and IL-8, after 48h of THP-1 addition. While untreated and 8nM PMA-stimulated THP-1 did not cause any inflammatory responses of the coculture according to sICAM, IL-6 and IL-8 release, 100nM PMA-stimulated THP-1 affected the coculture significantly. A significantly increased sICAM-level was detected in the basolateral compartment after addition of 100nM PMA-stimulated THP-1 with a cell number of 10.000 cells (1.35±0.15% related to coculture without THP-1) and 20.000 cells (1.5±0.15% related to coculture without THP-1) per coculture-well. Furthermore, addition of 20.000 PMA-treated (100 nM) THP-1 to the coculture resulted in a slight but still significant increase of IL-6 in both apical (1.13±0.06%) and basolateral (1.3±0.14%) compartments. While an apical response (IL-8 release) to 100nM PMA-stimulated THP-1 was already observed for 2.000 THP-1 cells/well (1.4±0.1%), IL-8 release further increased on augmenting the cell number (10.000 cell/well: 4±0.4% and 20.000 cell/well: 5.9±0.4%). Additionally, increased IL-8 levels were measured in the basolateral compartments with 10.000 (2.2±0.18%) and 20.000 (4.6±0.36%) THP-1 per well, which were pretreated with 100nM PMA. Finally, a correlation could be established between TER values and inflammatory responses in the triple-coculture with respect to stimulation of the THP-1 with 100nM PMA. Optimal triple-coculture conditions (regarding TER and inflammatory responses) were given by a pretreatment of the THP-1 cell line with 8nM PMA and a cell number of 10.000-20.000 THP-1 cells per well to be seeded on the apical side (epithelial) of the coculture.

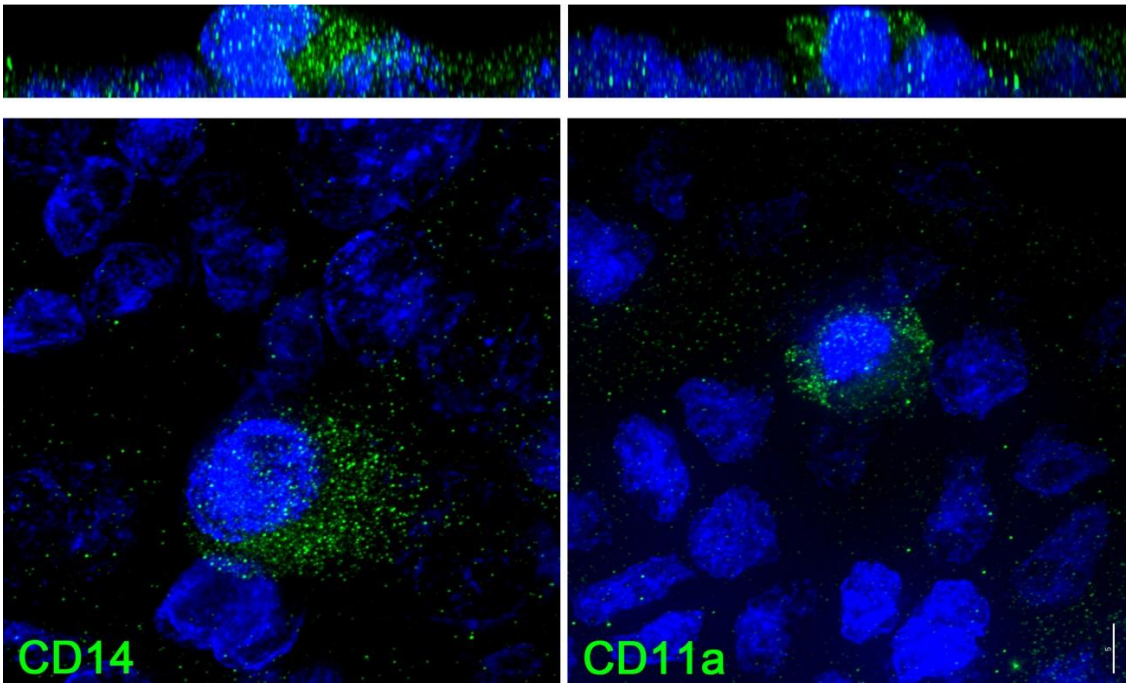

Figure 47: Immunofluorescence staining of CD14 and CD11a (green) of THP-1 on day 10 of coculture, prestimulated with 8nM PMA for four days and subsequent seeding on top of the epithelial layer of a coculture (H441/ISO-HAS-1). Nuclei are stained using Hoechst 33342 (blue), scale bar: 5 µm

Figure 47 shows exemplary immunofluorescently labelled THP-1 (CD14 and CD11a), which were added to the epithelial layer (H441) of the coculture. THP-1 were preteated with 8 nM PMA for 4 days prior to seeding on the coculture on day 8 and cultured with the coculture for 2 days. Premilinary results of aSNP treated triple cultures (THP-1/H441/ISO-HAS-1) are presented in Figure 48, which shows the transepithelial resistance measurement of aSNP treated coculture (H441/ISO-HAS-1) in comparison to the triple culture (THP-1/H441/ISO-HAS-1) with two different populations of THP-1 added (10.000 and 25.000 THP-1 cells/well). TER is depicted as the percentage of t_0, the time-point of each well prior to aSNP treatment. The untreated control (uc: without aSNP) and the positive control did not display any significant alterations concerning TER between coculture and triple culture. However, following TNF-α and aSNP treatment significant differences between the coculture and triple culture were observed. After 20h of the recovery period following a 4h exposure to 100 µg/ml Ludox TM-40 a noteworthy decrease of TER could be observed for the triple-

culture with 25.000 THP-1 cells compared to the triple-culture with 10.000 THP-1 cells and the coculture without THP-1 cells.

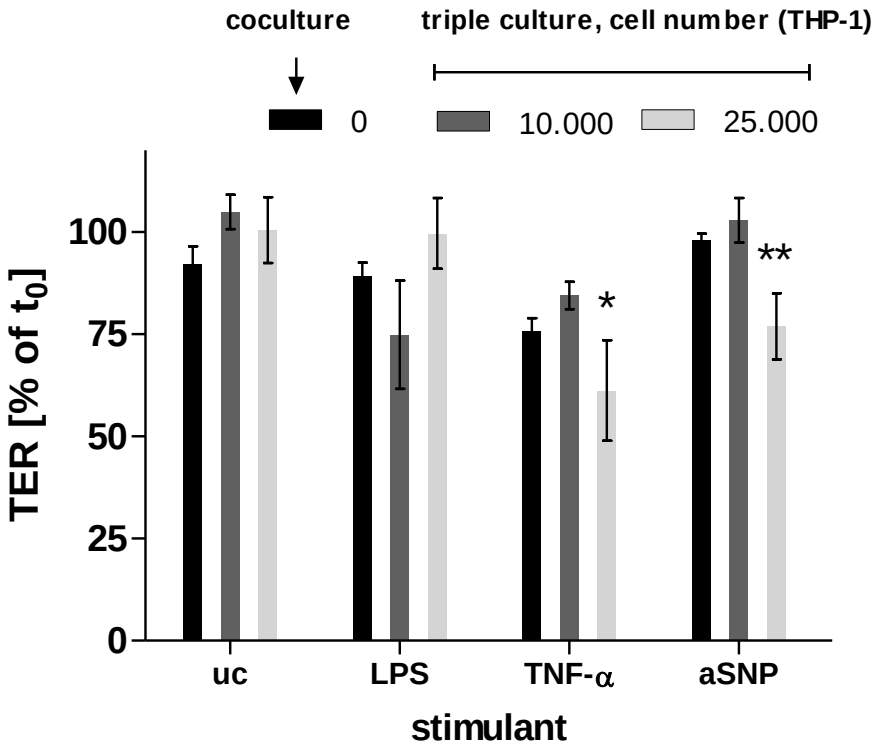

*Figure 48: Transepithelial resistance measurement of coculture (H441/ISO-HAS-1, THP-1=0) compared to the triple culture (H441/ISO-HAS-1 + THP-1=10.000 or THP-1=25.000) under different treatments. Uc: untreated control, LPS (1µg/ml), TNF-α (300 U/ml), aSNP (Ludox TM-40, 100 µg/ml). Data are depicted as means ± S.D. of one preliminary experiment with n=4 samples. For statistical analysis using two-way-anova with Bonferroni´s post test, the values of the untreated coculture (without THP-1) were used as control.*P <0.05, ** P <0.01 and *** P <0.001.*

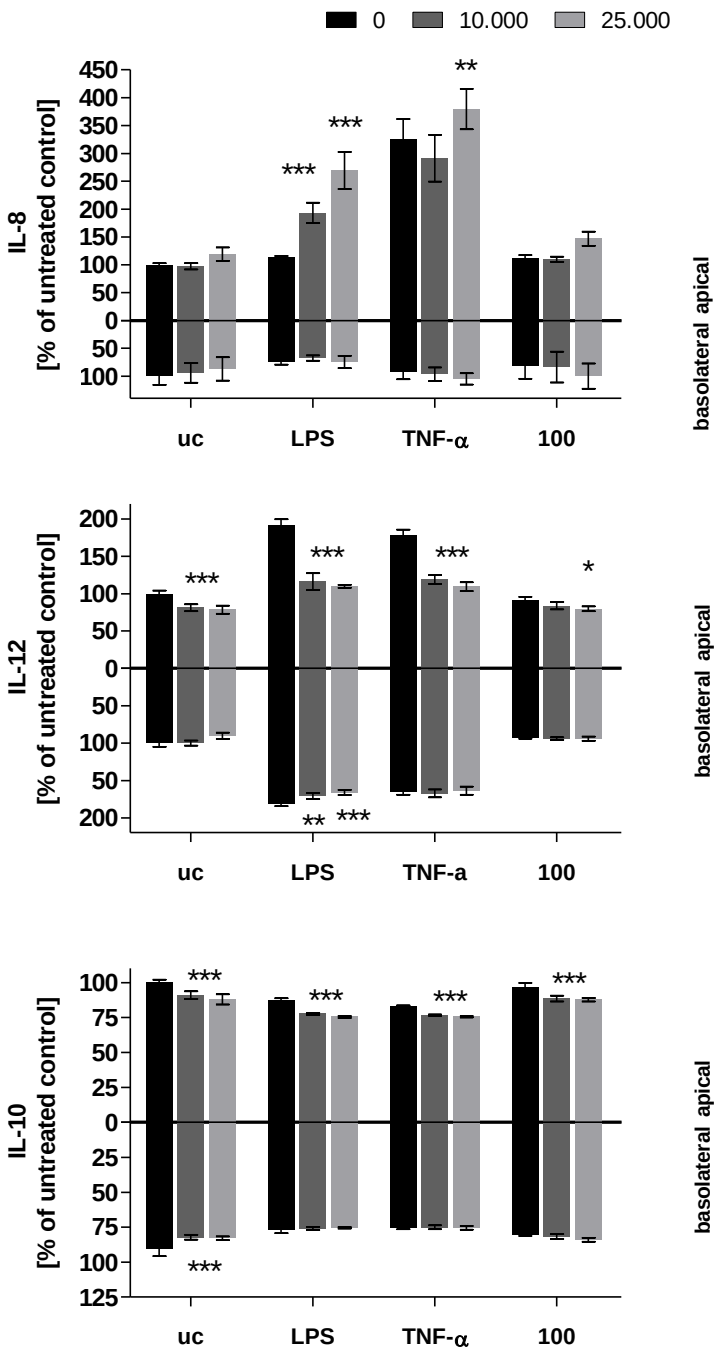

*Figure 49: Inflammatory responses (IL-8, IL-12, IL-10) of the coculture (H441/ISO-HAS-1, THP-1=0) compared to the triple culture (H441/ISO-HAS-1 + THP-1=10000 or THP-1=20000) under different treatments. Uc: untreated control, LPS (1µg/ml), TNF-α (300 U/ml), aSNP (Ludox TM-40, 100 µg/ml). Data are depicted as means ± S.D. of one preliminary experiment with n=4 samples. For statistical analysis using two-way-anova with Bonferroni´s post test, the values of the untreated coculture (without THP-1) was used as control. *P <0.05, ** P <0.01 and *** P <0.001.*

Figure 49 shows first results of the aSNP-treated triple culture in comparison with the coculture. In order to avoid cell loss of the THP-1 during washing steps as a result of the apparently loose adhesion of the THP-1 to the coculture, the coculture and the THP-1 (prestimulated with 8 nM PMA for 4h on fibronectin-coated 6-well plates) were incubated with aSNP, LPS and TNF-α prior to adding the THP-1 to the coculture. The untreated triple culture did not show an altered IL-8 release compared to the untreated coculture. After LPS (lipopolysaccharide) stimulation however, the triple culture responded with a cell number-dependent apical increase of IL-8 (0 THP-1: 114±1.7%, 10.000 THP-1:193±18%, 25.000 THP-1: 270±34% of untreated coculture without THP-1). TNF-α resulted in a significant IL-8 increase for the triple culture with 25.000 THP-1 (380±36%) compared to the TNF-α-treated coculture (326±35%). aSNP treatment did not reveal any differences concerning IL-8 release. With regard to IL-12, all stimulants (us, LPS, TNF-α and aSNP) caused a significantly suppressed response of the triple culture compared to the coculture. LPS stimulation for example showed an apical increase of IL-12 in the coculture (0 THP-1: 192±8.3% of untreated coculture), whereas IL-12 levels in the triple culture remained unaltered compared to the untreated coculture (10.000 THP-1:116±11%, 25.000 THP-1: 109±2% of untreated coculture without THP-1). Even basolaterally a significant reduction of IL-12 could be detected for the triple culture compared to the coculture (0 THP-1: 180±3.5%, 10.000 THP-1: 170±4, 25.000 THP-1: 166±3.5).

A similar tendency as observed for IL-12 release could be observed for IL-10 release, with apical IL-10 release being significantly suppressed in the triple culture compared to the coculture.

4 Discussion

4.1 Inflammatory and cytotoxic responses of an alveolar-capillary coculture model to aSNPs: comparison with conventional monocultures

Monocultures on tissue culture plastic are mostly used to study cytotoxicity and uptake of nanoparticles (NPs) in target cells. To investigate functional effects on biological diffusion barriers we investigated the effects of amorphous silica nanoparticles (aSNP) in a polarized barrier-forming coculture model compared to monocultures grown under conventional culture conditions. To detect aSNP cytotoxicity viability (MTS assay) and membrane integrity (LDH release) tests were performed. A good correlation of the MTS and LDH assays following aSNP treatment was observed for conventional monocultures. By contrast, the cocultures were less sensitive to aSNP exposure with respect to LDH release. Comparable to the results found for morphological changes, the responsiveness towards aSNP treatment was shifted from an aSNP concentration of 600 µg/ml in monoculture to 6000 µg/ml in coculture (factor 10). Under conventional tissue culture conditions monocultures of H441 show a fragmented immunostaining of tight junctional (TJ) and adherens junctional (AJ) proteins, whereas polarized cells (apical/basolateral differentiation) in coculture establish a functional TJ and AJ network [82]. The higher responsiveness towards amorphous silica toxicity by the non-polarized conventional monoculture may be due to the higher surface area accessible to the aSNPs, as these cells are much less cuboidal than in the coculture and tend to be much more flattened. For the cocultures another sensitive marker for toxic effects is the measurement of transbilayer electrical resistance (TER). For both aSNPs a concentration of 6000 µg/ml resulted in a complete breakdown of the TER for H441/ISO-HAS-1. At this high concentration the decrease of TER is a result of cell detachment. At a concentration of 600 µg/ml TER decreased to 25%, but staining of cell-cell contacts, such as E-cadherin or ZO-1, did not indicate a morphological change (Figure 14). For claudin-5 however, a reduction of the fluorescent signal (visual assessment) was observed (Figure 15). Thus, claudin-

5 might play a crucial role in maintaining intact barrier function as reflected in the TER value. A similar behaviour was seen in preliminary experiments with cocultures of primary alveolar epithelial (ATII) and endothelial cells (HPMEC), which is the gold standard model of the lower respiratory tract. While LDH measurement at a concentration of 600 µg/ml aSNPs resulted only in an insignificant LDH release, the TER-values decreased significantly. These data indicate that TER measurement is a highly sensitive method to evaluate slight changes in barrier properties, before any toxic effects are detectable by conventional membrane integrity assays.

Despite their toxicity aSNP induced a significant pro-inflammatory response (sICAM-1, IL-6, IL-8) in epithelial and endothelial cells in conventional monocultures, as well as in the polarized monoculture on transwell filter units. ICAM-1 (intercellular adhesion molecule-1) is a crucial mediator for the attraction and adhesion process of endothelial as well as epithelial cells to leukocytes. It is involved in numerous lung diseases, such as asthma [101], ARDS (acute respiratory distress syndrome) [102] and ALI (acute lung injury) [103]. Direct stimulation of rat lung tissue by pathogens caused an upregulation of ICAM-1 in bronchiolar epithelial cells, ATII, and in vascular endothelial cells [104]. Furthermore, increased soluble ICAM-1 levels were found in the bronchoalveolar fluid of mice and increased ICAM-1 expression was detected on alveolar macrophages and ATII cells exposed to ultrafine crystalline silica particles [105, 106]. For H441 cells in conventional monoculture a concentration of 60 µg/ml NexSil20, which showed no effects in MTS and LDH assays, induced a 3fold increased sICAM-1 release compared to the untreated control. Nevertheless, the responses of the monocultures differed markedly from that observed in cocultures. In coculture an inflammatory response was already detectable at much lower aSNP concentrations than in conventional monoculture. Thus, upper well exposure to 6 µg/ml resulted in a 10fold higher sICAM-1 release into the upper well compared to monocultures. Additionally, in coculture low concentrations of 6-60µg/ml aSNP, which had no effect on TER and LDH, resulted in an IL-6 and IL-8 release into the lower compartment, whereas no increase of both cytokines was measured on the exposed (apical)

side. By contrast, the polarized transwell-monocultures of H441 showed no changed basolateral release of both cytokines. Additionally, experiments with a fluorescent aSNP (SicaStar Red 30 nm) revealed that particles, when apically applied to H441, did not reach the ISO-HAS-1 seeded on the lower surface of the filter. However, on apical exposure without H441 on the top side the aSNP crossed the filter membrane and were detected in the ISO-HAS-1. Thus, it seems that it is not aSNPs transported to the ISO-HAS-1 cells, but rather crosstalk between the aSNP-stimulated H441 and the ISO-HAS-1 that resulted in increased IL-6 and IL-8 release into the lower compartment. The pro-inflammatory cytokines, IL-6 and IL-8, which play a decisive role in the recruitment and regulation of neutrophils, have been shown by other groups to be involved in the NP-induced inflammatory reaction [107, 108].

A functioning cytokine network across the alveolar-capillary barrier is pivotal for cellular communication during pulmonary inflammation. The polarized coculture allows a compartmentalisation with two biological barrier components apically facing the different compartments. This close topographical association further enables communication between epithelial and endothelial cells, although initially only the exposed epithelial cells might have contact with the nanoparticles. However, the present data indicate that the indirectly affected endothelial cells are able to forward various inflammatory signals, which in the *in vivo* situation could exert systemic effects.

The results of the apoptosis array show that the finely tuned balance of pro-apoptotic and anti-apoptotic factors which usually exists in healthy tissue is disturbed after exposure to 600 µg/ml aSNPs. A number of apoptosis markers are elevated after 4h aSNP exposure in coculture. The detected increase of HIF-1α, hypoxia inducible factor, and the phosphorylation of the p53-protein at Ser15, Ser46 and Ser392 is a sign of DNA damage or hypoxia due to the amorphous silica exposure. In keeping with p53 activation elevated pro-apoptotic markers were detected, contributing to the intrinsic pathway, such as Bad and Bax, with their counterparts, Bcl-2 and Bcl-x, and a concomitant increase in cytochrome c release, as well as the TRIAL receptor KILLER/DR5. Interestingly, XIAP (X-linked Inhibitor of apoptosis Protein), a member of the

Inhibitor of apoptosis family, was also upregulated following aSNP exposure. Since this protein binds and inhibits caspase 3, 7 and 9 this could explain why neither the procaspase nor the cleaved active product of caspase 3 was increased.

Numerous cytotoxicity studies also indicate that DNA damage or hypoxia and the subsequent mitochondria-regulated apoptosis are triggered by silica nanoparticles [109-113]. In an *in vivo* study in rats, high administered doses of amorphous silica to the lung led to increased cytotoxicity (LDH release in lung lavage), necrosis or apoptosis (increased TUNEL staining of epithelial cells)[114]. An induction of ER stress, which itself can initiate apoptotic processes [115-117], can be assumed by the upregulation of paraoxonase 2 (PON2) after 600 µg/ml aSNP treatment. For the H441 alone (monoculture on transwells) some apoptotic markers, such as i.e. p53, HIF-1α, or Bcl-x, Bcl-2 and Bax, do not seem to be affected following aSNP treatment. This might be an indication that the apoptotic response could originate from the indirectly exposed ISO-HAS-1 situated on the lower aspect of the filter membrane. This might be a further indication of cross-talk between the directly aSNP-exposed H441 and the ISO-HAS-1 at the other side of the filter membrane.

4.2 Endocytosis pathways as cellular uptake routes for NPs

The cell membrane is the first barrier which nanoparticles have to overcome in order to penetrate the intracellular compartment. There are several cellular uptake routes in focus to evaluate the entry mechanisms of nanoparticles. Current research is focussing on endocytotic pathways, such as phagocytosis, pinocytosis (clathrin-mediated and caveolae-mediated endocytosis as well as and macropinocytosis), and clathrin-independent mechanisms. Furthermore, recent studies emphasize several NP characteristics, such as size, shape and surface properties, to be crucial for entering respective pathways [118].

H441 grown under coculture conditions more closely mimic the phenotype of epithelial cells of the distal lung. By developing a tight barrier with continuous circumferential ZO-1 (zonula occludens-1) staining [82], H441 in coculture reach a more differentiated and polarized state compared to H441 kept under

conventional monoculture conditions. Thus, nanoparticle uptake behaviour of the epithelial cells was determined for H441 and compared under mono- and coculture conditions. Two silica-based NPs were investigated: 1. Sicastar Red (amorphous silica, ca. 30 nm in diameter), 2. AmorSil: (organosiloxane, ca. 60 nm in diameter) and as a control PEI-OG (poly(ethyleneimine)) coupled with Oregon green, abbreviated as PEI) used in parallel.

As reviewed by Kunzmann et. al. [119] silica-based NPs have been widely applied in nanobiomedicine research as drug/gene vehicles. Coating mesoporous silica nanoparticles (MSN) with, for example, polyethyleneimine (PEI) reduces cytotoxicity, enhances cellular uptake, increases delivery of siRNA or drugs such as paclitaxel [120]. PEI has been widely used in studies as a non-viral vehicle for drug and gene delivery [121-124]. Rejman and coworkers [125] indicated a clathrin- and caveolae-dependent uptake of PEI-polyplexes in A549 and HeLa. PEI transfection vectors have a high transfection efficiency, which may be a reflection of their ability to escape endosomes before they are cargoed to degradative lysosomes. PEI has a high buffering capacity, leading after their uptake by endocytosis to osmotic swelling and rupture of endosomes as well as a release of PEI into the cytoplasm [126]. Efficacious pulmonary gene delivery via PEI in concert with only mild inflammatory responses has already been described [127-129]. Transfection studies of H441 using PEI-GFP (PEI complexed to pDNA encoding enhanced green fluorescent protein gene) revealed a transfection rate of about 8% in conventional monoculture. Barrier-forming H441 under coculture conditions however, did not yield any transfection success, indicating the altered behaviour of differentiated and polarized cells compared to cells in conventional monoculture [82]. Poly(organosiloxane) core-shell nanoparticles have also gained attentiveness for prospective biomedical applications. The AmorSil NP used in this study have a magnetic core, giving the prospect of novel therapeutical applications [91, 92]. Magnetic NPs are already widely used for biomedical applications, such as hyperthermia, magnetic resonance imaging or drug delivery. A recent study investigated siRNA transfection efficiency in A549 cells of PEGylated, poly(ethyleneimine)-grafted silica nanoparticles with silanol and siloxane

functional groups [130]. The positively charged PEGylated-PEI enhances three factors which are indispensable for an efficient gene delivery. Thus, it enhances complexation with negatively charged siRNA, the interaction with negatively charged plasma-membrane surface, which results in an efficient internalisation of the NPs and finally, an endosomal escape may be meditated due to PEI. Coating of NPs with poly(ethylene glycol) (PEG) or as in our case poly(ethylene oxide) (PEO) is widely applied in research concerning nanoparticles generated for biomedical applications. Suh and co-workers [131] reported that PEGylation improved the stability of NPs in aqeuous solutions, gave a more efficient and constant crossing of NPs through biological obstacles and an improved cytoplasmic transport after endosomal escape, suggesting a reduction of non-specific adhesion to cytoskeletal elements.

In the present study, colocalisation studies using amorphous silica nanoparticles aSNP (Sicastar Red, 30 nm in diameter), the organosiloxane AmorSil and PEI revealed no specific classical uptake mechanism. Within the time points chosen in this study, all three NPs were not found colocalised either with markers for clathrin-mediated endocytosis (clathrin heavy chain: chc) or with markers for caveolin-dependent pathways (Caveolin-1: cav). Recent studies using unmodified mesoporous silica suggest a clathrin-dependent pathway for mesoporous silica uptake [132, 133]. By inhibiting the clathrin-mediated pathway with sucrose, which inhibits the clathrin-pathway by hypertonicity, Huang and co-workers [132] showed a reduction of internalized MSNs in the adipocyte-like 3T3-L1 and in human mesenchymal stem cells (hMSCs). Furthermore, Chung and co-workers [133] used i. a. phenylarsine oxide (PAO), another clathrin-endocytosis inhibitor, to demonstrate a decreased uptake of unmodified MSN in 3T3-L1. Inhibition of endocytosis pathways, unless clathrin-mediated or caveolae-mediated, is widely applied by researchers to reveal cellular uptake mechanisms of nanoparticles [125, 134, 135]. Glebov et. al. studied endocytosis mechanisms involving clathrin-, caveolae-, as well as flotillin-dependent machineries by applying several inhibition methods for these distinct endocytosis mechanisms [136].

In our study, labelling of flotillin-1- or flotillin-2-containing vesicles revealed a significant incorporation of Sicastar Red, AmorSil and PEI in such vesicles, thus indicating an involvement of flotillin-1/2 at least in traffic or storage mechanisms. Both in mono- and coculture NPs were found in flotillin-1/2-bearing vesicles of H441. The H441 cells in coculture only differed in the time-and dose-dependency of uptake. The polarized, barrier-forming H441 in coculture had to be exposed to a higher dose of NP for more then 10times than in monoculture to measure a visible uptake of Sicastar Red. Flotillin-1 and flotillin-2 (also called reggie-2 and reggie-1, respectively) are lipid raft-associated proteins and are thought to be involved in clathrin- and caveolae-independent endocytosis pathways [137-140]. Morrow and co-workers [137] demonstrated that flotillin-1, located in the plasma membrane, is present in caveolae to a very low extent (10%). On the other hand, Glebov et. al. demonstrated no colocalization events between flotillin-1 and caveolin-1 and confirmed the clathrin- and caveolae independency of flotillin-1-associated endocytosis in COS7 and HeLa cells [138]. Furthermore, this group observed a partial colocalisation of flotillins with the late- or lysosomal marker LAMP-1. Dermine et. al. [141] also found flotillin-1-containing lipid rafts in LAMP-1-bearing late, but not early phagosomes of J774 (a murine macrophage-like cell line) and deduced that flotillin-1 could be a novel marker of late endocytic/phagocytic organelles. Based on their findings Dermine et. al. argue that flotillin-1 associates after the maturation process of late phagosomes, since the group did not find flotillin-1 colocalized with early phagosomes [141]. Furthermore, Vercauteren and co-workers reported a flotillin-1-dependent uptake mechanism of polyplexes in retinal pigment epithelium (RPE) cells [142].

These results corroborate the findings provided in the present study, in which flottilin-1/2 were partially detected in LAMP-1-bearing vesicles of H441 and ISO-HAS-1 (see Figure 36). Since this phenomenon occurs in a variety of cell types such as macrophages (J774), epithelial cells (H441 and HeLa) or endothelial cells (ISO-HAS-1) it appears to be a general phenomenon. Thus, flotillins may play a key role in late- or lysosomal degradation or storage processes. Corroborating this hypothesis, not only amorphous silica but also

organosiloxane particles and nanoparticles of poly(ethyleneimine), which all are of therapeutical interest, localized in flotillin-1/2-bearing vesicles.

4.3 Size-dependent cytotoxicity and uptake of aSNPs

Using MTT and LDH assays Napierska and coworkers [86] already demonstrated a particle size-dependent cytotoxicic effect in a (supposed) human endothelial cell line (EAHY926) caused by aSNPs. The results of the present study corroborate their findings, as in this dissertation the smaller sized aSNP (30 nm) were found to cause greater damage to lung epithelial cells (H441) as determined by the MTT and LDH assays compared to larger sized (70nm, 300 nm) aSNPs. In summary cytotoxicity appears to increase with decreasing particle size. As in Napierska et. al. [86], the dose was expressed as a mass concentration. Choosing the right dosimetry is a double-edged sword. Comparing mass concentrations of different sized NPs leads to a comparison of different particle numbers. However, a mass concentration of, for example, 60 µg/ml (lowest concentration, for which a cytotoxic effect occurred with 30 nm aSNP) of the 30 nm aSNP matches with a particle number of 2×10^{12} particles/ml according to the manufacturer's specifications, whereas 60 µg/ml of 300 nm aSNP corresponds to 2×10^{9} particles/ml (i.e. 1000x less particles compared to 30 nm aSNP). However, adjusting the 300 nm aSNP to 2×10^{12} particles/ml would lead to a mass concentration of 60 mg/ml, which is far beyond any physiologically relevant amount. Additionally, the highest mass concentration of 300 nm which can be applied is 2×10^{11} particles/ml. However, this particle number corresponds to a mass concentration of 6 µg/ml for the 30 nm aSNPs, which is beyond the toxic range of the 30 nm aSNP. Lison et. al. [87] considered mass concentration, particle number, surface area and also the applied volume of NP-dispersion as crucial factors for reliable conclusions on nanoparticle cytotoxicity. In general, since the smaller the nanoparticle the bigger is the surface area per mass, the surface area is supposed to be a pivotal factor for the displayed biological activity, as reviewed by Oberdörster et. al. [143]. Although recent studies emphasize the size of NPs as a critical factor for entering the respective uptake pathways [118], in this study the size of

aSNPs, ranging from 30 nm to 300 nm, was not crucial for targeting flotillin-1/2-bearing vesicles in H441 and ISO-HAS-1 (see Figure 39 for Sicastar Red after 24h). This supports the findings of Shapero and coworkers [144], who detected an aSNP-accumulation (50 and 100 nm in size) in lysosomes of A549 cells after 24h. The latter group also found a colocalisation of aSNPs with early endosomes, multilamellar bodies and multivesicular bodies of A549 cells using electron microscopy, which is a more sensitive method to detect nanosized material than fluorescence-based detection methods, including immunofluorescence.

4.4 aSNP exposure to flotillin-1 and -2 depleted cells

A depletion/reduction of flotillin-1 and -2 expression in flotillin-1/2 siRNA-treated H441 cells was confirmed by real-time PCR studies. Furthermore, the fluorescence intensity of the immunofluorescent staining of flotillin-1/2 revealed a significant reduction of flotillin-1/2-containing vesicles in flotillin-1/2-depleted H441 cells. In this study, quantification of flotillin-1/2-depleted H441 cells showed a reduced uptake of Sicastar Red compared to non-transfected control cells. This finding may indicate an involvement of flotillin-1/2 in the uptake mechanisms of Sicastar Red. The control cells, which were transfected with Silencer® Negative siRNA (neg), also displayed a slight, but not significant reduction of the fluorescence intensity of the aSNP fluorescence signal. Real-time PCR results, however, did not indicate any reduction of flotillin-1/2 expression in non-targeted siRNA-transfected H441. Due to the fact that the transfection procedure using Gencarrier-1, which is a lipoplex-based transfection reagent, may influence endocytosis metabolism, since the lipoplexes follow the clathrin-dependent endocytosis route, nonspecific alterations in uptake of aSNPs may be explainable on the basis of these pre-treatments. For this reason, it is essential to carry out appropriate control experiments to verify nonspecific influences of pre-treatments, such as transfection reagents.

The mechanisms by which aSNPs exert their cytotoxic effect are still largely unknown. However, there are many possibilities, including damage to the

plasma membrane before particles penetrate the cells, intracellular interference after uptake in late- or lysosomal structures, and lysosomal escape. Therefore, further experiments were conducted to obtain more insight into these possible pathways. Cytotoxicity of flotillin-1/2-depleted H441 following aSNP (Sicastar Red) exposure was evaluated and compared to non-depleted cells. As Figure 40 shows, the toxic influence of aSNPs (Sicastar Red) at low concentrations (6-60 µg/ml) was increased in flotillin-1/2-depleted cells. After 4h a similar toxicity was observed for non-transfected, aSNP-treated cells and flotillin-1/2-depleted, aSNP-treated cells. However, after 20h of recovery differences between treatments became evident. While non-transfected cells appear to recover at low concentrations (6-60 µg/ml) within 20h after exposure, the toxic effects of aSNPs persisted in flotillin-1/2-depleted cells. For higher aSNP concenrations (300 µg/ml) similar toxicity was observed for all cellular treatments and time-points. Taking the results of Sicastar Red uptake in flotillin-1/2-depleted H441 into account, which indicated a decelerated uptake of aSNP as seen by decreased fluorescence intensity values, an increase in cytotoxicity appears at first sight to be contradictory. Assuming an involvement of flotillins in at least storage/degradation processes, which is corroborated by the localisation of NPs in flotillin-1/2-containing vesicles, even lower concentrations of incorporated aSNP might display higher cytotoxicity in flotillin-1/2-depleted cells compared to the higher amount taken up by the control cells (non-transfected). Glebov et. al. also studied the flotillin-dependent endocytosis mechanism by applying several inhibition methods [136, 138]. They stressed the need for careful interpretation of results which are obtained from such inhibition experiments, since evidence already exists that by inhibiting a distinct endocytosis pathway, another pathway may compensate instead [136]. A variety of controls have to be carried out in order to minimize other possible interpretations.

4.5 Approaching more closely the *in vivo* situation with a triple culture by adding the alveolar macrophage

Alveolar macrophages represent the front-line of alveolar defense mechanisms against aspirated pathogens or particles which have overcome proximal clearing mechanisms, such as the nasal passage-ways, or the mucociliary clearance machinery of the bronchioles [145]. Their function is it to phagocytose and subsequently kill phagocytosed microbes. Macrophages secrete antimicrobial metabolites, such as reactive oxygen species, lysozyme, peptides or proteases in order to prevent an accelerated inflammatory response of the alveolus due to such invading pathogens or particles [145, 146]. A triple-culture model of the barrier-forming alveolar cells, namely alveolar epithelial and capillary endothelial cells, together with alveolar macrophages has great potential to mimic more closely realistic cell interactions with nanoparticles in the deep lung.

Under physiological conditions the alveolar macrophage appears to be in a calmed or latent inflammatory state. *In vivo* studies using clodronate-filled liposomes designed to eliminate alveolar macrophages indicated an increased pulmonary immune response to normally innocuous particulate matter [147]. In order to prevent collateral damage to alveolar epithelial cells due to hypersensitive inflammatory responses upon daily aspirated microbes or dust, they actively suppress the adaptive immunity of all alveolus-associated cells. To achieve this, AMs secrete nitric oxide, prostaglandins, interleukin-10 (IL-10), and transforming growth factor-β (TGF-β) [10]. In the quiescent state, AMs closely adhere to the epithelial surface, produce minimal inflammatory cytokines and have a low phagocytotic activity [148]. After stimulation with higher doses of aspirated hazardous antigens, AMs detach from the alveolar surface and display innate immune functions, such as phagocytosis and secretion of pro-inflammatory cytokines, including TNF-α and IL-6 [10].

In vitro experiments using differentiated THP-1 as AMs in the coculture model of the alveolar-capillary barrier require a finely tuned induction to obtain THP-1 with AM-features which nevertheless possess a low activated state. Park and co-workers [149] stated that in order to detect responses to weak stimuli an

optimized THP-1 differentiation via PMA is required. These authors further reported that PMA has been used widely for research purposes at a concentration range from 10–400 ng/ml (ca. 16–540 nM) without regard to the upregulation of inflammatory markers. In their study they clearly showed increased levels of TNF-α and IL-8 upon treatment with high concentrations of PMA (50 and 100 ng/ml or 80 and 160 nM) and concluded a concentration of 5ng/ml (8 nM) PMA to be sufficient for AM-differentiation of THP-1.

In this study the stimulation with 8 nM and 100 nM PMA clearly induced cell adherence and spreading of the THP-1 cells (see Figure 44). Addition of THP-1, stimulated for 4 days with 8nM PMA (10.000 or 20.000 cells/coculture-well), to the established coculture of H441 and ISO-HAS-1 on day 8 of coculture resulted in a triple-culture with a stable barrier (Figure 45) and a cytokine release (sICAM, IL-6, IL-8) comparable to the coculture without THP-1 (Figure 46). A 4 day pre-treatment of THP-1 with high concentrations of 100 nM (62.5 ng/ml) PMA resulted in a drastic decrease of functional barrier properties (TER) in the triple-culture and distinctively elevated levels of IL-8. Therefore, a differentiaton to AM by a 4 day pre-treatment of THP-1 with 8 nM PMA was used to create a stable triple-coculture for cell communication studies. Under these conditions the AM-differentiated THP-1 could be visualized on top of the coculture´s epithelial layer (H441) by means of immunofluorescence of macrophage-specific markers, such as CD14 or CD11a. Finally, this novel triple-coculture was established to study cytotoxicity and inflammatory responses following nanoparticle interactions. Since the lung is composed of many different cell types, it is of great concern to conduct cytotoxicological studies with complex coculture systems consisting of more than one cell type, consequently allowing cellular communication rather than using monocultures with only one single cell type. Several studies focusing on nanoparticle-exposed human epithelial airway coculture models have already been performed to address this issue [150-153]. Müller et. al. [152] reported an altered response of IL-8 release following particle exposure on a triple cell coculture of A549 with MDMs (monocyte-derived macrophages) and MDDCs (monocyte-derived dendritic cells) compared to the respective monocultures. Wottrich et al. [153]

showed an increased sensitivity to particles with respect to cytokine release (IL-6, IL-8) from human epithelial cells A549 in coculture with macrophages, compared to the cells in monoculture. Corroborating these findings the alveolar-capillary barrier developed by the coculture model in this thesis was able to detect compartimentalized inflammatory responses following aSNPs exposure. Since the established triple-coculture with macrophage differentiated THP-1 displays sufficient barrier properties, it has great potential to complement the findings of the studies of the above mentioned research groups with respect to a directed cytokine release to the apical (alveolar) or basolateral (vascular lumen) side. In accordance with our approach other research groups also emphasized the essential nature of a functional alveolar-capillary barrier for studies on deep lung interaction with foreign material [154].

Initial studies used the triple-coculture under the same standard operational procedures (SOP) as applied for the aSNP-treated coculture (see Figure 48). Barrier properties measured by TER revealed an altered behaviour of the triple-coculture compared to the coculture composed of only two cell types following aSNP treatment. After 20h of recovery following 4h TNF-α as well as aSNP exposure (100 µg/ml Ludox-TM-40), a noteworthy decrease of TER was observed for the triple-culture compared to the coculture. Furthermore, cytokine release, for example, IL-8, IL-12 and IL-10, was examined following aSNP treatment. The triple-culture behaved more sensitively compared to the coculture after stimulation with LPS and TNF-α in regard to IL-8 release. aSNP-stimulation resulted in an slight but not significant increase of IL-8. Concerning IL-12 significant differences between coculture and triple-culture were observed for all stimulants (LPS, TNF-α and aSNP) and also for the untreated control, whereby the coculture responded more sensitively. IL-12 is normally produced by antigen-presenting cells, such as macrophages, dentritic cells or B cells [155] but is also shown for airway epithelial cells [156]. IL-12 is discussed as playing a crucial role in atopic asthma and airway hyper-responsiveness [157, 158], since it has been shown to have lower levels in asthmatic patients [159]. Lower IL-12 levels in the triple-culture may explain a higher responsiveness of the triple-culture compared to the coculture regarding IL-8 release. IL-10 is

additionally decreased in the triple-culture compared to the coculture. Depending on the priming stimulus, macrophages display a high functional plasticity and at least three distinct phenotypes have been recognized : 1. classically activated macrophages, 2. wound-healing macrophages and 3. regulatory macrophages. [160]. Among other factors the ratio of IL-10 and IL-12 is crucial for the characterisation of the three macrophage sub-populations [161]. In its quiescent state the alveolar macrophage normally produces high levels of IL-10 and this appears characteristic of the third population. PMA-prestimulation of the THP-1, however, leads to a more activated state, apparently with low levels of IL-10. Prospectivley, further characterisation of the triple-culture model and the differentiated THP-1 needs to be conducted to specify the macrophage phenotype in more detail. According to this preliminary data, completing the coculture with a third important cell type, the alveolar macrophage, may result in a more sensitive coculture model, which also possesses greater relevance for biomedical research. Indeed, it is inconceivable to have an *in vitro* model of the alveolus for the study of particle interaction with the lung without reference to the macrophage system. However, to corroborate these findings, additional tests have to be conducted to strengthen the statistical validity of the preliminary data presented in this thesis.
Additionally, a fine adjustment of the cell numbers of communicating cells is required, so as not to evoke cytokine release simply on the basis of an imbalance of cell types. A well designed and characterized triple-culture model will give us more insight into the complexity of cell communication which takes place in the alveolus.

5 Summary

5.1 Summary

In this study cytotoxicity and inflammatory responses of the lower respiratory tract following nanoparticle (NP) exposure were investigated. Special attention was also given to cellular uptake mechanisms, such as clathrin- or caveolae-mediated as well as clathrin- or caveolae-independent endocytosis pathways (possible involvement of flotillins) to evaluate specific entry routes for NPs. Three different types of NPs were chosen: amorphous silica (aSNP), organosiloxane (AmorSil) and poly(ethyleneimine) (PEI). All three NPs are gaining increasing interest for biomedical research (drug and gene delivery). In particular, aSNPs are widely used for industrial applications. Hence, attention has to be given to possible health hazards of inhalation of these NPs. The alveolar region of the lung with a surface area of 100-140 m^2, makes it an interesting target for drug and gene delivery, but at the same time it represents a serious area of attack for harmful nanomaterials. For that reason, toxic effects and the cellular pathways of internalized NPs should be addressed if a lung application is envisaged. The alveolar-capillary barrier of the deep lung is difficult to access by *in vivo* studies. Therefore, a coculture model that mimics the alveolar-capillary barrier *in vitro* has been established. The model consists of human lung epithelial cells (cell line NCI H441) and human microvascular endothelial cells (cell line ISO-HAS-1), on opposite sides of a transwell filter unit. NCI H441 differentiate to a polarized, barrier-forming epithelial layer. The tight barrier developed can be measured, for example, by transepithelial resistance (TER). NP interaction with cells in coculture was compared to interaction with the conventional monoculture, in which the cells are seeded on tissue culture plastic 24h prior to the experiment. This study demonstrates that not only the polarized nature of cells in coculture but also the close proximity of epithelial and endothelial cells plays an important role in the effects caused by aSNP exposure. With regard to inflammatory responses the coculture behaves more sensitively after aSNP exposure, i.e. sICAM, IL-6 and IL-8 release, than cells kept under conventional monoculture. On the other hand, the epithelial layer in coculture is more resistant than the conventional monoculture with regard to LDH release after aSNP treatment. Uptake studies revealed that the epithelial cells in coculture take

up NPs to a much lesser extent than the cells in conventional monoculture. Thus, NCI H441 in coculture show an epithelial character similar to the tight, protecting barrier found *in vivo*. Although sufficient uptake of NP to NCI H441 in coculture was induced, transport of NPs through the epithelial layer and following uptake in the endothelial layer was not detected within the chosen exposure times. In both mono- and coculture uptake mechanisms mediated by clathrin- or caveolae-dependent mechanisms could not be revealed using immunofluorescence . However, an accumulation of NPs in flotillin-1- and -2-containing vesicles was detected in the epithelial cells of both culture systems. Studies using flotillin-depleted epithelial cells showed a clearly decreased uptake of aSNPs. Additionally, the viability of cells after aSNP exposure was reduced. These findings indicate a contribution of flotillins in as yet unknown (clathrin or caveolae-independent) endocytosis mechanisms and (or) endosomal storage. In summary, although barrier properties differ considerably, uptake mechanisms were comparable between conventional monoculture and coculture for all NPs investigated. Nevertheless, toxicity studies should be carried out with cocultures, as the tight, protecting barrier is similar to the *in vivo* situation. This study clearly showed that the behaviour of cells alters when they are kept under coculture conditions. Cells reach a higher differentiation state and cell communication with other relevant cell types is possible. Adding a third relevant cell type to the coculture, the alveolar macrophage (cell line THP-1), which represents the first line of defence in the alveolus, corroborated these findings. Premilinary tests showed that this triple-culture reacted even more sensitively than the co-culture with changes in barrier function or IL-8 release upon stimulation with TNF-a (tumor necrosis factor α), LPS (lipopolysaccharide) or aSNPs. Compared to conventional monocultures, well designed multicellular culture models more closely mimic the cellular composition in the human body. Hence, nanoparticle interaction with the triple-culture model *in vitro* may predict effects of NP environmental exposure or drug and gene delivery to the deep lung more precisely than has been possible up to now.

5.2 Zusammenfassung

In dieser Arbeit wurden zytotoxische Effekte sowie die inflammatorische Reaktionen des distalen respiratorischen Traktes nach Nanopartikelexposition untersucht. Besondere Aufmerksamkeit lag auch auf der Untersuchung unterschiedlicher zellulärer Aufnahmewegen von Nanopartikeln wie z.B. Clathrin- oder Caveolae-vermittelte Endozytose oder auch Clathrin- und Caveolae-unabhängige Endozytose (mit möglicher Beteiligung von Flotillinen). Drei unterschiedliche Nanopartikel wurden hierbei gewählt: amorphes Silica (aSNP), Organosiloxan (AmorSil) und Poly(ethyleneimin) (PEI). Alle unterschiedlichen Materialien gewinnen zunehmend an Interesse für biomedizinische Forschungsrichtungen (drug and gene delivery). Insbesondere finden aSNPs auch in der Industrie vermehrt Anwendung, und stellen somit ein ernstzunehmendes Gesundheitsrisiko dar. Der alveoläre Bereich der Lunge besitzt eine enorm große Oberfläche (100-140 m^2). Dieser wird dadurch zu einem begehrten Angriffsziel für pharmazeutische Verabreichungen von Medikamenten über Nanopartikel als Vehikel aber bietet zugleich auch eine Angriffsfläche für gesundheitsschädliche Nanomaterialien. Aus diesem Grund sollten die gesundheitsschädigenden Risiken, sowie das Schicksal von zellulär aufgenommenen NPs sorgfältig untersucht werden. *In vivo* Studien an der alveolaren-kapillaren Barriere sind recht umständlich. Aus diesem Grund wurde in dieser Arbeit ein Kokulturmodel benutzt, dass die Alveolar-Kapillare Barrier *in vivo* nachstellt. Das Model besteht aus dem humanen Lungenepithelzelltyp (z.B. NCI H441) und einem humanen microvasculären Endothelzelltyp (z.B. ISO-HAS-1), die auf entgegengesetzten Seiten eines Transwell-Filters ausgesäht werden und eine dichte Barriere ausbilden. Diese kann mittels TER (transepithelial resistance) gemessen werden. Die NP Interaktion mit Zellen in Kokultur wurde mit denen in konventioneller Monokultur verglichen, in der Zellen 24h vor dem Experiment ausgesäht werden. Diese Studie zeigt, dass nicht nur die polarisierte Eigenschaft der Zellen in Kokultur sondern auch die unmittelbare Nähe von Epithel und Endothelzelle ausschlaggebend für durch aSNPs verursachte Effekte ist. Im Hinblick auf inflammatorische Marker (sICAM, IL-6, IL8-Ausschüttung), reagiert die Kokultur auf aSNPs empfindlicher als die konventionelle Monokultur, wohingegen die Epithelzellen in der Kokultur auf zytotoxikologischer Ebene (LDH-Ausschüttung)

unempfindlicher auf aSNPs reagierten als die Zellen in Monokultur. Aufnahmestudien haben gezeigt, dass die Epithelzellen in Kokultur entschieden weniger NPs aufnehmen. Somit zeigen die H441 in der Kokultur ähnliche epitheliale Eigenschaften einer schützenden Barriere, wie sie auch *in vivo* zu finden sind. Obwohl eine aureichende Aufnahme von NPs in H441 in Kokultur erreicht werden konnte, konnte ein Transport von NPs durch die epitheliale Schicht und eine Aufnahme in die endotheliale Schicht mit den gewählten Inkubationszeiten nicht gezeigt werden. Eine Clathrin- oder Caveolae-vermittelte Endozytose von NPs konnte mittels Immunfluoreszenz weder in der Mono- noch in der Kokultur nachgewiesen werden. Jedoch zeigte sich eine Akkumulation von NPs in Flotillin-1 und-2 enthaltende Vesikel in Epithelzellen aus beiden Kultursystemen. Ergebnisse mit Flotillin-inhibierten (siRNA) Epithelzellen, zeigten eine deutlich geringere Aufnahme von aSNPs. Zudem zeigte sich eine eine reduzierte Viabilität (MTS) von aSNP-behandelten Zellen. Dies deutet auf eine Beteiligung von Flotillinen an unbekannten (Clathrin oder Caveolae -unabhängig) Endozytosemechanismen und (oder) endosomaler Speicherung. Zusammenfassend waren die Aufnahmemechanismen für alle untesuchten NPs in konventioneller Monokultur und Kokultur vergleichbar, obwohl sich die Barriereeigenschaften deutlich unterscheiden. Dennoch sollten Toxizitätsstudien an Kokulturen, aufgrund ihrer *in vivo*-ähnlichen, dichten und schützenden Barriere, durchgeführt werden. Diese Arbeit zeigt deutlich, dass sich die Zellen in Kokultur anders verhalten. Die Zellen erreichen hierbei einen höheren Differenzierungsgrad und eine Zellkommunikation mit anderen relevanten Zelltypen wird ermöglicht. Durch das Einbringen eines dritten relevanten Zelltyps in die Kokultur, des Alveolarmakrophagen (cell line THP-1), welcher die erste Verteidigungsfront im Alveolus bildet, wird diese Aussage weiter bekräftigt. Erste Versuche haben gezeigt, dass die Triplekultur bezüglich ihrer Barriereeigenschaften und IL-8-Ausschüttung sensitiver auf z.B. TNF-α oder LPS-Stimulation reagiert als die Kokultur. Verglichen mit konventionellen Monokulturen imitieren gut ausgebildete, multizelluräre Kokulturmodelle viel präziser das zelluläre Zusammenspiel im Körper. Darum liefern Nanopartikelinteraktionen mit dem *in vitro*-Triplekulturmodel aufschlussreichere Ergebnisse bezüglich umweltbedingter oder pharmazeutischer NP-Exposition in der distalen Lung als es uns bisher möglich war.

6 References

1. Dorit RL, Walker WF, Barnes RD: **Zoology**. Philadelphia, FT. Worth, Chicago, San Fransisco, Montreal, Toronto, London, Sydney, Tokyo: Saunders College Publishing; 1991.
2. Hoet PH, Bruske-Hohlfeld I, Salata OV: **Nanoparticles - known and unknown health risks**. *J Nanobiotechnology* 2004, **2**(1):12.
3. Berthiaume Y, Voisin G, Dagenais A: **The alveolar type I cells: the new knight of the alveolus?** *J Physiol* 2006, **572**(Pt 3):609-610.
4. Fehrenbach H: **Alveolar epithelial type II cell: defender of the alveolus revisited**. *Respir Res* 2001, **2**(1):33-46.
5. Devendra G, Spragg RG: **Lung surfactant in subacute pulmonary disease**. *Respir Res* 2002, **3**:19.
6. Nkadi PO, Merritt TA, Pillers DAM: **An overview of pulmonary surfactant in the neonate: Genetics, metabolism, and the role of surfactant in health and disease**. *Molecular Genetics and Metabolism* 2009, **97**(2):95-101.
7. Whitsett JA, Kingma PS: **COLLECTINS**. In: *Encyclopedia of Respiratory Medicine.* Edited by Geoffrey JL, Steven DS. Oxford: Academic Press; 2006: 534-540.
8. Crouch E, Wright JR: **Surfactant proteins A and D and pulmonary host defense**. *Annu Rev Physiol* 2001, **63**:521-554.
9. Ochs M: **The closer we look the more we see? Quantitative microscopic analysis of the pulmonary surfactant system**. *Cell Physiol Biochem* 2010, **25**(1):27-40.
10. Lambrecht BN: **Alveolar macrophage in the driver's seat**. *Immunity* 2006, **24**(4):366-368.
11. Orfanos SE, Mavrommati I, Korovesi I, Roussos C: **Pulmonary endothelium in acute lung injury: from basic science to the critically ill**. *Intensive Care Med* 2004, **30**(9):1702-1714.
12. Nel AE, Diaz-Sanchez D, Li N: **The role of particulate pollutants in pulmonary inflammation and asthma: evidence for the involvement of organic chemicals and oxidative stress**. *Curr Opin Pulm Med* 2001, **7**(1):20-26.
13. Fichtner F, Koslowski R, Augstein A, Hempel U, Rohlecke C, Kasper M: **Bleomycin induces IL-8 and ICAM-1 expression in microvascular pulmonary endothelial cells**. *Exp Toxicol Pathol* 2004, **55**(6):497-503.
14. Azuma A, Takahashi S, Nose M, Araki K, Araki M, Takahashi T, Hirose M, Kawashima H, Miyasaka M, Kudoh S: **Role of E-selectin in bleomycin induced lung fibrosis in mice**. *Thorax* 2000, **55**(2):147-152.
15. Beck GC, Yard BA, Breedijk AJ, Van Ackern K, Van der Woude FJ: **Release of CXC-chemokines by human lung microvascular endothelial cells (LMVEC) compared with macrovascular umbilical vein endothelial cells**. *Clin Exp Immunol* 1999, **118**(2):298-303.
16. Hashimoto S, Gon Y, Matsumoto K, Takeshita I, Asai Y, Asai Y, Machino T, Horie T: **Regulation by intracellular glutathione of TNF-alpha-induced p38 MAP kinase activation and RANTES production by**

human pulmonary vascular endothelial cells. *Allergy* 2000, **55**(5):463-469.
17. Grau GE, Mili N, Lou JN, Morel DR, Ricou B, Lucas R, Suter PM: **Phenotypic and functional analysis of pulmonary microvascular endothelial cells from patients with acute respiratory distress syndrome**. *Lab Invest* 1996, **74**(4):761-770.
18. Gehr P, Bachofen M, Weibel ER: **The normal human lung: ultrastructure and morphometric estimation of diffusion capacity**. *Respir Physiol* 1978, **32**(2):121-140.
19. Dudek SM, Garcia JG: **Cytoskeletal regulation of pulmonary vascular permeability**. *J Appl Physiol* 2001, **91**(4):1487-1500.
20. Furuse M, Hirase T, Itoh M, Nagafuchi A, Yonemura S, Tsukita S: **Occludin: a novel integral membrane protein localizing at tight junctions**. *J Cell Biol* 1993, **123**(6 Pt 2):1777-1788.
21. Fanning AS, Jameson BJ, Jesaitis LA, Anderson JM: **The tight junction protein ZO-1 establishes a link between the transmembrane protein occludin and the actin cytoskeleton**. *J Biol Chem* 1998, **273**(45):29745-29753.
22. Van Itallie CM, Anderson JM: **The molecular physiology of tight junction pores**. *Physiology (Bethesda)* 2004, **19**:331-338.
23. Van Itallie CM, Anderson JM: **Claudins and epithelial paracellular transport**. *Annu Rev Physiol* 2006, **68**:403-429.
24. Wang F, Daugherty B, Keise LL, Wei Z, Foley JP, Savani RC, Koval M: **Heterogeneity of claudin expression by alveolar epithelial cells**. *Am J Respir Cell Mol Biol* 2003, **29**(1):62-70.
25. Ando-Akatsuka Y, Yonemura S, Itoh M, Furuse M, Tsukita S: **Differential behavior of E-cadherin and occludin in their colocalization with ZO-1 during the establishment of epithelial cell polarity**. *J Cell Physiol* 1999, **179**(2):115-125.
26. Napierska D, Thomassen LC, Lison D, Martens JA, Hoet PH: **The nanosilica hazard: another variable entity**. *Part Fibre Toxicol* 2010, **7**(1):39.
27. Kreyling WG, Semmler-Behnke M, Chaudhry Q: **A complementary definition of nanomaterial**. *Nano Today* 2010, **5**(3):165-168.
28. Service RF: **Nanotoxicology: Nanotechnology grows up**. *Science* 2004, **304**(5678):1732-1734.
29. Ellsworth DK, Verhulst D, Spitler TM, Sabacky BJ: **Titanium nanoparticles move to the marketplace**. *Chem Innov* 2000, **30**(12):30-35.
30. **Institute of Nanotechnology, http://www.nano.org.uk/**
31. **AEROSIL®, EVONIK Industries, http://www.aerosil.com**
32. Waters KM, Masiello LM, Zangar RC, Tarasevich BJ, Karin NJ, Quesenberry RD, Bandyopadhyay S, Teeguarden JG, Pounds JG, Thrall BD: **Macrophage responses to silica nanoparticles are highly conserved across particle sizes**. *Toxicol Sci* 2009, **107**(2):553-569.
33. Borm PJ, Robbins D, Haubold S, Kuhlbusch T, Fissan H, Donaldson K, Schins R, Stone V, Kreyling W, Lademann J *et al*: **The potential risks of**

nanomaterials: a review carried out for ECETOC. *Part Fibre Toxicol* 2006, **3**:11.
34. Bonner JC: **Nanoparticles as a potential cause of pleural and interstitial lung disease**. *Proc Am Thorac Soc* 2010, **7**(2):138-141.
35. Morgan WK: **Industrial bronchitis**. *British Journal of Industrial Medicine* 1978, **35**(4):285-291.
36. Yao S, DellaVentura G, Petibois C: **Analytical characterization of cell-asbestos fiber interactions in lung pathogenesis**. *Anal Bioanal Chem*, **397**(6):2079-2089.
37. Castranova V, Vallyathan V: **Silicosis and coal workers' pneumoconiosis**. *Environ Health Perspect* 2000, **108 Suppl 4**:675-684.
38. Hnizdo E, Sluis-Cremer GK: **Risk of silicosis in a cohort of white South African gold miners**. *Am J Ind Med* 1993, **24**(4):447-457.
39. Hnizdo E, Murray J: **Risk of pulmonary tuberculosis relative to silicosis and exposure to silica dust in South African gold miners**. *Occup Environ Med* 1998, **55**(7):496-502.
40. Calvert GM, Rice FL, Boiano JM, Sheehy JW, Sanderson WT: **Occupational silica exposure and risk of various diseases: an analysis using death certificates from 27 states of the United States**. *Occup Environ Med* 2003, **60**(2):122-129.
41. Steenland K, Stayner L: **Silica, asbestos, man-made mineral fibers, and cancer**. *Cancer Causes Control* 1997, **8**(3):491-503.
42. Pelucchi C, Pira E, Piolatto G, Coggiola M, Carta P, La Vecchia C: **Occupational silica exposure and lung cancer risk: a review of epidemiological studies 1996-2005**. *Ann Oncol* 2006, **17**(7):1039-1050.
43. Vida S, Pintos J, Parent ME, Lavoue J, Siemiatycki J: **Occupational exposure to silica and lung cancer: pooled analysis of two case-control studies in Montreal, Canada**. *Cancer Epidemiol Biomarkers Prev* 2010, **19**(6):1602-1611.
44. **Cancer fact sheet (Fact sheet N°297)** [http://www.who.int/mediacentre/factsheets/fs297/en/print.html]
45. Suvatne J, Browning RF: **Asbestos and lung cancer**. *Dis Mon*, **57**(1):55-68.
46. Borm PJ, Kreyling W: **Toxicological hazards of inhaled nanoparticles--potential implications for drug delivery**. *J Nanosci Nanotechnol* 2004, **4**(5):521-531.
47. Kreyling WG, Scheuch G: **Particle Lung Interactions**. New York-Basel; 2000.
48. Stone V, Johnston H, Clift MJ: **Air pollution, ultrafine and nanoparticle toxicology: cellular and molecular interactions**. *IEEE Trans Nanobioscience* 2007, **6**(4):331-340.
49. Vallyathan V, Castranova V, Pack D, Leonard S, Shumaker J, Hubbs AF, Shoemaker DA, Ramsey DM, Pretty JR, McLaurin JL *et al*: **Freshly Fractured Quartz Inhalation Leads to Enhanced Lung Injury and Inflammation - Potential Role of Free-Radicals**. *American Journal of Respiratory and Critical Care Medicine* 1995, **152**(3):1003-1009.

50. Fubini B, Hubbard A: **Reactive oxygen species (ROS) and reactive nitrogen species (RNS) generation by silica in inflammation and fibrosis**. *Free Radic Biol Med* 2003, **34**(12):1507-1516.
51. Finkelstein JN, Johnston C, Barrett T, Oberdorster G: **Particulate-cell interactions and pulmonary cytokine expression**. *Environ Health Perspect* 1997, **105 Suppl 5**:1179-1182.
52. Crestani B, Seta N, Palazzo E, Rolland C, Venembre P, Dehoux M, Boutten A, Soler P, Dombret MC, Kahn MF *et al*: **Interleukin-8 and neutrophils in systemic sclerosis with lung involvement**. *Am J Respir Crit Care Med* 1994, **150**(5 Pt 1):1363-1367.
53. Paine R, 3rd, Rolfe MW, Standiford TJ, Burdick MD, Rollins BJ, Strieter RM: **MCP-1 expression by rat type II alveolar epithelial cells in primary culture**. *J Immunol* 1993, **150**(10):4561-4570.
54. Zhao MQ, Foley MP, Stoler MH, Enelow RI: **Alveolar epithelial cell chemokine expression induced by specific antiviral CD8+ T-cell recognition plays a critical role in the perpetuation of experimental interstitial pneumonia**. *Chest* 2001, **120**(1 Suppl):11S-13S.
55. Matsukura S, Kokubu F, Kubo H, Tomita T, Tokunaga H, Kadokura M, Yamamoto T, Kuroiwa Y, Ohno T, Suzaki H *et al*: **Expression of RANTES by normal airway epithelial cells after influenza virus A infection**. *Am J Respir Cell Mol Biol* 1998, **18**(2):255-264.
56. Rosseau S, Selhorst J, Wiechmann K, Leissner K, Maus U, Mayer K, Grimminger F, Seeger W, Lohmeyer J: **Monocyte migration through the alveolar epithelial barrier: adhesion molecule mechanisms and impact of chemokines**. *J Immunol* 2000, **164**(1):427-435.
57. Paine R, 3rd, Christensen P, Toews GB, Simon RH: **Regulation of alveolar epithelial cell ICAM-1 expression by cell shape and cell-cell interactions**. *Am J Physiol* 1994, **266**(4 Pt 1):L476-484.
58. Hance AJ, Douches S, Winchester RJ, Ferrans VJ, Crystal RG: **Characterization of mononuclear phagocyte subpopulations in the human lung by using monoclonal antibodies: changes in alveolar macrophage phenotype associated with pulmonary sarcoidosis**. *J Immunol* 1985, **134**(1):284-292.
59. Hoogsteden HC, van Dongen JJ, van Hal PT, Delahaye M, Hop W, Hilvering C: **Phenotype of blood monocytes and alveolar macrophages in interstitial lung disease**. *Chest* 1989, **95**(3):574-577.
60. Schwartz J: **Air pollution and hospital admissions for heart disease in eight U.S. counties**. *Epidemiology* 1999, **10**(1):17-22.
61. Poloniecki JD, Atkinson RW, de Leon AP, Anderson HR: **Daily time series for cardiovascular hospital admissions and previous day's air pollution in London, UK**. *Occup Environ Med* 1997, **54**(8):535-540.
62. Mills NL, Amin N, Robinson SD, Anand A, Davies J, Patel D, de la Fuente JM, Cassee FR, Boon NA, MacNee W *et al*: **Do inhaled carbon nanoparticles translocate directly into the circulation in humans?** *American Journal of Respiratory and Critical Care Medicine* 2006, **173**(4):426-431.

63. Peters A, Dockery DW, Muller JE, Mittleman MA: **Increased particulate air pollution and the triggering of myocardial infarction**. *Circulation* 2001, **103**(23):2810-2815.
64. Nemmar A, Hoylaerts MF, Hoet PH, Dinsdale D, Smith T, Xu H, Vermylen J, Nemery B: **Ultrafine particles affect experimental thrombosis in an in vivo hamster model**. *Am J Respir Crit Care Med* 2002, **166**(7):998-1004.
65. Nemmar A, Hoet PH, Vanquickenborne B, Dinsdale D, Thomeer M, Hoylaerts MF, Vanbilloen H, Mortelmans L, Nemery B: **Passage of inhaled particles into the blood circulation in humans**. *Circulation* 2002, **105**(4):411-414.
66. Soldati T, Schliwa M: **Powering membrane traffic in endocytosis and recycling**. *Nat Rev Mol Cell Biol* 2006, **7**(12):897-908.
67. Doherty GJ, McMahon HT: **Mechanisms of endocytosis**. *Annu Rev Biochem* 2009, **78**:857-902.
68. Mukherjee S, Ghosh RN, Maxfield FR: **Endocytosis**. *Physiol Rev* 1997, **77**(3):759-803.
69. Gaidarov I, Santini F, Warren RA, Keen JH: **Spatial control of coated-pit dynamics in living cells**. *Nat Cell Biol* 1999, **1**(1):1-7.
70. Ghitescu L, Fixman A, Simionescu M, Simionescu N: **Specific binding sites for albumin restricted to plasmalemmal vesicles of continuous capillary endothelium: receptor-mediated transcytosis**. *J Cell Biol* 1986, **102**(4):1304-1311.
71. Soda R, Tavassoli M: **Transendothelial transport (transcytosis) of iron-transferrin complex in the bone marrow**. *J Ultrastruct Res* 1984, **88**(1):18-29.
72. King GL, Johnson SM: **Receptor-mediated transport of insulin across endothelial cells**. *Science* 1985, **227**(4694):1583-1586.
73. Ge S, Song L, Serwanski DR, Kuziel WA, Pachter JS: **Transcellular transport of CCL2 across brain microvascular endothelial cells**. *J Neurochem* 2008, **104**(5):1219-1232.
74. Kawashima Y, Yamamoto H, Takeuchi H, Fujioka S, Hino T: **Pulmonary delivery of insulin with nebulized DL-lactide/glycolide copolymer (PLGA) nanospheres to prolong hypoglycemic effect**. *J Control Release* 1999, **62**(1-2):279-287.
75. Yamamoto H, Kuno Y, Sugimoto S, Takeuchi H, Kawashima Y: **Surface-modified PLGA nanosphere with chitosan improved pulmonary delivery of calcitonin by mucoadhesion and opening of the intercellular tight junctions**. *J Control Release* 2005, **102**(2):373-381.
76. Zhang Q, Shen Z, Nagai T: **Prolonged hypoglycemic effect of insulin-loaded polybutylcyanoacrylate nanoparticles after pulmonary administration to normal rats**. *Int J Pharm* 2001, **218**(1-2):75-80.
77. Surti N, Naik S, Bagchi T, Dwarkanath BS, Misra A: **Intracellular delivery of nanoparticles of an antiasthmatic drug**. *AAPS PharmSciTech* 2008, **9**(1):217-223.
78. Bailey MM, Berkland CJ: **Nanoparticle formulations in pulmonary drug delivery**. *Med Res Rev* 2009, **29**(1):196-212.

79. Hermanns MI: **Etablierung einer Ko-Kultur von Alveolarepithel und Mikrovaskul„rem Endothel als in vitro Modell einer humanen respiratorischen Einheit** 2005.
80. Masuzawa M, Fujimura T, Hamada Y, Fujita Y, Hara H, Nishiyama S, Katsuoka K, Tamauchi H, Sakurai Y: **Establishment of a human hemangiosarcoma cell line (ISO-HAS)**. *Int J Cancer* 1999, **81**(2):305-308.
81. Unger RE, Krump-Konvalinkova V, Peters K, Kirkpatrick CJ: **In vitro expression of the endothelial phenotype: comparative study of primary isolated cells and cell lines, including the novel cell line HPMEC-ST1.6R**. *Microvasc Res* 2002, **64**(3):384-397.
82. Hermanns MI, Kasper J, Dubruel P, Pohl C, Uboldi C, Vermeersch V, Fuchs S, Unger RE, Kirkpatrick CJ: **An impaired alveolar-capillary barrier in vitro: effect of proinflammatory cytokines and consequences on nanocarrier interaction**. *J R Soc Interface* 2010, **7 Suppl 1**:S41-54.
83. Greenberg MI, Waksman J, Curtis J: **Silicosis: a review**. *DisMon* 2007, **53**(8):394-416.
84. Barnes CA, Elsaesser A, Arkusz J, Smok A, Palus J, Lesniak A, Salvati A, Hanrahan JP, Jong WH, Dziubaltowska E *et al*: **Reproducible comet assay of amorphous silica nanoparticles detects no genotoxicity**. *Nano Lett* 2008, **8**(9):3069-3074.
85. Brunner TJ, Wick P, Manser P, Spohn P, Grass RN, Limbach LK, Bruinink A, Stark WJ: **In vitro cytotoxicity of oxide nanoparticles: comparison to asbestos, silica, and the effect of particle solubility**. *Environ Sci Technol* 2006, **40**(14):4374-4381.
86. Napierska D, Thomassen LC, Rabolli V, Lison D, Gonzalez L, Kirsch-Volders M, Martens JA, Hoet PH: **Size-Dependent Cytotoxicity of Monodisperse Silica Nanoparticles in Human Endothelial Cells**. *Small* 2009.
87. Lison D, Thomassen LC, Rabolli V, Gonzalez L, Napierska D, Seo JW, Kirsch-Volders M, Hoet P, Kirschhock CE, Martens JA: **Nominal and effective dosimetry of silica nanoparticles in cytotoxicity assays**. *Toxicol Sci* 2008, **104**(1):155-162.
88. Tsuchiya S, Yamabe M, Yamaguchi Y, Kobayashi Y, Konno T, Tada K: **Establishment and characterization of a human acute monocytic leukemia cell line (THP-1)**. *Int J Cancer* 1980, **26**(2):171-176.
89. Hermanns MI, Unger RE, Kehe K, Peters K, Kirkpatrick CJ: **Lung epithelial cell lines in coculture with human pulmonary microvascular endothelial cells: development of an alveolo-capillary barrier in vitro**. *Lab Invest* 2004, **84**(6):736-752.
90. Hermanns MI, Fuchs S, Bock M, Wenzel K, Mayer E, Kehe K, Bittinger F, Kirkpatrick CJ: **Primary human coculture model of alveolo-capillary unit to study mechanisms of injury to peripheral lung**. *Cell Tissue Res* 2009, **336**(1):91-105.
91. Utech S, Scherer C, Maskos M: **Multifunctional, multicompartment polyorganosiloxane magnetic nanoparticles for biomedical applications**. *J Magn Magn Mater* 2009, **321**(10):1386-1388.

92. Utech S, Scherer C, Krohne K, Carrella L, Rentschler E, Gasi T, Ksenofontov V, Felser C, Maskos M: **Magnetic polyorganosiloxane core-shell nanoparticles: Synthesis, characterization and magnetic fractionation**. *J Magn Magn Mater* 2010, **322**(21):3519-3526.
93. micromod Partikeltechnologie GmbH, Teller. J, Grüttner. C, Rudershausen. S, Westphal. F: **Verfahren zur Herstellung gefärbter und fluoreszenter Polykieselsäure-Partikel**. In*.* Edited by Office EP. Germany; 2000: 2001/2049.
94. Dubruel P, Christiaens B, Rosseneu M, Vandekerckhove J, Grooten J, Goossens V, Schacht E: **Buffering properties of cationic polymethacrylates are not the only key to successful gene delivery**. *Biomacromolecules* 2004, **5**(2):379-388.
95. Kasper J, Hermanns MI, Bantz C, Maskos M, Stauber R, Pohl C, Unger RE, Kirkpatrick JC: **Inflammatory and cytotoxic responses of an alveolar-capillary coculture model to silica nanoparticles: Comparison with conventional monocultures**. *Part Fibre Toxicol* 2011, **8**(1):6.
96. Berridge MV, Tan AS: **Characterization of the cellular reduction of 3-(4,5-dimethylthiazol-2-yl)-2,5-diphenyltetrazolium bromide (MTT): subcellular localization, substrate dependence, and involvement of mitochondrial electron transport in MTT reduction**. *Arch Biochem Biophys* 1993, **303**(2):474-482.
97. Gillies RJ, Didier N, Denton M: **Determination of cell number in monolayer cultures**. *Anal Biochem* 1986, **159**(1):109-113.
98. Diabaté S, Völkel K, Wottrich R, Krug HF: **Macrophages and epithelial cells in co-culture as sensitive targets for pulmonary toxicity assessment**. In: *Effects of Air Contaminants on the Respiratory Tract - Interpretations from Molecules to Meta Analysis.* Edited by Heinrich U. Stuttgart, Germany: Fraunhofer IRB Verlag; 2004: 233-243.
99. Diabate S, Mulhopt S, Paur HR, Krug HF: **The response of a co-culture lung model to fine and ultrafine particles of incinerator fly ash at the air-liquid interface**. *Altern Lab Anim* 2008, **36**(3):285-298.
100. Erickson HP: **Size and Shape of Protein Molecules at the Nanometer Level Determined by Sedimentation, Gel Filtration, and Electron Microscopy**. *Biological Procedures Online* 2009, **11**(1):32-51.
101. Miao H, Xue QF, Hu QH, Zhang H, Wang LR, Niimi H, Zhuang FY: **In situ expression of ICAM-1 and its mRNA in the lung tissue of asthmatic rats**. *Clin Hemorheol Microcirc* 1997, **17**(4):325-331.
102. Muller AM, Hermanns MI, Cronen C, Kirkpatrick CJ: **Comparative study of adhesion molecule expression in cultured human macro- and microvascular endothelial cells**. *Exp Mol Pathol* 2002, **73**(3):171-180.
103. Fenoglio I, Tomatis M, Lison D, Muller J, Fonseca A, Nagy JB, Fubini B: **Reactivity of carbon nanotubes: free radical generation or scavenging activity?** *Free Radic Biol Med* 2006, **40**(7):1227-1233.
104. Yu ML, Limper AH: **Pneumocystis carinii induces ICAM-1 expression in lung epithelial cells through a TNF-alpha-mediated mechanism**. *Am J Physiol* 1997, **273**(6 Pt 1):L1103-1111.

105. Nario RC, Hubbard AK: **Localization of intercellular adhesion molecule-1 (ICAM-1) in the lungs of silica-exposed mice**. *EnvironHealth Perspect* 1997, **105 Suppl 5**:1183-1190.
106. Hubbard AK, Thibodeau M, Giardina C: **Cellular and molecular mechanisms regulating silica-induced adhesion molecule expression in mice**. *J EnvironPatholToxicolOncol* 2001, **20 Suppl 1**:45-51.
107. Cho WS, Choi M, Han BS, Cho M, Oh J, Park K, Kim SJ, Kim SH, Jeong J: **Inflammatory mediators induced by intratracheal instillation of ultrafine amorphous silica particles**. *Toxicology Letters* 2007, **175**(1-3):24-33.
108. Hetland RB, Schwarze PE, Johansen BV, Myran T, Uthus N, Refsnes M: **Silica-induced cytokine release from A549 cells: importance of surface area versus size**. *HumExpToxicol* 2001, **20**(1):46-55.
109. Hu S, Zhao H, Yin XJ, Ma JK: **Role of mitochondria in silica-induced apoptosis of alveolar macrophages: inhibition of apoptosis by rhodamine 6G and N-acetyl-L-cysteine**. *J ToxicolEnvironHealth A* 2007, **70**(17):1403-1415.
110. Gwinn MR, Leonard SS, Sargent LM, Lowry DT, McKinstry K, Meighan T, Reynolds SH, Kashon M, Castranova V, Vallyathan V: **The role of p53 in silica-induced cellular and molecular responses associated with carcinogenesis**. *J ToxicolEnvironHealth A* 2009, **72**(23):1509-1519.
111. Panduri V, Surapureddi S, Soberanes S, Weitzman SA, Chandel N, Kamp DW: **P53 mediates amosite asbestos-induced alveolar epithelial cell mitochondria-regulated apoptosis**. *Am J Respir Cell Mol Biol* 2006, **34**(4):443-452.
112. Upadhyay D, Kamp DW: **Asbestos-induced pulmonary toxicity: role of DNA damage and apoptosis**. *ExpBiolMed(Maywood)* 2003, **228**(6):650-659.
113. Msiska Z, Pacurari M, Mishra A, Leonard SS, Castranova V, Vallyathan V: **DNA Double Strand Breaks by Asbestos, Silica and Titanium dioxide: Possible Biomarker of Carcinogenic Potential?** *Am J Respir Cell Mol Biol* 2009.
114. Johnston CJ, Driscoll KE, Finkelstein JN, Baggs R, O'Reilly MA, Carter J, Gelein R, Oberdorster G: **Pulmonary chemokine and mutagenic responses in rats after subchronic inhalation of amorphous and crystalline silica**. *ToxicolSci* 2000, **56**(2):405-413.
115. Zhang K, Kaufman RJ: **The unfolded protein response: a stress signaling pathway critical for health and disease**. *Neurology* 2006, **66**(2 Suppl 1):S102-109.
116. Horke S, Witte I, Wilgenbus P, Altenhofer S, Kruger M, Li H, Forstermann U: **Protective effect of paraoxonase-2 against endoplasmic reticulum stress-induced apoptosis is lost upon disturbance of calcium homoeostasis**. *Biochem J* 2008, **416**(3):395-405.
117. Horke S, Witte I, Wilgenbus P, Kruger M, Strand D, Forstermann U: **Paraoxonase-2 reduces oxidative stress in vascular cells and**

decreases endoplasmic reticulum stress-induced caspase activation. *Circulation* 2007, **115**(15):2055-2064.

118. Vivero-Escoto JL, Slowing, II, Trewyn BG, Lin VS: **Mesoporous silica nanoparticles for intracellular controlled drug delivery**. *Small* 2010, **6**(18):1952-1967.
119. Kunzmann A, Andersson B, Thurnherr T, Krug H, Scheynius A, Fadeel B: **Toxicology of engineered nanomaterials: Focus on biocompatibility, biodistribution and biodegradation**. *Biochim Biophys Acta* 2011, **1810**(3):361-373.
120. Xia T, Kovochich M, Liong M, Meng H, Kabehie S, George S, Zink JI, Nel AE: **Polyethyleneimine Coating Enhances the Cellular Uptake of Mesoporous Silica Nanoparticles and Allows Safe Delivery of siRNA and DNA Constructs**. *ACS Nano* 2009.
121. Boussif O, Lezoualc'h F, Zanta MA, Mergny MD, Scherman D, Demeneix B, Behr JP: **A versatile vector for gene and oligonucleotide transfer into cells in culture and in vivo: polyethylenimine**. *Proc Natl Acad Sci U S A* 1995, **92**(16):7297-7301.
122. Dubruel P, Christiaens B, Vanloo B, Bracke K, Rosseneu M, Vandekerckhove J, Schacht E: **Physicochemical and biological evaluation of cationic polymethacrylates as vectors for gene delivery**. *Eur J Pharm Sci* 2003, **18**(3-4):211-220.
123. Dubruel P, Dekie L, Christiaens B, Vanloo B, Rosseneu M, Van De Kerckhove J, Mannisto M, Urtti A, Schacht E: **Poly-l-glutamic acid derivatives as multifunctional vectors for gene delivery. Part B. Biological evaluation**. *Biomacromolecules* 2003, **4**(5):1177-1183.
124. Gabrielson NP, Pack DW: **Efficient polyethylenimine-mediated gene delivery proceeds via a caveolar pathway in HeLa cells**. *J Control Release* 2009, **136**(1):54-61.
125. Rejman J, Bragonzi A, Conese M: **Role of clathrin- and caveolae-mediated endocytosis in gene transfer mediated by lipo- and polyplexes**. *Mol Ther* 2005, **12**(3):468-474.
126. Akinc A, Thomas M, Klibanov AM, Langer R: **Exploring polyethylenimine-mediated DNA transfection and the proton sponge hypothesis**. *J Gene Med* 2005, **7**(5):657-663.
127. Gautam A, Densmore CL, Xu B, Waldrep JC: **Enhanced gene expression in mouse lung after PEI-DNA aerosol delivery**. *Mol Ther* 2000, **2**(1):63-70.
128. Gautam A, Densmore CL, Waldrep JC: **Pulmonary cytokine responses associated with PEI-DNA aerosol gene therapy**. *Gene Ther* 2001, **8**(3):254-257.
129. Gautam A, Densmore CL, Golunski E, Xu B, Waldrep JC: **Transgene expression in mouse airway epithelium by aerosol gene therapy with PEI-DNA complexes**. *Mol Ther* 2001, **3**(4):551-556.
130. Lee H, Sung D, Veerapandian M, Yun K, Seo SW: **PEGylated polyethyleneimine grafted silica nanoparticles: enhanced cellular uptake and efficient siRNA delivery**. *Anal Bioanal Chem* 2011.

131. Suh J, Choy KL, Lai SK, Suk JS, Tang BC, Prabhu S, Hanes J: **PEGylation of nanoparticles improves their cytoplasmic transport**. *Int J Nanomedicine* 2007, **2**(4):735-741.
132. Huang DM, Hung Y, Ko BS, Hsu SC, Chen WH, Chien CL, Tsai CP, Kuo CT, Kang JC, Yang CS *et al*: **Highly efficient cellular labeling of mesoporous nanoparticles in human mesenchymal stem cells: implication for stem cell tracking**. *FASEB J* 2005, **19**(14):2014-2016.
133. Chung TH, Wu SH, Yao M, Lu CW, Lin YS, Hung Y, Mou CY, Chen YC, Huang DM: **The effect of surface charge on the uptake and biological function of mesoporous silica nanoparticles in 3T3-L1 cells and human mesenchymal stem cells**. *Biomaterials* 2007, **28**(19):2959-2966.
134. Fazlollahi F, Angelow S, Yacobi NR, Marchelletta R, Yu AS, Hamm-Alvarez SF, Borok Z, Kim KJ, Crandall ED: **Polystyrene nanoparticle trafficking across MDCK-II**. *Nanomedicine* 2011.
135. Jiang X, Dausend J, Hafner M, Musyanovych A, Rocker C, Landfester K, Mailander V, Nienhaus GU: **Specific effects of surface amines on polystyrene nanoparticles in their interactions with mesenchymal stem cells**. *Biomacromolecules* 2010, **11**(3):748-753.
136. Damke H, Baba T, van der Bliek AM, Schmid SL: **Clathrin-independent pinocytosis is induced in cells overexpressing a temperature-sensitive mutant of dynamin**. *J Cell Biol* 1995, **131**(1):69-80.
137. Morrow IC, Rea S, Martin S, Prior IA, Prohaska R, Hancock JF, James DE, Parton RG: **Flotillin-1/reggie-2 traffics to surface raft domains via a novel golgi-independent pathway. Identification of a novel membrane targeting domain and a role for palmitoylation**. *J Biol Chem* 2002, **277**(50):48834-48841.
138. Glebov OO, Bright NA, Nichols BJ: **Flotillin-1 defines a clathrin-independent endocytic pathway in mammalian cells**. *Nat Cell Biol* 2006, **8**(1):46-54.
139. Ait-Slimane T, Galmes R, Trugnan G, Maurice M: **Basolateral internalization of GPI-anchored proteins occurs via a clathrin-independent flotillin-dependent pathway in polarized hepatic cells**. *Mol Biol Cell* 2009, **20**(17):3792-3800.
140. Langhorst MF, Reuter A, Jaeger FA, Wippich FM, Luxenhofer G, Plattner H, Stuermer CA: **Trafficking of the microdomain scaffolding protein reggie-1/flotillin-2**. *Eur J Cell Biol* 2008, **87**(4):211-226.
141. Dermine JF, Duclos S, Garin J, St-Louis F, Rea S, Parton RG, Desjardins M: **Flotillin-1-enriched lipid raft domains accumulate on maturing phagosomes**. *J Biol Chem* 2001, **276**(21):18507-18512.
142. Vercauteren D, Piest M, van der Aa LJ, Al Soraj M, Jones AT, Engbersen JF, De Smedt SC, Braeckmans K: **Flotillin-dependent endocytosis and a phagocytosis-like mechanism for cellular internalization of disulfide-based poly(amido amine)/DNA polyplexes**. *Biomaterials* 2011, **32**(11):3072-3084.
143. Oberdorster G, Oberdorster E, Oberdorster J: **Nanotoxicology: an emerging discipline evolving from studies of ultrafine particles**. *Environ Health Perspect* 2005, **113**(7):823-839.

144. Shapero K, Fenaroli F, Lynch I, Cottell DC, Salvati A, Dawson KA: **Time and space resolved uptake study of silica nanoparticles by human cells**. *Mol Biosyst* 2011, **7**(2):371-378.
145. Rubins JB: **Alveolar macrophages: wielding the double-edged sword of inflammation**. *Am J Respir Crit Care Med* 2003, **167**(2):103-104.
146. Sibille Y, Reynolds HY: **Macrophages and polymorphonuclear neutrophils in lung defense and injury**. *Am Rev Respir Dis* 1990, **141**(2):471-501.
147. Thepen T, Van Rooijen N, Kraal G: **Alveolar macrophage elimination in vivo is associated with an increase in pulmonary immune response in mice**. *J Exp Med* 1989, **170**(2):499-509.
148. Holt PG: **Inhibitory activity of unstimulated alveolar macrophages on T-lymphocyte blastogenic response**. *Am Rev Respir Dis* 1978, **118**(4):791-793.
149. Park EK, Jung HS, Yang HI, Yoo MC, Kim C, Kim KS: **Optimized THP-1 differentiation is required for the detection of responses to weak stimuli**. *Inflammation Research* 2007, **56**(1):45-50.
150. Alfaro-Moreno E, Nawrot TS, Vanaudenaerde BM, Hoylaerts MF, Vanoirbeek JA, Nemery B, Hoet PH: **Co-cultures of multiple cell types mimic pulmonary cell communication in response to urban PM10**. *EurRespir J* 2008, **32**(5):1184-1194.
151. Diabate S, Mulhopt S, Paur HR, Krug HF: **The response of a co-culture lung model to fine and ultrafine particles of incinerator fly ash at the air-liquid interface**. *AlternLab Anim* 2008, **36**(3):285-298.
152. Muller L, Riediker M, Wick P, Mohr M, Gehr P, Rothen-Rutishauser B: **Oxidative stress and inflammation response after nanoparticle exposure: differences between human lung cell monocultures and an advanced three-dimensional model of the human epithelial airways**. *J RSocInterface* 2010, **7 Suppl 1**:S27-S40.
153. Wottrich R, Diabate S, Krug HF: **Biological effects of ultrafine model particles in human macrophages and epithelial cells in mono- and co-culture**. *IntJ HygEnvironHealth* 2004, **207**(4):353-361.
154. Lehmann AD, Daum N, Bur M, Lehr CM, Gehr P, Rothen-Rutishauser BM: **An in vitro triple cell co-culture model with primary cells mimicking the human alveolar epithelial barrier**. *Eur J Pharm Biopharm* 2011, **77**(3):398-406.
155. Trinchieri G, Scott P: **Interleukin-12: basic principles and clinical applications**. *Curr Top Microbiol Immunol* 1999, **238**:57-78.
156. Walter MJ, Kajiwara N, Karanja P, Castro M, Holtzman MJ: **Interleukin 12 p40 production by barrier epithelial cells during airway inflammation**. *Journal of Experimental Medicine* 2001, **193**(3):339-351.
157. Meyts I, Hellings PW, Hens G, Vanaudenaerde BM, Verbinnen B, Heremans H, Matthys P, Bullens DM, Overbergh L, Mathieu C *et al*: **IL-12 contributes to allergen-induced airway inflammation in experimental asthma**. *J Immunol* 2006, **177**(9):6460-6470.
158. Durrant DM, Metzger DW: **IL-12 can alleviate Th17-mediated allergic lung inflammation through induction of pulmonary IL-10 expression**. *Mucosal Immunol* 2010, **3**(3):301-311.

159. Plummeridge MJ, Armstrong L, Birchall MA, Millar AB: **Reduced production of interleukin 12 by interferon gamma primed alveolar macrophages from atopic asthmatic subjects**. *Thorax* 2000, **55**(10):842-847.
160. Mosser DM, Edwards JP: **Exploring the full spectrum of macrophage activation**. *Nat Rev Immunol* 2008, **8**(12):958-969.
161. Martinez FO, Sica A, Mantovani A, Locati M: **Macrophage activation and polarization**. *Front Biosci* 2008, **13**:453-461.